Doctoral Dissertation
Doctoral Program in Chemical Engineering (30th Cycle)

Syngas production by electrocatalytic reduction of CO_2 using Ag-decorated TiO_2 nanotubes

By

Mohammad Amin Farkhondehfal

******

Supervisor(s):
Prof. N. Russo
Dr. S. Hernàndez , Co-Supervisor

Doctoral Examination Committee:
Prof. M.C. Paganini, Referee, Università degli Studi di Torino
Prof. I. Nova , Referee, Politecnico di Milano
Prof. F. Scala, Referee, Università di Napoli
Prof. A. Ktarba , Referee, Jagiellonian University
Prof. R.Pirone, Referee, Politecnico di Torino

Politecnico di Torino
2018

Declaration

I hereby declare that, the contents and organization of this dissertation constitute my own original work and does not compromise in any way the rights of third parties, including those relating to the security of personal data.

Mohammad Amin Farkhondehfal

2017

* This dissertation is presented in partial fulfillment of the requirements for **Ph.D. degree** in the Graduate School of Politecnico di Torino (ScuDo).

I would like to dedicate this thesis to my loving parents for their support throughout these years

Acknowledgment

I would like to thank my supervisor Prof. Nunzio Russo for his help and support during this period and for letting me to have this opportunity.

I would like to thank Prof. G. Saracco for his precious support and guidance.

I would like to thank Prof. M. Makkee and his research group for allowing us to use some of their facilities in TUDelft. Also Andrea Lamberti for his kind support in the synthesis process.

And a very special thank to my Co-Supervisor Dr. Simelys Hernández for her unconditional support in my research activities from the first day of my career.

Abstract

The CO_2 that comes from the use of fossil fuels accounts for about 65% of the global greenhouse gas emission, and it plays a critical role in global climate changes. Among the different strategies that have been used to address the storage and reutilization of CO_2, the transformation of CO_2 into chemicals or fuels with a high added-value has been considered a winning approach. This transformation is capable of reducing the carbon emission and induce a "fuel switching" that exploits renewable energy sources. This work aims to focus on electrocatalytic reduction of CO_2 to produce syngas as a raw material for many other chemical industries. The chosen electrocatalyst for this purpose is Ag decorated Titania nanotubes.

The presented work has been divided in 3 parts: Initially, a thorough analysis of state of the art about syngas production by electrocatalysis of CO_2 has been presented which includes current status, the catalyst used so far and the parameter that effects the process and also how to improve them. Next chapter is about the synthesis of catalyst. As for this work, Ag decorated Titania nanotubes has been chosen as the electrocatalyst. The synthesis also divided in two sub sessions. First, how to synthesize the substrate which is Titania nanotubes and the next sub session is concerned with Ag deposition methods used in this work. After a brief description of existing methods for the growth of Titania nanotubes, anodization method has been described and used for the fast and well oriented vertically aligned nanotubes regarding the aforementioned sub session. In the next sub session, two different deposition methods have been described and used. One of the methods described in the current study is UV deposition in which Ag particles are being deposited on nanotubes by UV illumination of Silver nitrate solution. Furthermore, the next

method has been carried out using sputtering of Ag nanoparticles on nanotubes in which the deposition time and applied currents for sputtering has been changed to achieve the best dispersed Ag nanoparticles.

In the third chapter, different Ag decorated Titania nanotubes has been evaluated and tested in order to analyze the performance of each electrocatalyst. Additionally, different electrochemical tests from chronoamperometry to cyclic voltammetry and electrochemical surface area measurement has been taken into account so as to evaluate the performance of the catalysts. All the mentioned analysis has been carried out in ambient conditions. In these tests the maximum current density of 60mA.cm^{-2} with H_2/CO ratio of 3 to 1 has been achieved by Titania nanotube decorated with Ag nanoparticles by sputtering at 60mA for 90s. Furthermore, to investigate the effect of pressure, chronoamperometry analyzes has been done in 7 bar which showed to increase the production rate due to higher solubility of CO_2 into electrolyte. Moreover, for stability analysis of electrocatalyst, Titania nanotube which decorated by Ag nanoparticles by sputtering method at 60mA for 90s has been chosen for a 21-hour chronoamperometry test. Surface analysis by Transmission Electron Microscopy (TEM) and Electrochemically Active Surface Area (ECSA), before and after the reaction, confirmed that the decay in the activity of this electrocatalyst happened due to agglomeration and dissolution of some nanoparticles. Also, in order to investigate the effect of Titania nanotubes as a co-catalyst for Ag nanoparticles in CO_2 reduction, different substrates with the same amount of Ag loading have been tested and analyzed. Consequently, it is concluded that Titania can act as a facilitating medium for stabilizing *rate determining step* radicals. Also, using Titania in the form of nanotubes proved to be beneficial by increasing the active surface area of electrocatalyst and decreasing the resistance of mass transfer and electrical transportation in the electrodes’ surface.

Contents

List of Figures

List of Tables

Chapter 1

State of the art

1.1 The importance of the work

CO_2 as a main greenhouse gas plays a key role in global warming along with other greenhouse gases (CFCs-24%, CH_4-15%, and N_2O-6%), and considered to be a global challenge in our era [20, 21]. In Figure 1 Global GHG emission produced by human activities are categorized on the basis of the economic sectors that lead to their production. Therefore, in the recent years many regulations and platforms have been put to control CO_2 emission by human activities and control the level of CO_2 in the atmosphere. The major goal of Paris agreement in December 2015 during the 21st Conference of Parties on Climate change (COP21) is to reduce this impact on global level. The objective is to maintain the mean increase of global temperature below 2 °C during this century to prevent the catastrophic effect of global warming.

Another prospective to the importance of this issue is restriction of fossil fuels and scarcity of them in some parts of the world and most importantly the depletion of these fuels [22]. So, finding a sustainable way for the deployment of alternative fuels is considered to be a possible solution to this challenge.

The challenge is to reduce the carbon footprint, reuse CO_2 and convert intermittent renewable energy into continuous energy that can be stored into chemicals and fuels. Current strategy of many research groups have put in place to address CO_2 storage [23] and reuse [24]. By this latter, the intention of this work is to change CO_2 to value added products using sustainable processes. Among all the proposed methods, electrochemical reduction of CO_2 is an attractive alternative from both economic and environmental point of view [2].Main products of electrochemical CO_2 reduction are CO, formic acid or higher molecular weight hydrocarbons like methanol and ethanol. The main challenge for the implantation of this technology at industrial level is to find suitable electro-catalyst and optimized process condition for the selective production of the desired product with a high conversion and scalable production rate and efficiency.

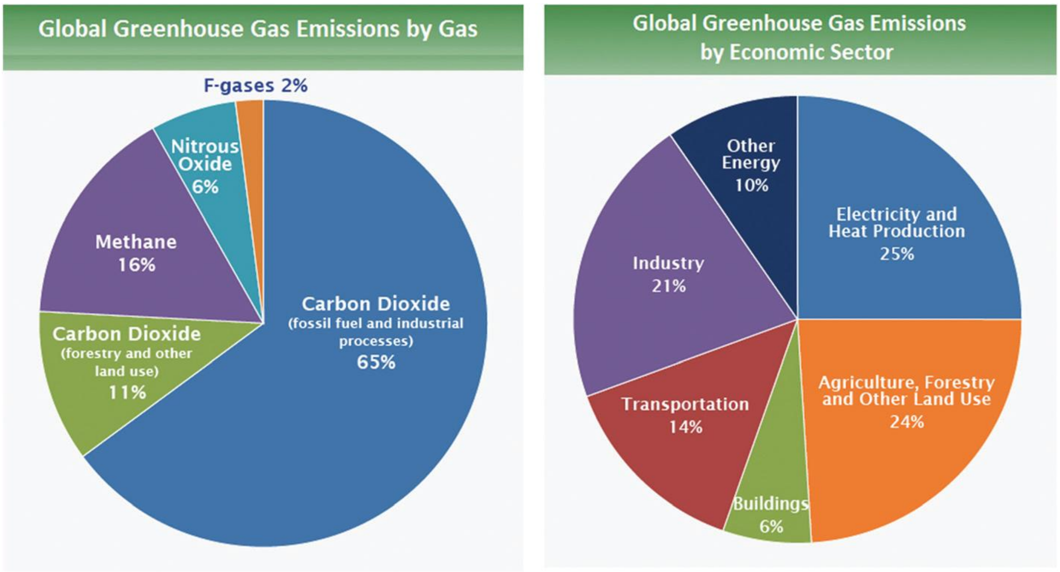

Figure 1.Global GHG emission produced by human activities and categorized on the basis of the economic sectors that lead to their production.

1.2 Syngas from Carbon Dioxide: the opportunity

Due to the use of aqueous media for electrochemical reduction of CO_2, Hydrogen Evolution reaction (HER) is an inevitable competitor for CO_2 conversion. So since reduction of water or protons (H^+) is a side product, the best way is to combine two reactions for production of Syngas. This way, the feedstock for many downstream processing in order to produce variety of chemical product from ammonia to alcohols and hydrocarbons would be provided.

The major advantage of producing syngas instead of directly producing other possible products of CO_2 reduction is that further development of engineered products based on the ratio of CO/H_2 is possible. Different possible products and intermediates for other bulk chemicals, solvents, plastics, pharmaceutical and other chemical intermediates, which can be produced from Syngas can be seen in Figure 2. As mentioned above the ratio of CO/H_2 plays a key role on its application so adjusting this ratio during the CO_2 reduction would be a wise choice. This adjustment can be done either by catalyst and/or the configuration of the reactor.

A recent report on “Syngas & Derivatives: A Global Strategic Business Report” by Global industry Inc. [25] emphasizes the growing usage of syngas on developing countries which are now the leading market for that and also Middle eastern, African and Asian pacific countries consume two third of global consumption of Syngas. Also due to high rising demand of Chinese market on Syngas for production of methanol , Asia-Pacific had the fastest annual growth of 3.2% within 2007-2013 period [25] which can create significant opportunities for production of Syngas from renewable energy sources. Moreover, because of widely application of Syngas as a fuel in internal combustion engines and an intermediate for the production synthetic natural gas, based on the forecasts the global consumption of Syngas will reach 146 thermal GW by 2020 [25].

Highly increasing demand of Syngas is not only due to increase in the rate of electricity and transport energy consumption and the growth in exploitation of its derivatives but also to avoid emission of greenhouse gases, which makes it a perfect value added product for the renewable energy sector to be exploited more and more.

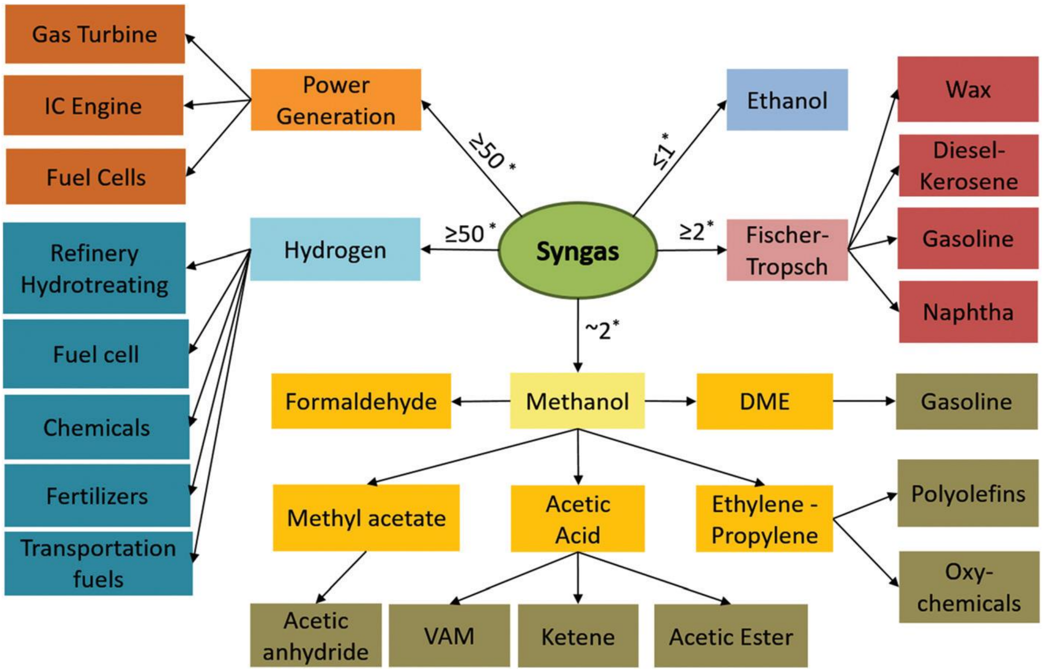

Figure 2. Syngas derivatives (* H_2/CO ratio) reproduced with permission from [1]

1.3 State of the art of electrochemical reduction of Carbon dioxide to Carbon monoxide in heterogeneous catalyst

1.3.1 Thermodynamics of CO_2 reduction

Due to high stability of CO_2 molecule (free Gibbs formation energy ΔG = −394 kJ mol^{-1}) high amount of energy required to change it into value added products. Below (Table 1) there is a list of the free Gibbs energies and the standard Nernst potentials (at 1 bar, 25 °C, pH = 7) for such products. Also, the effect of variation of temperature on the redox potential can be calculated by Gibbs-Helmholtz equation as follows:

$$E(T) = \frac{-\Delta G}{nF} = -\frac{(\Delta H(T) - T\Delta S(T))}{nF} \qquad (1)$$

Where G is the Gibbs free energy, H is the enthalpy and S in entropy.

Due to low contribution of entropy in room temperature, the term (–TΔS) is negligible and the effect of thermodynamic feasibility is being considered through the term ΔH [26]. As can be seen in the table (1) the standard potential of CO_2 reduction to the products is not so high except for the production of CO_2^- radical which is considered to be the necessary intermediate for major products like CO, formic acid and methane, in another word the rate determining step for CO_2 reduction to these products. Apart from production of RDS radical in CO_2 reduction, the kinetic barriers of multi-electron transport plays a key role on high over potentials and restrictions on the reaction. This can push or in some cases replace the reduction of CO_2 reduction in aqueous electrolyte toward Hydrogen Evolution Reaction (HER) which is kinetically more favourable [27].

Theoretically in aqueous electrolyte CO_2 can be reduced to CO, formic acid and methanol, considering standard water oxidation in anode at E^0 =1.23 V vs NHE , by applying minimum cell potential of 1.47 to 1.94 V but due to the reasons mentioned earlier, higher potentials need to be applied to overcome the thermodynamic barriers which called overpotentials to initiate CO_2 reduction [28]. To be more precise the definition of overpotential is the difference between the thermodynamic potential needs for a half reaction to occur and the applied potential, which needed for the reaction to occur experimentally [29]. The major causes of this overpotential can be listed as 1) the activation energy needed for electron transport 2) ohmic loss due to conductivity of the means between electrodes 3) mass transport restrictions. Among the CO_2 reduction products, CO is the most thermodynamically favored one since it requires only two electrons and presents a lower Nernst standard potential with respect to formic acid as the next rival. As has been demonstrated in Figure 3 the overpotential of CO production can vary from few mV to 3V depending on experimental conditions in which CO_2 reduction occurred, from using different catalysts to different setup configuration and different electrolytes. The details of these parameters in each experiment are being summed up in section 4.

Table 1. The standard ΔG° (25°C; pH = 0) and standard Nernst potentials (E°) at 25 °C, 1 bar, pH=7[30]

Reaction	ΔG^0 (kJ/mol)	E^0 (V vs. SHE)
$CO_2 + 2H^+ + 2e^- \rightarrow CO + H_2O$	19.9	-0.53
$CO_2 + 2H^+ + 2e^- \rightarrow HCOOH$	38.4	-0.61
$CO_2 + 4H^+ + 4e^- \rightarrow H_2CO + H_2O$	27.5	-0.48
$CO_2 + 8H^+ + 8e^- \rightarrow CH_4 + 2H_2O$	-130.8	-0.38
$CO_2 + 6H^+ + 6e^- \rightarrow CH_3OH + H_2O$	-17.3	-0.24
$CO_2 + e^- \rightarrow {CO_2}^{\circ -}$	183.32	-1.9

1.3.2 Efficiency quantification of the electrodes

One of the most reported parameter to quantify the efficiency of an electrode is current density. It is defined as the electric current per unit of surface of electrode and it’s magnitude is the electric current per cross-sectional area at a given point in space and applied potential [31]. So more current density means more electron has passed through the surface of the electrode and being consumed for that specific reaction. In Figure 3 current density according to the applied potentials has been demonstrated. In this chart, higher the current density better is the performance of the electrode and on the other hand, lower the applied potentials means lower overpotentials and more efficient the system is.

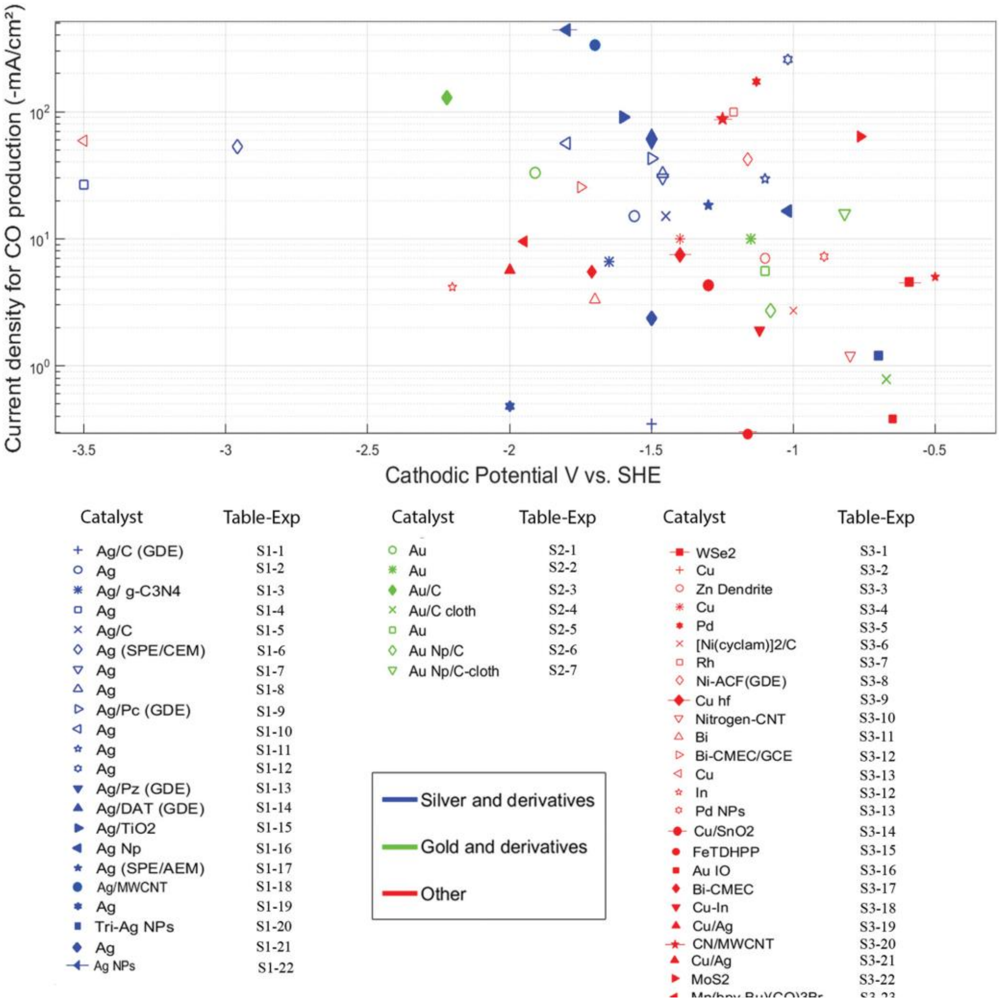

Figure 3.Maximum cathodic current densities vs. cathodic potential for CO_2 electrochemical reduction to CO (as main C-based product).The details of each experiment can be find in details in [1]. Reproduced with the permission from [1].

In addition, in most of the cases apart from the desired product in CO_2 reduction , other product(*e.g.* CO, CH_4 , *etc*) and side products(*e.g* H_2) might be produced. In order to quantify the selectivity of the electrocatalyst toward the desired product and the yield of the reaction the term Faradaic Efficiency (FE) has been introduced. FE is defined as the ratio of coulombs required to form a certain amount of product to the total charge over a specific time interval[1]. FE calculation for CO as the desired product can be calculated as below:

$$\text{FE} = \frac{2 \cdot F \cdot mol\ CO\ produced}{j \cdot A \cdot t} \qquad (2)$$

where F is the faraday constant (96485.33 s A/mol), j is the current density (A/m^2), A is the area of the electrode (m^2), and t is the reaction time (s).

Theoretically the sum of FE of all products should be 100% to be able to close the mass balance cycle during the reaction but in many papers the sum of FEs of the products are more than 100% and many other works they only report the FEs for CO without giving details on the other products.

Another important parameter which defines the practical applicability of a specific electrocatalyst is Production rate (PR). The CO production rate at a given applied potential can be calculated as follows [1]:

$$\text{PR} = \frac{j \cdot FE}{2 \cdot F} \qquad (3)$$

In most of the research this parameter is not being reported due to loss of activity or selectivity of the electrocatalyst during the reaction but for practical implementation it is necessary to be calculated after long lasting experiments.

1.3.3 Reaction mechanism

The major kinetical barrier for CO_2 reduction is to find a catalyst which is able to break the symmetric bond of C-O and form C-H bond in another word be able to do proton-coupled transfer [32].

As can be seen in Figure 4 each metal electrodes used for electrocatalytic reduction of CO_2 is selective toward a specific product. As mentioned before changing the symmetry molecule of CO_2 to form a nonlinear radical of $CO_2^{\cdot-}$ is an initial step toward electroreduction of CO_2 which causes significant overpotentials

[30]. The importance of this rate determining step is that its coordination can determine the possibility of $2e^-$ reduction toward CO or formate [4]. Due to high energy demand of interaction of $CO_2^{-\cdot}$ radical in aqueous (-2.21 vs. SCE), other subsequent reaction to form other derivatives for CO_2 reduction considered to be instantaneous [2, 33]. That is why its stabilization considered to be crucial for efficiency and production rate of the desired product.

Recently J.P. Jones *et al.* [2] divided the electrocatalysts for CO_2 reduction in three groups (Figure 4), based on their ability to: a) coordinate the $CO_2^{\bullet -}$ intermediate; b) reduce CO. Group 1 consists of metals like Sn, Pb, Hg, In and Cd. These metals in this report considered to neither bind the $CO_2^{-\cdot}$ Intermediate nor reduce CO thus formate (formic acid) is the main product of this group of metals. Next group which is constituted of metals like Au, Ag, Ga and Zn claimed to be able to bind $CO_2^{-\cdot}$ and cannot reduce CO which results in CO formation as the main product [34].

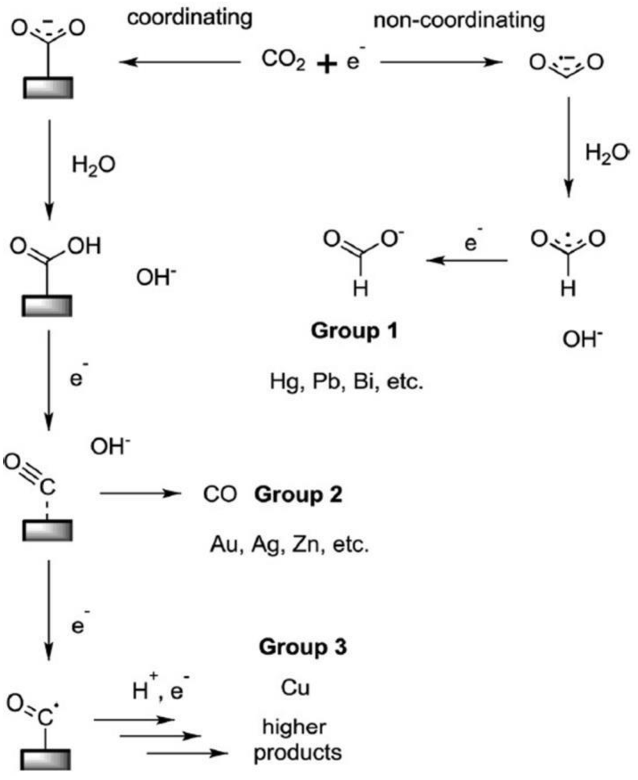

Figure 4.Mechanism for electrochemical CO_2 reduction on metal surfaces in presence of water. Reproduced with permission from [2]

As an alternative to the above systems, application of ionic liquids (usually N-containing salts) gains a lot of attention. The target is to manipulate the above-mentioned mechanism to increase the stabilization of intermediates and also increasing the amount of available dissolved CO_2 for electro reduction. The role of ionic liquid is to decrease the overpotential of the reaction by complexation among the weak bond of CO_2 and the anion in the ionic liquid (*e.g.* BF_4^- , PF_6^-) [35, 36]. In Figure 5 a simplified mechanism of interaction between a commonly used anion of a ionic liquid (BF_4^-) and slightly bent molecule of CO_2 which causes a decrease in radical formation for the subsequent reactions. In most of non-aqueous systems CO is the main product in comparison with other products which need C-H bonding. However, in some cases adding some aqueous electrolyte can decrease the viscosity and conductivity of electrolyte and also by suppressing HER the ratio of CO to H_2 can be manipulated.

Figure 5. Schematic interaction between CO_2 and BF_4^- . Reproduced with permission from [2]

1.4 Syngas production

Syngas consists of CO and H_2 both of which considered to be major products in aqueous electrolyte due to very similar standard potential reaction (*i.e.* -0.41 V and -0.54 V *vs* NHE at pH 7.0 for H_2 and CO production, respectively). Hence, in water based media the production of H_2 is somehow inevitable but the catalysts and operational conditions can play a key role on adjusting the ratio between CO and H_2.The focus of major recent works in this era is the development of appropriate catalyst for selective CO production. The basic challenges to overcome are a) high selectivity toward CO in comparison with other possible products b) a sufficient rate of production and high current density c) the stability of the performance of the catalyst over the time. Different metal catalyst which has been used so far for this purpose is discussed in the following sub-sessions.

1.4.1 CO production

The most famous metal electrocatalyst for reduction of CO_2 to CO are Au and Ag due to their ability on bonding $CO_2^{-\cdot}$ and inability to produce other side products. The cost of these noble metals is the main problem so using them in nanostructured way to reduce the metal loading and increase the conversion rate is one logical solution to this issue. Another solution is to use co-catalysts and support materials to increase the stability of the catalyst nano particles and to enhance conductivity and mass transport [37, 38]. Also, in some reports, co-catalysts have been used to decrease the overpotential of the reaction [3]. Other materials also have been used as electrocatalyst for CO production to substitute noble metals. In the following sections a thorough investigation on the major works in this era has been presented and categorized based on the type of catalyst.

1.4.1.1 Ag based catalysts

Silver is considered to be a favourite catalyst due to its fairly high performance and lower cost in comparison with other noble metals like Gold or Platinum. The metallic surface of Ag showed to have a good selectivity toward reduction CO_2 to CO [3, 39-41] with lower overpotential than many other metallic surfaces [42]. Table 2 summarizes the major works with their experimental details. It is noteworthy that the current density reported in this table is according to total current density and does not take in to account for a specific product. Therefore, to illustrate the result in a more comparable way in Figure 6 the FE and current density for CO production has been demonstrated.

Major drawbacks of using Ag are its high cost compared to other abundant element (i.e. Mn, Ni, Co, Fe) and its high overpotential in bulk form (Ag foil). To tackle this issue, using Ag in its nanoparticle form and also application of co-catalyst to achieve high-performance electro-catalyst with efficiently used surface area are being introduced. Lu *et. al.*[42] developed a de-alloying process to synthesize a nano-porous Ag catalyst with a monolithic structure and highly curved inner surfaces. They achieved a current density of 18 $mAcm^{-2}$ at 500 mV of overpotential and 92 % of faradaic efficiency under atmospheric pressure conditions. In another interesting work Liu *et. al.* [43] used a pre-dominant shape dependent electrocatalytic reduction of CO_2 to CO on triangular silver (Tri-Ag) nanoplates which result in high FE (96.7%) and energy efficiency (61.7%) with low current density and as a result low production rate.

Table 2. Detailed conditions and results achieved on experiments made with Ag-based electrodes for the CO_2 reduction to C (as main C-based product). Reproduced with permission from [1]

EXP. NR	Cathodic Potential (V *vs.* NHE)	Electro-catalyst	Electrode size (cm²)	Ag loading (wt %)	FE (%)	Current density ǂ (-mA/cm²)	Catholyte	Anolyte	Test time (h)	Ref.
1	-1.5	Ag/C (GDE)	N/A	60	7	5	1 M KOH	1 M KOH	N/A	[44]
2	-1.56	Ag	1	-	30	50	0.5 M $KHCO_3$	0.5 M $KHCO_3$	2	[4]
3	-1.65	Ag/ g-C_3N_4	6.25	40	33	20	0.1 M KH_2PO_4 / K_2HPO_4	0.1 M KH_2PO_4 / K_2HPO_4	20	[45]
4	-3.5	Ag	N/A	-	33	80	0.2 M $KHCO_3$	KOH	7	[5]
5	-1.45	Ag/C	1	-	30	50	0.5 M $KHCO_3$	0.1 M KOH	8	
6	-2.96	Ag (SPE/CEM)	0.2	-	52.7	100	0.2 M K_2SO_4	0.2 M K_2SO_4	2	[40]
7	-1.46	Ag	N/A	-	60	50	0.5 M $KHCO_3$	KOH	7	[5]
8	-1.46	Ag	N/A	-	64.6	50	0.2 M K_2SO_4	0.2 M K_2SO_4	2	[40]
9	-1.5	Ag/Pc (GDE)	N/A	6.25	78	55	1 M KOH	1 M KOH	N/A	[44]
10	-1.8	Ag	N/A	-	80	70	0.5 or 0.8M K_2SO_4	2.5M KOH	1.5h	[9]
11	-1.1	Ag	N/A	-	84	35	1 M $KHCO_3$	1 M $KHCO_3$	1	[46]
12	-1.02	Ag	1	-	86	300	0.5 M $KHCO_3$ (20 atm)	0.5M $KHCO_3$	N/A	[47]
13	-1.5	Ag/Pz (GDE)	N/A	2.51	88	65	1 M KOH	1 M KOH	N/A	[44]
14	-1.5	Ag/DAT (GDE)	N/A	8.62	89	73	1 M KOH	1 M KOH	N/A	[44]
15	-1.6	Ag/TiO_2	0.09	40	90	101	1M KOH	1M KOH	N/A	[3]
16	-1.02	Ag Np	N/A	-	92	18	0.5 M $KHCO_3$		N/A	[42],[48]
17	-1.3	Ag (SPE/AEM)	0.2	-	92.3	20	0.2 M K_2SO_4	0.2 M K_2SO_4	2	[40]
18	-1.7	Ag/MWCNT	-	-	95	350	1M KOH	1M KOH	N/A	[49]
19	-2	Ag	1.5	-	96	0.5	18 mol% EMIN-BF_4 in H_2O	100mM H_2SO_4	0-7	[36]
20	-0.7	Tri-Ag NPs	0.785	-	96	1.25	0.1 M $KHCO_3$	0.1 M $KHCO_3$	168	[43]
21	-1.5	Ag	1.6	-	99	2.4	BMImCl with 20wt% H_2O	BMImCl with 20 wt% H_2O	10	[39]
22	-1.9	Ag NPs on GDE	10	-	100	440	3M KOH	3M KOH	N/A	[6]

ǂ Total current density not considering the selectivity toward any product.

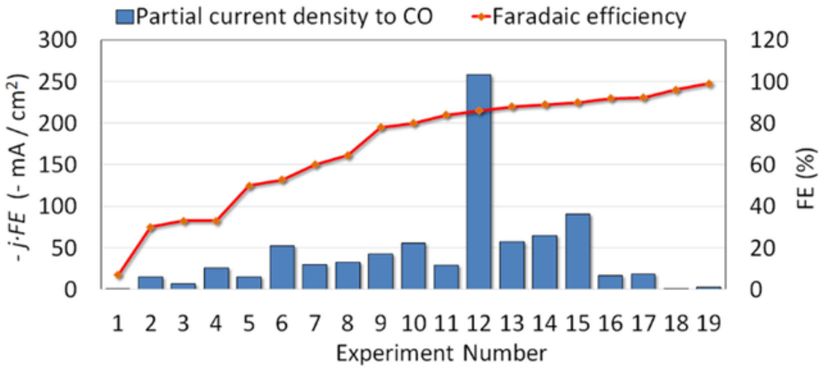

Figure 6.Current densities and Faradaic efficiencies related to the CO production from the electrochemical reduction of CO_2 for Ag based electrodes Reproduced with permission from [1]

Using different substrates is also of a great interest in recent works. The most frequently used substrate is TiO_2 because of its application to be used as a co-catalyst for photo-electro reduction of CO_2[50-52].In an interesting work, Ma *et. al.* [3] synthesized Ag nanoparticles on TiO_2 support to investigate the role of TiO_2 on electro catalytic reduction of CO_2 to CO. Among different Ag loading which they used, the best results have been achieved by 40% Ag/TiO_2 NPs with FE of 90% and fairly high current density (-101 mA/cm^2). Recently they also have reported a significant enhancement in current density (350 mA/cm2 with 95% FE for CO production)in alkaline electrolyte (1M KOH) at cell potential of -3V by using multi-walled carbon nanotubes (MWCNTs) in the Ag catalyst layer of gas diffusion electrode [49]. To date this result is one of the most promising attempts for CO_2 reduction to CO. In another work Tornow *et. al.* [44] also investigated the application of carbon supported, nitrogen organometallic silver catalyst for CO_2 reduction through addition of an amine ligand to Ag/C. They found that among four different N-based organometallic support for Silver, 3,5-diamino-1,2,4-triazole supported on carbon (AgDAT/C) produced about −70 mA cm^{-2} of current density and almost 90% of Faradaic efficiency for CO production. This way they manage to use lower Ag loading. Sastre et. al. also reported the effect of graphitic carbon nitride as a co-catalyst to nano-structered Silver for syngas production [41]. The highest CO productivity (~ 60 $mmolcm^{-2}h^{-1}$) was achieved by using 40 wt% Ag loading at -1.15 V *vs* RHE.

Moreover, different reactor configuration with Ag based catalyst is also gained attraction. Hori *et. al.* [40] used silver-coated ion-exchange membrane electrodes (solid polymer electrolyte, SPE) and they achieved 53 % of CO faradaic efficiency, with a high overpotential of 2.43 V. Using a pH buffer layer with the aim to adjust the CO/H_2 ratio for a new electrochemical cell configuration has been proposed by Delacourt *et. al.* [5]. The result was current density of 80 mA/cm^2 with CO/H_2 ratio of 2/1 which can be adopted later on for the production of methanol. The only drawback is that they reported a loss of selectivity in long term tests.

It is noteworthy that one of the major challenges in most of the works so far is to maintain the performance and selectivity of the catalyst over the time. But in major part of the reported researches the tests last less than 7 hours. Also, the scale up of these catalysts and reactors are still a challenge. Most of the tests performed with electrodes smaller than 6.25 cm^2. So as a sum up, the problem of scale up and stability of the catalyst remains the major challenge for technological research and development.

1.4.1.2 Au based electrodes

Gold showed to be one of the best electrocatalyst with highest activity and selectivity toward CO production by CO_2 reduction, among the polycrystalline metals [34]. Development of different technics of synthesis of Au nanoparticles helped a lot to increase the reaction rate by controlling active surface area and its morphology. In table 3 the details of the different experiments carried out with Au electrocatalyst in different forms has been presented. Also in Figure 7 the corresponding current densities and FE for CO production is being illustrated.

Usually electrodeposition of metals from counter electrodes like Pt can poison the cathodic parts of electrocatalyst by influencing CO bonding energy on the surface of the cathodic electrode. One of the major advantages of Au nanoparticles (Nps) are their ability to resist the poisoning and maintaining the longevity of the catalyst compare to other noble metals. A significant improvement on the durability of an Au NP electrode compared to bulk gold was observed by Chen *et. al.* [53]. Also they achieved one of the lowest overpotentials (*i.e.* 140 mV, see Figure. 3) so far reported for CO production by using Au NPs in which they reached 78 % of FE but with a low current density of -1 $mAcm^{-2}$. They reduced Au oxide into Au particles with metastable surfaces that accelerated the CO_2 reduction catalysis by stabilizing intermediates in the process. The system stability was proved for a maximum of 8 h [53]. A thorough study of different mono-dispersed Au NPs (of 4, 6, 8 and 10 nm) has been done by Zhu and *et. al.*[28]. They showed that 8 nm Au NPs results in maximum CO faradaic efficiency (up to 90 % at -1.08 V vs. SHE) during the CO_2 electrolysis in 0.5 M $KHCO_3$ at 25 °C.

Table 3. Detailed conditions and results achieved on experiments made with Au-based electrodes for the CO_2 reduction to C (as main C-based product).

Exp. Nr.	**Cathodic Potential (V *vs.* NHE)**	**Electro-catalyst**	**Electrode size (cm²)**	**Au loading (%)**	**FE (%)**	**Current density ǂ (-mA/cm²)**	**Electrolyte**	**Test time (h)**	**Ref.**
1	-1.91	Au	N/A	-	33	100	0.5 M $KHCO_3$	N/A	*[4]*
2	-1.15	Au	N/A	-	50	20	0.5 M $KHCO_3$	N/A	*[34]*
3	-2.22	Au/C	N/A	40	64	200	0.5 M $KHCO_3$	N/A	*[4]*
4	-0.96	Au/CNT	N/A	-	70	10	0.5 M $NaHCO_3$	4	*[54]*
4	-0.67	Au Np/ C cloth	0.6	-	78	1	0.5 M $KHCO_3$	8	*[53]*
5	-1.1	Au	N/A	-	80	7	0.1 M $KHCO_3$	0.5	*[55, 56]*
6	-1.08	Au Np/C	N/A	-	90	3	0.5 M $KHCO_3$	N/A	*[28]*
7	-0.82	Au Np/C-cloth	0.6	-	98	16	0.5 M $KHCO_3$	N/A	*[53]*

ǂ Total current density not considering the selectivity toward any product.

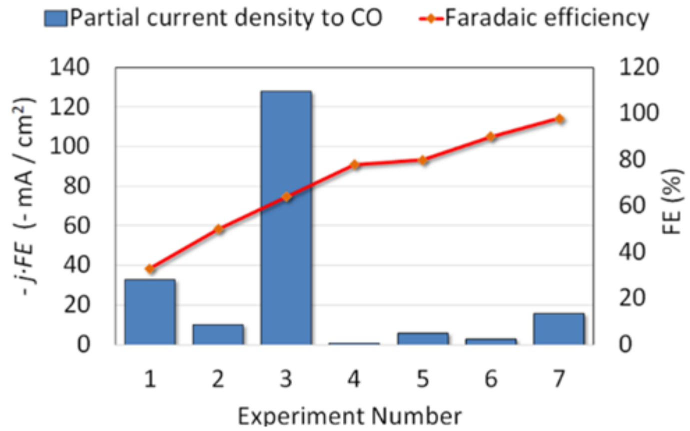

Figure 7 Current densities and Faradaic efficiencies related to the CO production from the electrochemical reduction of CO_2 for Au based electrodes.

In a different approach Delacourt *et. al.* [5] used a buffer layer BL-type cell for studying Au plates and Au NPs dispersed in C-based supports as cathodic electrodes. They demonstrated that by controlling the buffer layer thickness, the passing of the protons from proton exchange membrane (PEM) can be controlled and as a result different ratio of CO/H_2 can be achieved. The best result in this experiment was 128 $mAcm^{-2}$ with a FE of 64 %, although the stability of such systems in long-term tests have not yet been demonstrated.

1.4.1.3 Other systems

High price of noble metals which considered to be the most favorite electrocatalyst for CO_2 reduction to CO, makes the efforts to find other abundant metals with comparable performance to Au and Ag, more significant. In table 4 a summary of different works on variety of more affordable non-noble metals such as Cu, In, Bi, Mn, Fe, Mo, Ni, and Zn, among others, as well as other precious metals like Pd and Rh has been demonstrated. Also an illustrative comparison of their performance can be found in Figure 3 and 8. Evidently high current density (i.e. -172.5 and -99.4 $mAcm^{-2}$) and faradaic efficiency has been achieved by using noble metals like Pd and Rh in high pressure reactors by Hara *et. al.* [47, 57]. In this work which has been made 20 years ago, they studied different electrocatalyts (Co, Rh, Ni, Pd, and Pt) supported in gas diffusion electrodes (GDE) under high pressure (20 bar) and the maximum of -300 mA/cm² and almost 60 % FE for CO production had been achieved.

Among non-noble electrocatalyst for CO_2 reduction, the vast majority of researches on low cost and abundant electrocatalysts have been focused on Cu and Sn. They showed to be highly active for CO_2 reduction but not very selective toward production of CO [58, 59]. In a recent work by Kas *et. al.* using compact Cu hollow fibre as both gas diffuser and cathode leads to comparable results to those achieved by noble metals [60]. The good performance of these hollows can be contributed to a defect-rich porous structure and less mass transport resistance. Tin(Sn) as an electrochemical catalyst for CO_2 reduction is mostly favourable for formate production but in a very recent work by Li *et. al.* thin layer of SnO_2 is coated over Cu nanoparticles the reduction becomes Sn-thickness dependent: the thicker (1.8 nm) shell shows Sn-like activity to generate Formate whereas the thinner (0.8 nm) shell is selective to the formation of CO but with low current densities [61]. Moreover, using Bismuth based electrocatalyst gained lot of attention as a potential substitute for noble metals. In a work by Median-Ramos *et. al.* a Bi-based carbon monoxide evolving catalyst (Bi-CMEC) has been synthesized by an electrodeposition method and it produced CO with 95 % of FE and current density of - 31 $mA\cdot cm^{-2}$ [62].

It is worth mentioning that with the current advances in homogenous catalysts for CO_2 very good results has been achieved for a system with $Ni(cyclam)_2^+$ (cyclam = 1,4,8,11-tetraazacyclotetradecane) [63] or enzymic catalyst of Ni-CODH in which microbial interconversions between CO and CO_2 were catalyzed by carbon monoxide dehydrogenases (CODH) [64, 65]. These interesting works indeed opened up new ways for scale up purposes but still far away from industrialization and commercialization.

Table 4.Detailed conditions and results achieved on experiments made with electrodes different than Ag and Au for the CO_2 reduction to C (as main C-based product).Reproduced with permission from [1]

Exp. Nr.	Cathodic Potential (V *vs.* NHE)	Electrocatalyst	Electrode size (cm²)	FE (%)	Current density ǂ (-mA/cm²)	Electrolyte	Test time (h)	Ref.
1	-0.59	WSe_2	N/A	24	18.95	$EMIMBF_4$	27	[66]

2	-1.4	Cu	0.002	38.1	20	BmimPF_6	N/A	[67]
3	-1.1	Zn Dendrite	N/A	50	14	0.5 M $NaHCO_3$	3	[68]
4	-1.4	Cu	N/A	50	20	Bmim-PF_6	N/A	[67]
5	-1.13	Pd	N/A	57.5	300	20 atm	N/A	[47]
6	-1	[Ni(cyclam)]$_2$/C	N/A	60	4.5	0.1 M KNO_3 pH 4.1	3.5	[63, 69]
7	-1.21	Rh	N/A	61	163	30 atm	N/A	[57]
8	-1.16	Ni-ACF(GDE)	0.49	67	63	0.5 M $KHCO_3$, 20 atm	N/A	[70]
9	-1.4	Cu hf		75	10	0.3 M $KHCO_3$	24	[60]
10	-0.8	Nitrogen-CNT	N/A	80	1.5	0.1 M $KHCO_3$	10	[71]
11	-1.7	Bi	0.3	81	4.1	MeCN containing 100 mM [BMIM]OTf	8	[72]
12	-1.75	Bi-CMEC/GCE	0.3	82	31	[BMIM]PF_6(MeCN solvent)	3	[62]
13	-3.5	Cu	3	84	70	MeOH	N/A	[73]
14	-2.2	In	N/A	85.3	4.9	Propylene Carbonate	N/A	[74]
15	-0.89	Pd NPs	1	90	8	0.1 M $KHCO_3$	N/A	[75]
16	-1.3	Cu/SnO_2		93	4.6	0.3 M $KHCO_3$		[61]
17	-1.16	FeTDHPP	N/A	94	0.31	DMF 0.1 M n-Bu_4NPF_6, H_2O	4	[76]
18	-0.65	Au IO (inverse opal)	N/A	95	0.4	0.1 M $KHCO_3$	3.5	[77]
19	-1.71	Bi-CMEC	0.3	95	5.8	Bmim-BF_4 in MeCN	12	[78]
20	-1.12	Cu-In	N/A	95	2	0.1 M $KHCO_3$	7	[79]
21	-2	Cu/Ag	1.6	98	5.8	EMIMBF_4+ BMIMNO_3 with CoCl2	150	[80]
22	-1.25	CN/MWCNT		98	90	KCl	N/A	[81]
23	-0.764	MoS_2	N/A	98	65	4 mol% EMIM-BF_4 in H_2O	10	[82]
24	-1.95	Mn(bpy-Bu)$(CO)_3$Br	N/A	100	9.5	1.4 M CF_3CH_2OH/MeCN	0.5	[83]

25	-0.5	Ni-CODH	N/A	100	5	0.1 M Phosphate	N/A	[64, 84]

ǂ Total current density not considering the selectivity toward any product.

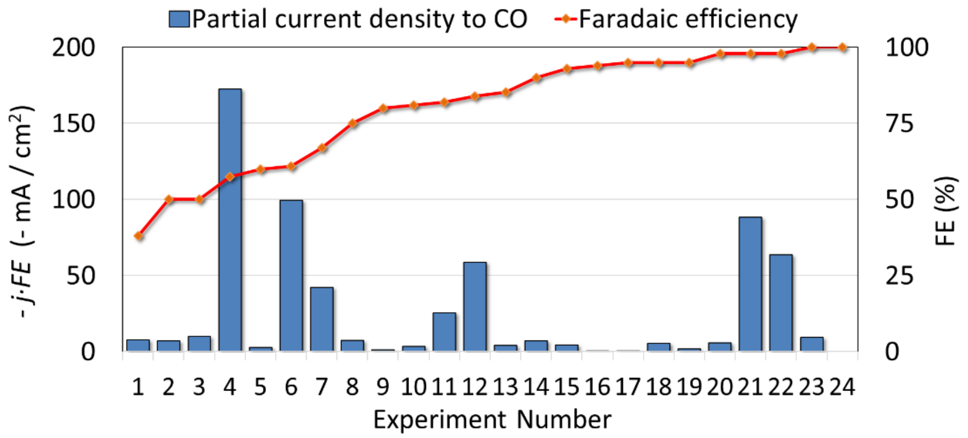

Figure 8. Faradaic efficiency and current density for the CO production in systems using electrodes different than Ag or Au. Reproduced by permission form [1]

1.4.2 H_2 production

Another content of Syngas is Hydrogen. Thus, considering the kinetics of Hydrogen Evolution Reaction (HER) by knowing the catalysts that improve the rate and efficiency of HER is of the essence for combining HER and CO_2 reduction. Further, a brief description of catalyst for HER and different system has been discussed.

1.4.2.1 Alloyed Catalyst

During the last decade investigation on several elements like Cu, Au, Pd, Rh, Fe [85-87], Ni [86, 88, 89], RuO_2 [90, 91] has been done. These efforts emphasized that coated alloys show better performance and lower overpotentials. The increase of the surface area of cathode is the key parameter of the coating for decreasing overpotential [92]. Coatings are applied using one of the four following techniques i) plasma or thermal spraying, ii) thermal decomposition, iii) electroplating including electrodes deposition, and iv) in-situ activation. Electrodeposition may be performed either in one- or in multistep deposition [93].

1.4.2.2 Fe based

A considerable surface area of Fe-Mo alloys will cause a high rate hydrogen evolution [94]. The experiments on electrodeposited Fe-Mo alloys showed an overpotential drop of 0.15-0.3 V for HER as compared to mild steel in a simulated commercial electrolyte for chlorate production[95]. Rosalbino *et. al.* [96] followed the studies of the HER on crystalline alloys with the composition $Fe_{90}R_{10}$ where R = Ce, Sm, Y and Mm (mischmetal) in 1 M NaOH solution at 25 C. The evaluation of electrocatalytic efficiency was obtained to be better for $Fe_{90}Ce_{10}$ and $Fe_{90}Mm_{10}$ than for $Fe_{90}Y_{10}$ and $Fe_{90}Sm_{10}$, essentially because of the synergetic composition effects of these alloys [92]. Rosalbino *et. al.* published the results of the other researches on electrocatalytic activity efficiency for some other crystalline alloys containing Fe-Zn-R [R =rare earth metals; La, Y, Gd and mischmetal] in the presence of 1M NaOH solution at 25 C [97]. They also concluded that the multiphase microstructure of alloys promotes the hydrogen adsorption leading to the increase of kinetics of hydrogen evolution on electrode surface.

1.4.2.3 Co and Ni based

Interesting properties of Co-Mo alloys such as high melting point, good corrosion resistance and high efficiency hydrogen evolution make it a center of attention for recent researches in this area [98-103]. A Co-Mo coating on titanium and steel substrate has been done by Spasojevic *et. al.* [103]. They reported a highly catalytic activity of this alloy for HER. Subramania *et. al.* on the hand studied the influence of variation of current density, pH and temperature on molybdenum content in Co-Mo alloy and they succeeded to reach 40 mA/cm² of current density with 50% of Mo content [104]. Ni and its alloys or its composites are the most investigated materials for HER electrode applications [92]. The most interesting property of Ni is its resistance toward alkaline solutions [105]. Low catalytic activity of Ni make the researchers to alter its structure by active carbon fiber [70] or alloyed with different metals or metal oxide like MoO_2, MoO_3 [106-108] , W [109, 110] , Fe [111, 112], Mo, Cr, Pd [113].

Arul Raj *et. al.* [114] obtained the HER with over-potential (0.187 V) for their best ternary cathode; Ni-Fe-Mo similar to the best binary cathode of Ni-Mo, over 1500 h of continuous electrolysis in typical industrial conditions. Moreover, Shervedani *et. al.* [93] studied the electrocatalytic activities in an alkaline solution of nickel-phosphorous- graphite (Ni-P-C_g) and found good electrochemical stabilities and a high electrocatalytic activity for this alloy as compared with Ni-P and Ni electrodes. In a recent study, McCrory *et al.*[11] benchmarked 18 HER electro-catalysts for evaluating their activity under acid (1M H_2SO_4) or basic conditions (1M NaOH). As can be seen in Figure 9, several non-noble metals based HER catalysts has been tested that were able to operate at -10 $mAcm^{-2}$ with overpotentials < 0.1 V in acidic and/or alkaline solutions.

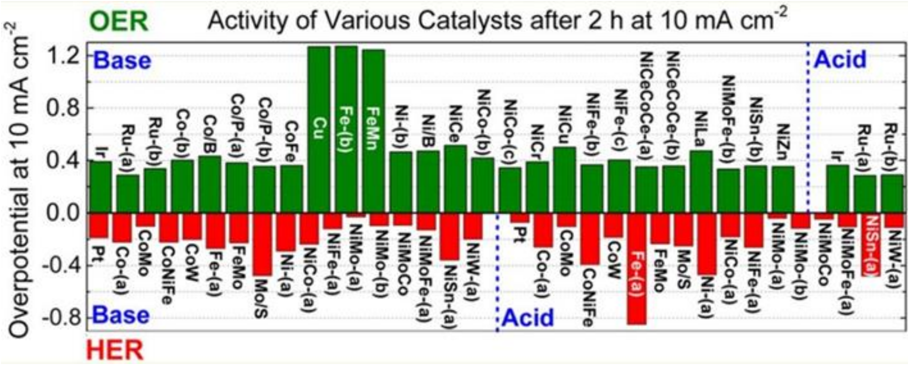

Figure 9. Benchmarking of Hydrogen Evolving Reaction and Oxygen Evolving Reaction Electro-catalysts. Reprinted with permission from [11]

1.4.2.4 Au based

Gold (Au) is the most favorable noble metal for HER due to its properties of being catalytically active and quite stable in acid medium [115-120]. Xu [121] investigated hydrogen evolution in single crystal gold electrode. This electrode was used as a substrate to investigate the influence of some organics on hydrogen evolution process. The kinetics of hydrogen evolution on gold electrode has been described by Khanova *et. al.* [122] as a barrierless discharge. In this study, they have obtained the polarization curves consisting of two linear segments with Tafel slopes 0.06 V at lower overpotentials and 0.12 V at the higher ones. In another report, Smiljanic *et. al.* [123] used bimetallic surfaces of Au/Pd in alkaline solution. In this study Pd/Au(1 1 1) electrodes have shown a significant catalytic activity toward hydrogen evolution reaction in 0.1 M NaOH solution with respect to the pure Au(1 1 1) surface, where HER occurs at very high overpotential. Electrocatalysis of the HER in acid and alkaline media by Cu, Ag, Au, Pt, Ru, Ir and Ti electrodes has been described by Danilevoc *et. al.* [124].This study proposed that due to coverage by spectator species, even in the HER potential region, it is still questionable if it would be possible to establish experimentally a true relationships between M–H_{ad} (M = Cu, Ag, Au, Pt, Ru, Ir and Ti) energetics and catalytic activity , therefore, with the exception of Pt, Ir and Au, the experimentally established positions of the other metal catalysts in the observed volcano relations are uncertain over the entire pH range [124]. Hydrogen has been proposed as the green fuel of the future in the wake of depleting fossil fuels. Recently, carbon paste electrodes (CPE) modified with nanomaterials as electrocatalysts have drawn wide attention for hydrogen evolution reaction (HER) in acid medium [125]. Siddhardha *et. al*. [126] modified CPE with novel gold composites as electro-catalysts for HER in acid medium. The nanocomposites have shown ~100 fold increased current density than unmodified CPE at -0.3 V.

1.5 Factors influencing the process of Carbon Dioxide reduction to Carbon Monoxide

Different parameters can affect the performance of CO_2 reduction to CO. The logic for many research works is that to adjust different parameters (*i.e.* reactor configuration, electrode material, electrolyte, pressure, temperature, *etc.*) to enhance the performance toward the desired products. Although many thorough studies has been done so far, yet the trend of combination of the above mentioned parameters is not clear. In the following sub-sessions, the effect of each parameter on electrocatalytic reduction of CO_2 to CO is being discussed.

1.5.1 Electrochemical reactor configuration

The electrochemical *reactor configuration* is a determining factor and strongly affects the results, especially the global current density. Therefore, the variety of different designs makes the results obtained in different setups, not completely comparable. However, in this session the most promising concepts in reactor design are being discussed. A summary of different reactor configurations is illustrated in Figure 10.

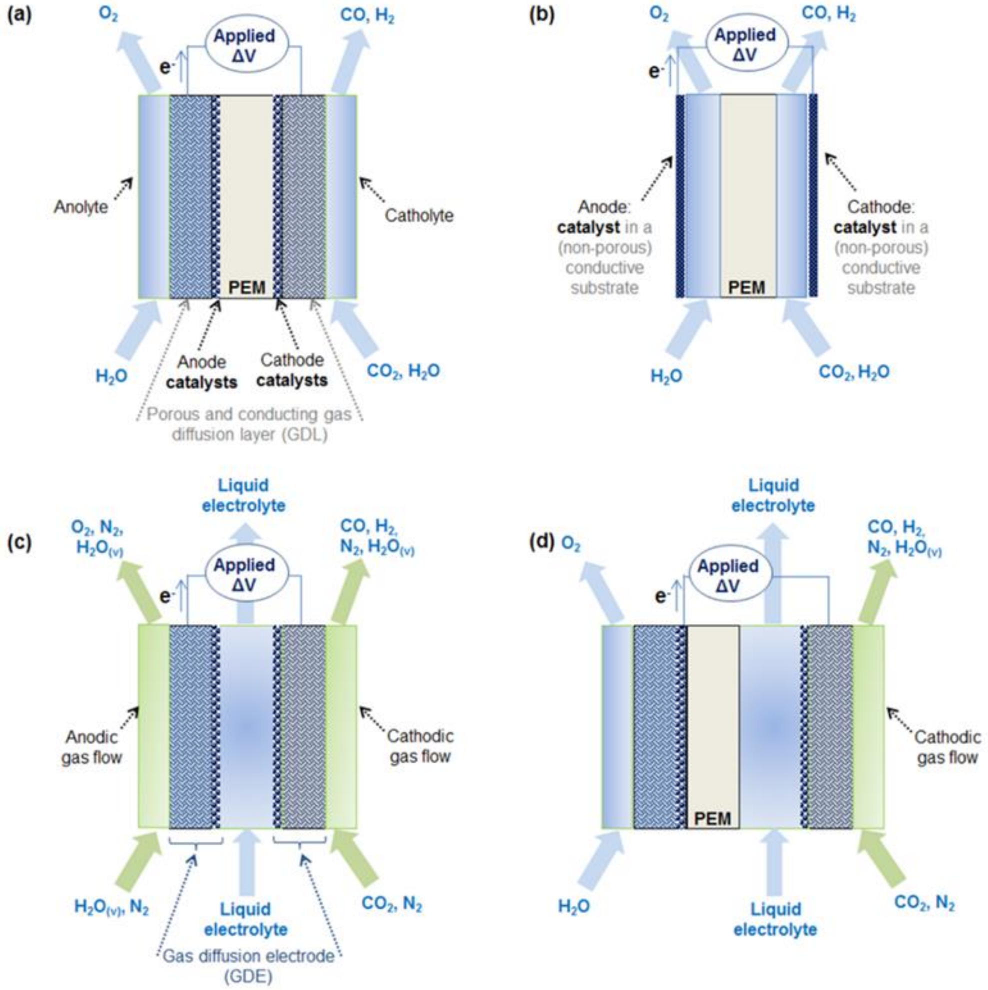

Figure 10. Schemes of some interesting reactor configurations used to reduce CO2 to CO: (a) use of gas diffusion layers (GDL) and a PEM with liquid streams; (b) use of conductive non-porous substrates and a PEM between liquid catholyte and anolyte with liquid streams; (c) use of gas diffusion electrodes (GDE) separated by a liquid electrolyte, gas feeds; (d) use of both a PEM and a liquid electrolyte between GDE, liquid anodic feed and gaseous cathodic feed. Reproduced with permission from [1]

The most common configuration of reactor is a two compartment cell reactor in which two parts are separated by a PEM membrane, very similar to a PEM fuel cell configuration (Figure 10a). In this configuration the electrodes are either deposited on PEM membrane [40] or the catalyst can be coated on a Gas Diffusion layer (GDL) which is conductive and permeable [127]. The major constraints in this type of configurations are the product crossovers in both compartments and also selective ion transportation considering the possible difference of pH on each side. [12]. A common choice for membranes in this configuration is Cation Exchange Membrane (CEM) which allows the H^+ ions which are produced in anode as a product of oxidation of water and also other protons like K^+ from the anolyte to transfer from anodic compartment to cathodic one. It is worth mentioning that in this configuration in anodic part which Oxygen Evolution Reaction (OER) is taking place the acidic ambient is more favored and to achieve high efficiency of OER noble electrodes are needed [11] (Figure 9).

Another option is to use Anodic Exchange Membrane (AEM) in order to allow the diffusion of OH^-, HCO_3^- and CO_3^{2-} ions, typically when basic electrolytes (*e.g.* bicarbonate) are used in the cathodic chamber [40]. The major consequence of application of AEM is lower anodic efficiency and higher crossover of anionic products like Methanol and Formate [12]. In a quasi-neutral solution (e.g. K_2SO_4), using CEM or AEM can have some restrictions due to formation of OH^- ions in aqueous media during the electrocatalytic reduction as follows:

$$CO_2 + H_2O \quad + 2e^- \rightarrow CO + 2OH^- \qquad (5)$$

OH^- will interact with dissolved CO_2 and results in formation of HCO_3^- or CO_3^{-2} and with presence of metallic cations like K^+, $KHCO_3$ or K_2CO_3 is formed at the metal-membrane interface. This accumulation of these ions can peel of the metals form the membrane and deactivate the surface of the catalyst. Also, CEM membranes are better to be used in acidic ambient which then as a result of H^+ ions HER is more favourable and CO_2 reduction will be supressed but instead on an AEM both OH^- and CO_3^{2-} can be easily eliminated from the metal-membrane interface due to their mobility within the membrane and, thus, the CO_2 reduction reaction is favoured [1]. Another proposed configuration is again a two-compartment cell but with electrodes immersed into electrolyte (Figure 10b) in which electroactive surfaces of catalysts supported on not porous nor water permeable materials. As an example Kuhl and co-workers were able to to optimize the efficiency of the reactor by minimizing ohmic losses with characterizing it by a geometry that maximize the cathode exposed area vs. the catholyte volume, *i.e.* 4.5 cm^2 *vs* 8 ml (Figure 11a) [13]. In another work Hatsukade *et. al.* reduced CO_2 to CO as a major product along with Formic acid, Methanol , Ethanol and Methane on metallic Silver in a similar configuration of reactor (Figure 11b) [46]. They also reported the reaction rate of CO_2 vs. potential by which they concluded that at potentials more negative than - 1.1 V *vs* RHE the reaction is limited by mass transport rather than that by kinetics control. A novel configuration of reactor to overcome the problems which occurs by using CEM and AEM membrane is being proposed by Kenis *et. al.* which its scheme can be seen in Figure 10c [16, 71]. In

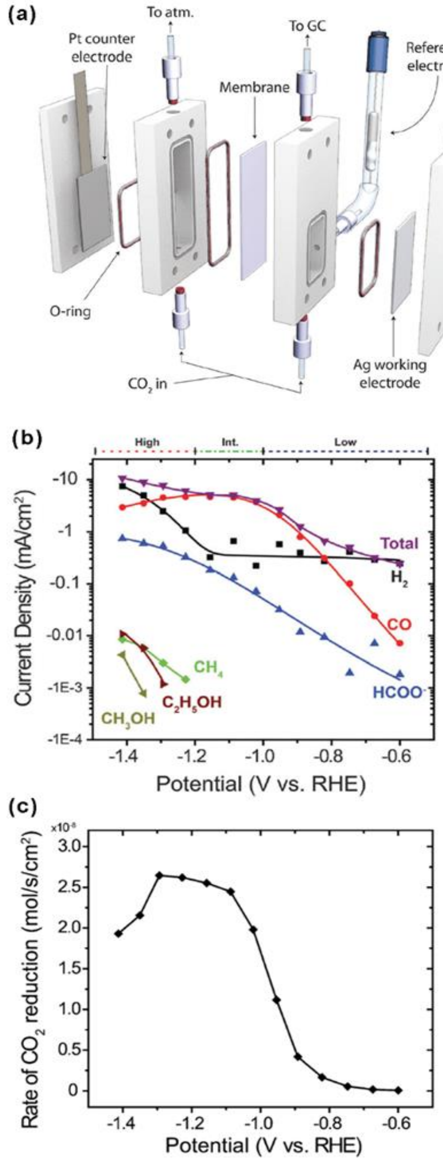

Figure 11. a) A schematic view of the electrochemical cell reported by Jaramillo and co-workers, b) Tafel plot of the partial current density corresponding to each product of the CO_2 reduction on Ag surface and c) Total rate of CO_2 reduction as a function of potential. Reproduced and adapted from [13].

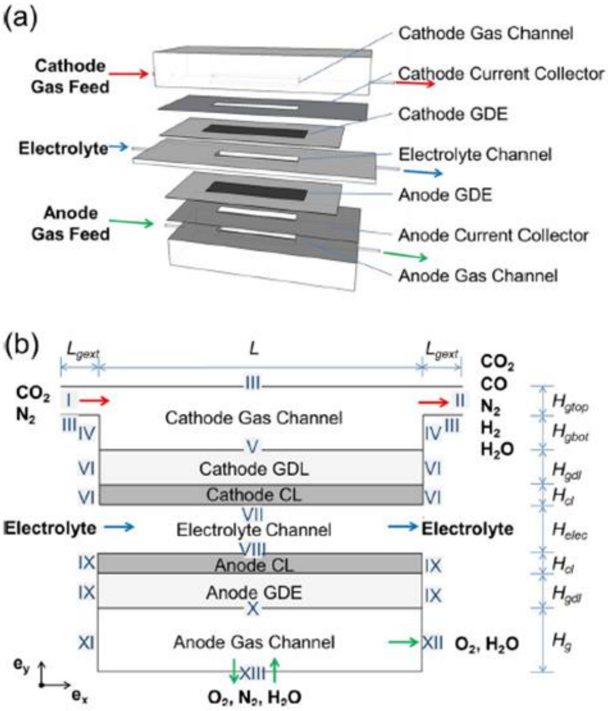

Figure 12. A schematic view of the microfluidic cell reported by Wu et al. for the CO_2 reduction to CO with details of: a) various functional layers and b) a simplified schematic used in modelling. Reproduced from [16].

this configuration gas diffusion electrode (GDE) has been used to directly introduce gaseous CO_2 as reactant to the cathode surface, with the advantage of increase the selectivity toward the CO_2 conversion. This reactor consists of different layers and active sides of both anode and cathode are in a continuous contact with the electrolyte which are passing through the layers (see Figure.12). The main advantage of such system is that different parameters like CO_2 concentration of the feed and feed flow rates, porosity of GDEs, channel length and also electrolyte contact time can be modified and studied to find out the effect of each parameter on CO_2 reduction to syngas. The illustrated configuration of Figure.10d has been proposed by Delacourt *et. al.* [4, 5] and Dufek *et. al*. [17] in which an electrolyte is being used as a medium between cathodic side and the PEM. By this configuration the passage of H^+ ions can be controlled by a buffer layer. As a result, by controlling HER, CO/H_2 ratio can be adjusted (Figure 13).

One of the most recent technologies in reactor configuration is adoption of bipolar membrane combined with GDLs or GDEs. These kinds of membranes are consisting of two laminated layers of cation and anion exchange membrane often with a catalyst in between to promote water dissociation at the interface. The goal is to made the protons and hydroxides to move toward the respective electrode [12]. In a report by Li *et. al*. [12] a CO_2 electrolyzer system, based on a commercial BPM with an alkaline NiFeOx OER catalyst, was studied with both Ag/aqueous bicarbonate and BiOx/ionic liquid/gasphase CO_2 catalyst/catholyte compositions[1] (Figure 13b). The onset potential for CO_2 reduction by Ag catalyst was -1.05 V vs. Ag/AgCl with -30 mA cm^{-2} of current density at -1.5 V in an electrolyte of $KHCO_3$. The result of the comparison of BPM membrane with two other commercially membranes of CEM and AEM showed a shift of -0.6V when using BPM because of the additional thermodynamic driving force required by the cell by acid−base neutralization and a loss of ∼300 mV occurs in the BPM cell because of the reaction of protons with HCO_3^- ions [12]. The drawback for CEM and AEM membranes are still their instability toward alkaline or acidic ambient which can be occurred during the reduction of CO_2 by migration of H^+ or OH^- ions and pH change in cathode and anode side are inevitable. On the other hand, BPM membranes showed to be more stable due to dissociation of water which drove the H^+ and OH^- ions toward cathode and anode, respectively.

A major challenge in this era is the scale up process of the above-mentioned configurations. So far, the major researches dealt with laboratory scales and few works reported the scale up procedure for these processes. For instance, Oloman *et. al*. [128] achieved the current density of 0.6 and 3.1 kA m^{-2} with applied cell potential of -2.7 to -4.45 V for Formate production with FE of 63 to 91 % for a scale up from 45 to 320 cm^2 respectively.

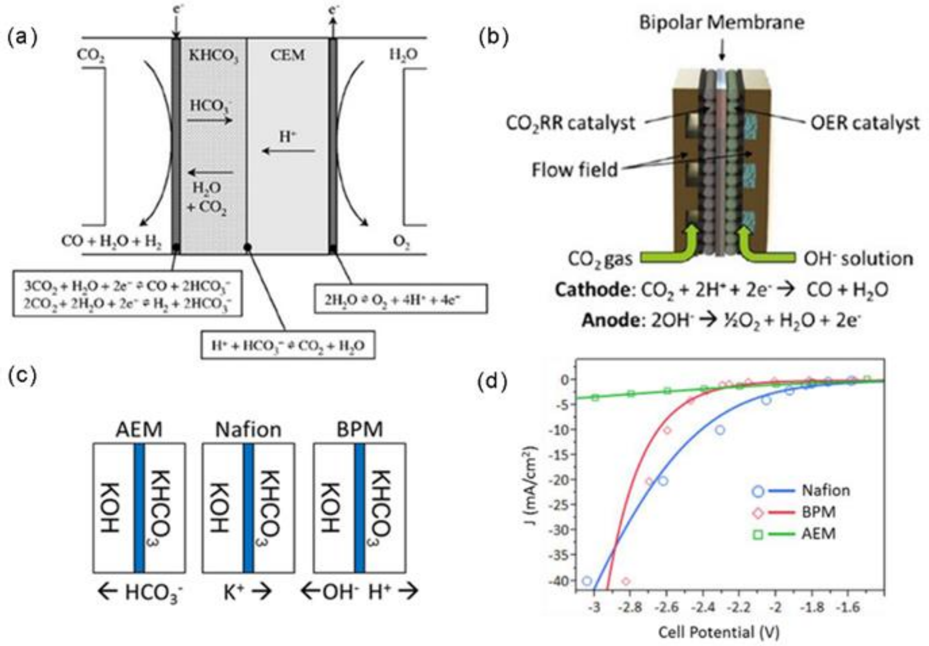

Figure 13. CO_2 reduction cells for syngas production based on GDE: a) schematic of buffer layer-type electrolysis cell by Delacourt *et. al.* [4, 5]; b) schematic drawing of the gas-fed CO_2 electrolyzer by Li *et. al.* [12]; c) illustration of the predominant ion transport processes during electrolyzer operation with AEM, Nafion, and bipolar membranes; d) j−V curves for a BiOx/$BMIM^+OTf^-$-catalyzed GDE-based cell comparing BPM, AEM, and CEM membranes. Adapted with permission from [4, 5, 12].

1.5.2 Adjusting H_2/CO ratio

The significance of controlling the products ratio of CO_2 reduction is due to the fact that these products can directly be used in another reactor for the production of other value-added products, avoiding the separation equipment to decrease the capital cost of the production line.

As can be seen in Figure 2, due to the ratio of H_2/CO in syngas, different pathways can result in different products. This ratio depends on different parameters such as current density, applied potentials, reactor configuration, pH, electrolyte and also electrocatalyst. Hence, production of a steadily stable products composition and a facile and doable way to implement these systems on the existing infrastructures are very important, regarding the complexity of electroreduction of

CO_2 [5]. There have been only few reports on this issue so far. For instance, Hori *et. al.*[40] developed a PEM-based electrode by the deposition of silver directly onto ion exchange membranes (Figure 10a without GDL).This PEM electrodes were able to reduce CO_2 to CO with partial current density of -5 to -60 mA cm_2 for about 2h and CO/H_2 ratio of 30 to 1.33, respectively. Since the PEM electrodes made with an AEM its high anionic conductivity enhances the electron and CO_2 adsorption on the surface of the porous metal layer. As a result, OH^- and CO_3^{2-} can be easily removed from the metal membrane interface by passing through the AEM membrane allowing detoxication of the electrocatalyst surface for CO_2 reduction and being sustained for 2 h. This way a fixed composition of products can be maintained.

Another proposition is using an aqueous buffer layer of potassium bicarbonate between a CEM and a gas diffusion cathode which has been reported by Delacourt *et. al.* [5] (see Figure 10d and 13). In this configuration the electrochemical reactions of H_2 and CO evolution is going forward with a proton donor, *i.e.* H_2O or HCO_3^- rather than H^+ due to non-acidic nature of cathodic part. This buffer layer prevents the excessive protons to intervene the process of CO_2 reduction and as a result by manipulating the thickness of buffer layer, mass transfer barrier is likely to change and as a result the amount of transferred protons can be controlled. Adjusting the number of transferred protons will result in adjusted H_2 production during the process of CO_2 reduction. The drawbacks of such system are that, while this arrangement enabled the stable operation of the cell, a Pt−Ir OER catalyst was used to ensure anode stability and low overpotential in the acidic anolyte, and it also entailed a free-energy loss associated with the acid−base neutralization reaction of H^+ and $HCO_3^−$ at the interface between the CEM and the buffer layer [12].

In another work, the size dependency of the catalytic activity of Au nanoparticles and its effect on manipulation of CO/H_2 ratio has been reported by Mistery *et. al.* [129]. An increase on current density with a decrease on CO faradaic efficiency by decreasing the particle size and based on DFT calculations, made them concluded that the trends were related to the increase in the number of low-coordinated sites on small NPs, which favored the evolution of H_2 over the reduction of CO_2 to CO [129].

1.5.3 Electrolytes

In most of liquid electrolytes has been adopted at least in one part of the cathodic part in most of the works which adds more complexity to the system. The heterogeneous electrochemical reduction of CO_2 employs aqueous electrolytes commonly composed of alkali cations (e.g. Na^+, K^+), various anions such as halide anions, bicarbonate (HCO_3^-), or hydroxide (OH^-), due to their high conductivity in water[17, 130]. So, the adoption of electrolyte can have a profound effect on product selectivity.

Hori *et. al* [131] investigated the effect of different electrolyte in the selectivity of the products of CO_2 reduction. They found a remarkable dependency on the presence of H^+ protons and as a result the pH of the surface of electrode on production selectivity over Cu electrodes.

The importance of the effect of pH arises because depending on the reaction of CO_2 reduction (see Table 1) production of OH^- ions or the consumption of H^+, could increase the pH. Moreover, CO_2 can act as both reactant and a buffer which makes the effect of pH more complicated. In a bicarbonate CO_2 solution the major equilibria reactions are as follows [132] :

$$CO_2 + H_2O \leftrightarrow H_2CO_3 \leftrightarrow H^+ + HCO_3^- \quad \mathrm{p}K_a=6.4 \tag{5}$$

$$\mathrm{HCO_3^-} \leftrightarrow \mathrm{H^+} + \mathrm{CO_3^{2-}} \quad \mathrm{p}K_a=10.3 \tag{6}$$

$$CO_{2(aq)} + OH^- \leftrightarrow HCO_3^- \tag{7}$$

Based on the concentration bicarbonate, reaction 6 can result in pH value of 6 to 8. So, because of reactions 5 and 6 and from direct reaction of CO_2 with hydroxide ions (reaction 7) the buffer capacity near the electrodes can be justified.

Gupta *et. al*. [19] analysed the local pH changes for Cu electrodes. As can be seen in Figure 14 by increasing the pH to 10 current density is increased, too. It seems that in higher overpotentials by increasing the pH, HER suppresses and by decreasing the local concentration of CO_2, CO production decreased and the reaction moved toward production of Methane and Ethane [19].

Another important aspect is the effect of cations in the electrolytes [133]. Wu *et. al.* [134] investigated the effect of a wide range of electrolyte (*i.e.* $KHCO_3$, K_2SO_4, KCl, Na_2SO_4, Cs_2SO_4, $NaHCO_3$, and $CsHCO_3$) on the selectivity of Sn electrode. In another work Kenis *et. al.* [133] reported the size dependency of cations on selectivity of Ag electrode for CO_2 reduction. They concluded that larger cations (salts used in the electrolyte) favor CO production and suppress H_2 evolution.

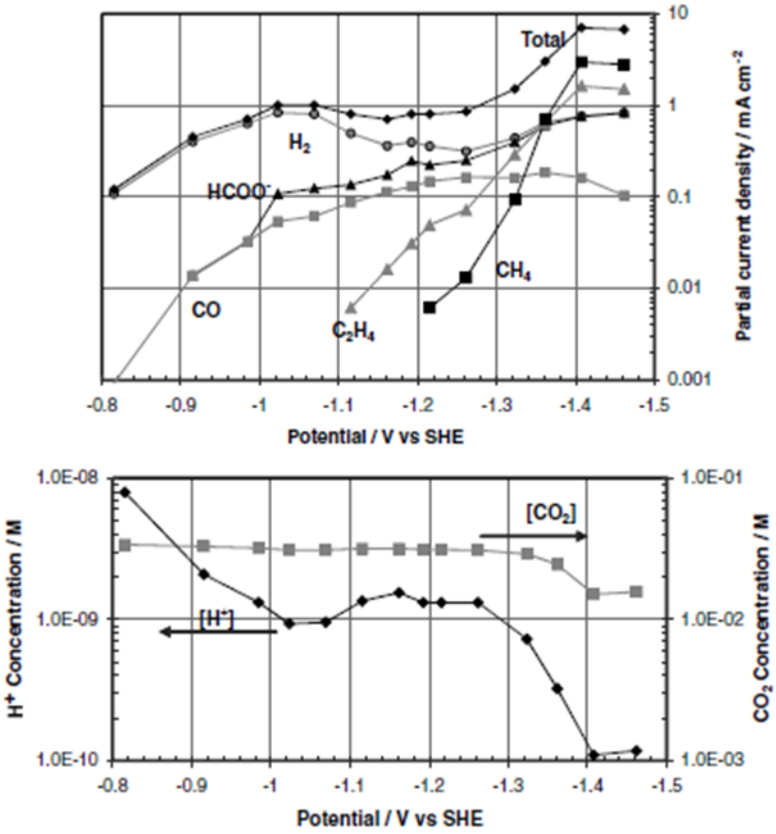

Figure 14. Partial current data from Hori et al.[10] (Conditions: 0.1M $KHCO_3$, 19 C, CO_2 bubbled, bulk $[H^+] = 1.55 \cdot 10^{-7}$ M, bulk $[CO_2] = 3.41 \cdot 10^{-2}$ M. Estimated local $[H^+]$ and $[CO_2]$ values for polarization measurements from [19]

In a more recent work Verma *et.al.* [6] have reported the effect of electrolyte on the electroreduction of CO_2 to CO on Ag based gas diffusion electrodes. In this report the effect of different concentration of electrolytes (KOH, KCl, $KHCO_3$) in

CO_2 production to CO has been discussed. As a result, in this study, using highly alkaline electrolyte of KOH (3M) have showed to be the best electrolyte by reaching a very high current density in comparison with other electrolytes. This effect can be attributed to an improved stabilization of the rate limiting $CO_2^{\cdot -}$ radical intermediate by a higher concentration of K^+ ions in the outer Helmholtz plane (OHP) of the electrical double layer. Higher concentrations of K^+ and OH^- will lead to a more compact double layer at the electrode-electrolyte interface leading to a smaller Debye length or an OHP closer to the electrode surface [29]. The conclusion indicated that by using KOH as the electrolyte, considering the O_2 evolution reaction takes place at the anode, the OH^- generated at the cathode has a greater chance to get consumed at the anode. Such a continuous removal of the OH^- species from the cathode can enhance CO_2 reduction [6] (see Figure 15).

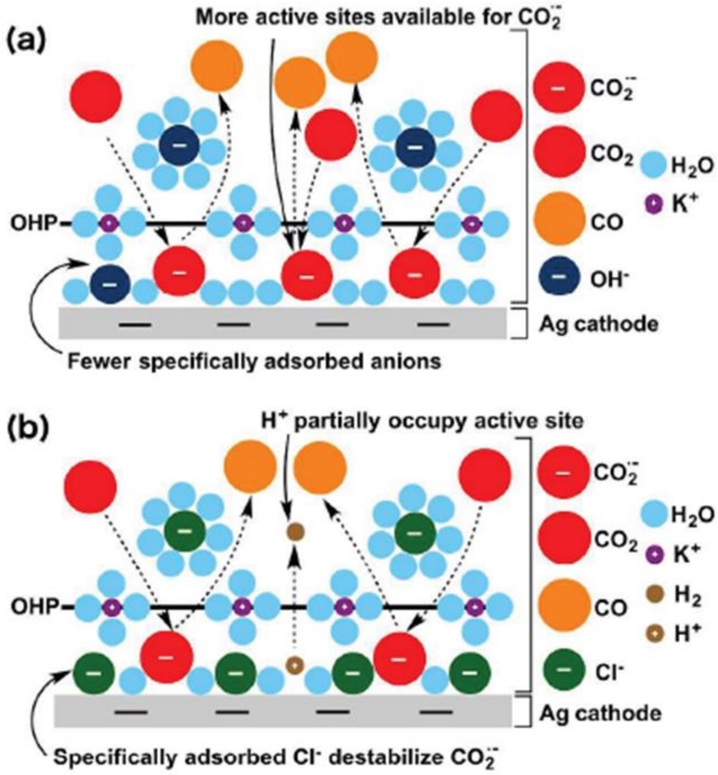

Figure 15. The effect of using a)KOH or b)KCl in the processes of double layer and their role in CO_2 reduction to CO. Reprinted and adapted from [6].

Other less common electrolytes are ionic liquids. They have been reported by different groups, but their major drawback is that they mostly are expensive and sensitive to moisture. Salehi Khojin *et.al.* [135] used dried EMIM-BF_4 as catholyte and 0.5 M sulfuric acid as anolyte with Silver nanoparticles as cathodic electrocatalyst. They also modified the catholyte by using 18 mol% WMIN-BF_4 in water in the cathodic compartment and 100 mM aqueous sulfuric acid in the anode compartment to achieve a more selective with low overpotential CO_2 reduction [36]. In addition, Asadi *et. al.* [82] have used 4 mol% EMIN-BF_4 in water (pH=4) for both compartments for selective production of CO by molybdenum bisulphate as cathode. FE of 98% and current density of -65 mA cm^{-2} were achieved. In another work Dung *et. al.* [136] used an aqueous solution of 1-butyl-3 methylimidazoliumchloride (BMImCl) with 20 wt.% H_2O with Ag metal as cathode. In a more recent work Verma *et. al.* [6] investigated the effect of ionic salts on the performance of famous carbon capture ionic liquids like EMIM Cl, choline Cl and their deep eutectic solvents. They concluded that adding ionic salts like KCl can enhance the performance of these ionic liquids for CO_2 reduction and helps the integration of two parallel process of CO_2 capture and CO_2 reduction.

1.5.4 Temperature

Most of the reported works have been held in ambient temperature and pressure. However, due to exothermic nature of the reaction in most of commercial electrolysers the operation takes place in 80-150°C. Hence the temperature can play a significant role in thermodynamic of the reaction. In a recently reported work Dufek *et. al*. [9] have investigated the effect of operating conditions like temperature, CO_2 flow and current densities on the production of syngas on a GDE containing an Ag catalyst. In this work a monotonic drop of overpotential has been reported at -70 mA cm^{-2} by increasing the temperature from 18 to 70°C with overall cell potential drop of 1.57V. This can be attributed to both kinetic and thermodynamic for H_2 and CO evolution reaction. From thermodynamic data, it was calculated that the thermodynamic change in the reduction potential for both CO_2 and H_2O reduction, as the temperature is increased from 25 to 125 ^{o}C, is less than 0.1 V[9]. This can approve that temperature can have a more significant effect on kinetics at the surface of catalyst than that of thermodynamics. Also the ohmic drop on the resistance of the cell and the membrane by increasing the temperature can also contribute to this effect [9] (Figure 16).

Moreover, Solubility of CO_2 in the electrolyte directly depends on the temperature in a way that by increasing the temperature the dissolved amount of CO_2 will decrease which then leads to mass-transport limitation for CO_2 reduction and favours the HER reaction.

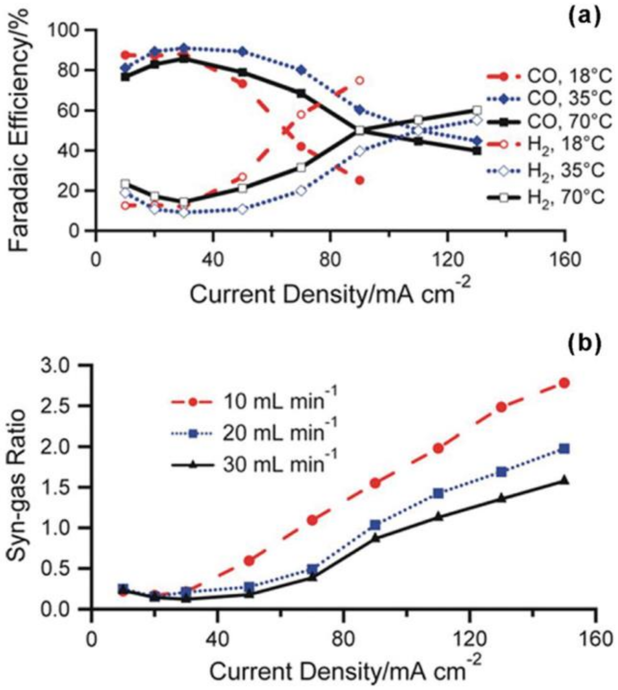

Figure 16. a) FE for CO and H_2 at 18, 35, and 70 °C at a CO_2 flow of 20 mL min^{-1}. b) Syngas (H_2/CO) ratio as a function of CO_2 flow rate at 70 °C. Catholyte: 0.8 M K_2SO_4. Taken with permission from [9]

1.5.5 Pressure

Pressure is another influential aspect in CO_2 reduction. As discussed above higher amount of dissolved CO_2 results in higher feedstock for electrochemical reduction and higher production rate. The major challenge is the configuration of reactor in which electrocatalytic process should happen in high pressures. Figure 17 summarizes the results of few research groups who report this process in high pressure. One of the first reports in high pressure CO_2 reduction has been done by Hara *et. al.* in which they used a two-compartment electrochemical cell at 20 and

30 bar and they achieved current density as high as 300 mA/cm² by using Ag and Pd cathodes, and reached over 50 % of faradaic efficiency for the CO production at 20 atm [47]. In a more recent work Dufek *et. al.* reported a CO_2 reduction to CO with current densities up to -225 mA cm^{-2} with 80% faradaic efficiency for CO production by using a pressurized cell at 20 bar (see Figure 18) [17]. This amount is 5 times higher than that of the ambient operating conditions which confirms that pressure can plays an important role in increasing the production rate and efficiency of CO_2 reduction.

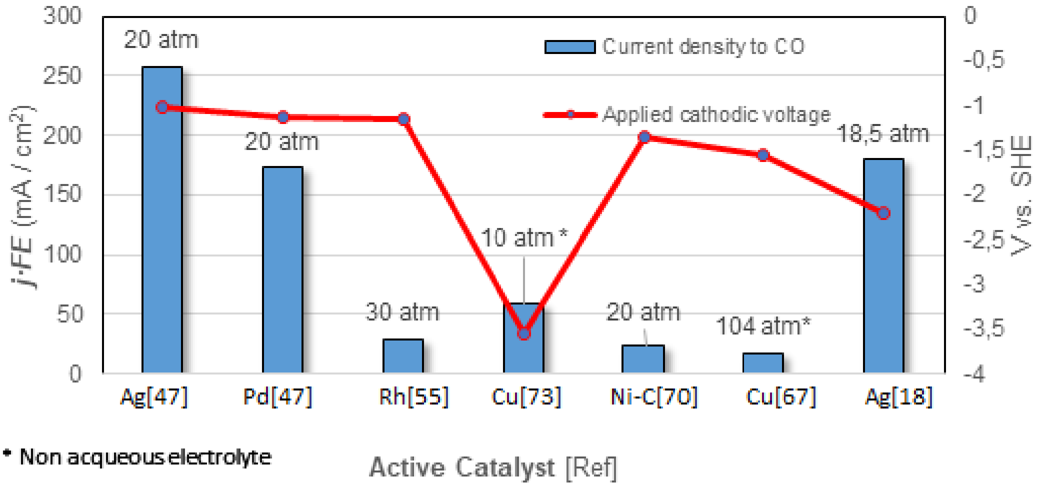

Figure 17. CO current densities and respective cathodic potentials for the CO_2 reduction to CO production in high pressure systems. Reproduced with permission from [1]

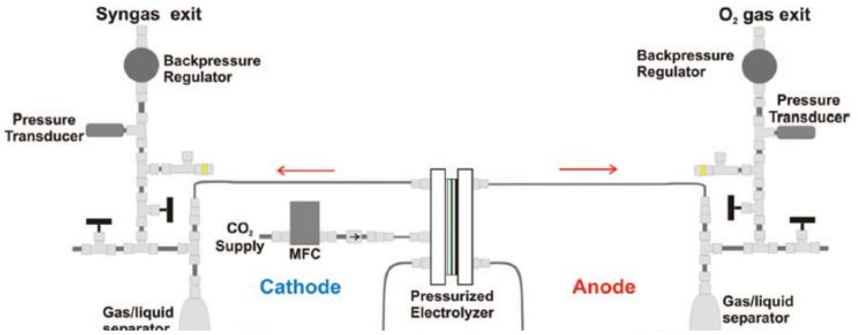

Figure 18. Schematic of the pressurized electrolysis system reported by Dufek *et. al.* Taken with permission from [17].

Chapter 2

Electrocatalyst synthesis

2.1 Suitable electrocatalyst

As it has been described in the previous chapter different catalyst can result in different selectivity and different efficiency toward the desired product. The goal is to find an electrocatalyst which can produce syngas with the desired CO/H_2 ratio with low overpotentials and high current density. Also, by analyzing different steps in the mechanism of CO_2 reduction, finding the best co-catalyst could help to improve kinetical and thermodynamic barriers for a better and more efficient CO_2 reduction to syngas. As it has been mentioned before Silver and Gold are considered to be among the most favorite electrocatalyst for CO production. The major drawbacks of these materials are their high cost and high overpotentials. Hence, one of the resolutions toward lowering the overpotentials is the application of nanostructured Au and Ag particles [41, 43, 48]. Also using co-catalyst is another modification that gains lots of attentions recently [3, 44, 53]. The goal in this work is to find a suitable electrocatalyst which performs CO_2 reduction to Syngas and a proper support as co-catalyst which facilitate the process in a more efficient way by using low noble metal loadings. For this purpose, in this chapter after a brief state of the art review on the methods used for both TiO_2 nanotubes synthesize and Ag deposition, the selected recipe for electrocatalyst synthesis will be discussed and the prepared catalysts will be analyzed from the morphological point of view.

2.1.1 Why Ag-TiO_2 nanotube

Ag is the most favorite electrocatalyst for CO_2 reduction to CO, but the challenge is its high overpotential and low stability. To overcome this issue, many support has been used to lower Ag loading as a noble metal and to stabilize the rate determining steps in CO_2 reduction to CO. In an interesting work Ma *et. al.* [3] used Ag supported on TiO_2 nanoparticles. As can be seen in Figure 3, they achieved a fairly high current density of 100 mA cm^{-2} with Ag loading of 40%. Moreover, they concluded in this report that TiO_2 improves CO_2 reduction kinetics, probably through the adsorption and stabilization of the $CO_2^{\cdot-}$ intermediate, which then can react to form CO on adjacent Ag particles [3]. The schematic of proposed mechanism can be seen in Figure 19.

On other hand since Iijima discovered Titania nanotubes [137], these 1D nanostructures provide unique and exceptional properties like high electron transport and very high surface area. As a result, among all transition metal oxide, TiO_2 is one of the most investigated compounds in materials science [7]. TiO_2 is semiconductor (bandgap ≈ 3 eV) mainly available in three crystalline forms: anatase, rutile and brookite; as mentioned before, it is the most investigated transition-metal oxide due to remarkable proprieties like [7]:

- photoactivity (photovoltaic cells and water splitting);
- biocompatibility (used for medical tools) ;
- non-toxic for the environment;
- good resistance to corrosion;
- low-cost.

Since 1972, when Fujishima and Honda discovered TiO_2 photoactivity [138] , great efforts have been made to deepen the knowledge about this phenomenon and the number of TiO_2 applications has grown. In brief, semiconductors are excited by the light, with higher or equal energy respect to the semiconductor bandgap, forming photo-holes in the valence band and photo-electrons in the conduction band; such charge carriers can rapidly recombine, but they can also migrate to the surface and oxidize or reduce adsorbed species [138].

Nanostructured forms of Titania, like nanoparticles, nanorods and nanotubes, have been studied to increase the superficial area. In particular, one-dimensional nanostructures like nanotubes and nanorods should present a faster electron transport and lower charge recombination, with respect to nanoparticles [18], since the grain boundaries can act as recombination centers [139] (Figure 20).

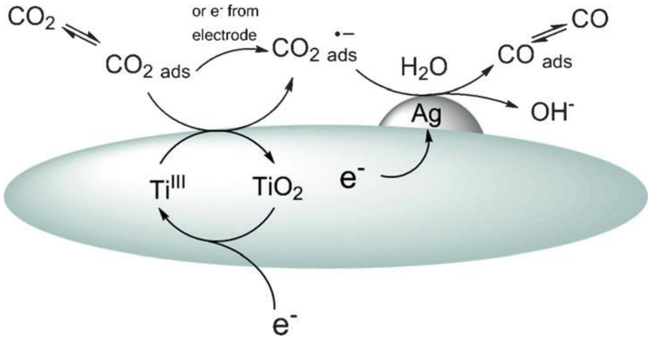

Figure 19. A scheme of the proposed pathway for CO_2 reduction to CO on the Ag/TiO_2 catalyst. Reproduced with permission from [3]

Hence because of the aforementioned properties, herein vertically oriented TiO_2 nanotubes (NTs) were chosen and due to quasi one-dimensional arrangement, TiO_2 NTs are able to provide high surface area for Ag loading and superior electron transport properties [140]. The goal is to enhance the stability of CO_2^- intermediate formed because of Titania oxidation as well as to improve CO production in presence of silver nanoparticles. Particular attention has been devoted to reduce the noble metal loading in the electrode and to increase the catalyst`s active surface area with the attempt to decrease the required overpotential.

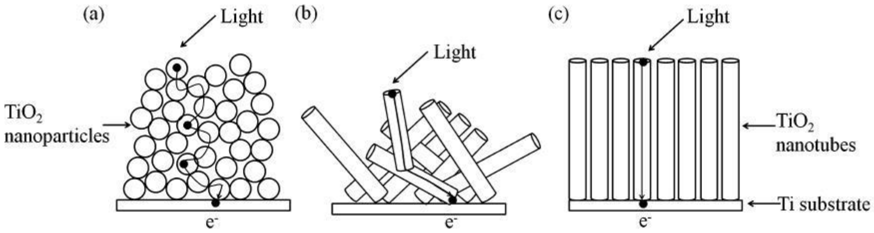

Figure 20. Schemes of the electron pathways through (a) nanoparticles, (b) randomized and (c) oriented TiO_2 nanotubes. Reproduced from [18]

2.2 Titania nanotube synthesis techniques

Self-organized oxide tube arrays or pore arrays can be obtained by different methods. Table 5 shows a comparison between the three most diffused methods for the synthesis of Titania nanotubes: template-assisted, electrochemical anodization and hydrothermal. Other techniques include sol-gel methods, solvothermal techniques and atomic layer deposition (ALD) [141]. The pioneer work by Hoyer *et. al.* is an example of template assisted method which is based on the use of polymeric mould in which the semi-conductor is electrochemically deposited and then the polymeric template is being dissolved [142].The other synthesis technique is electrochemical anodization. In this method by applying high potentials to a Ti foil which is used as a substrate, nanotubes can be synthesized. The hydro/solvothermal method, in the other hand, is based on a thermal treatment in a NaOH solution and subsequent treatment in an HCl solution [143]. By taken in to account all the advantages and drawbacks of these different methods, anodization has been chosen for the synthesis of TiO_2 nanotubes in this work due to its controllability of synthesis and the growth of well-ordered nanotubes. Hence, before jumping to experimental part, in the following sub session a more detailed description of the method has been presented.

Table 5. Comparison between synthesis methods of TiO_2 nanotubes. Reproduce from [18]

Synthesis method	**Order**	**Advantages**	**Drawbacks**
Template-assisted	Ordered arrays	(a) Dimension control through the template (b) Uniformity	(a) Possible damage during template removal (b) Template dissolution may contaminate nanotubes
Electrochemical anodization	Oriented arrays	(a) Dimension control through conditions applied (b) Well attached and ordered arrays	(a) Not separated nanotubes (b) Length distribution not uniform
Hydrothermal	Random alignment	(a) Easy method (b) large amounts of nanotubes	(a) Uneven size distribution (b) Less ordered arrays

2.2.1 Electrochemical Anodization

The electrochemical oxidation of certain metals can lead to five different situations, depending on the conditions and on the electrolyte (Figure 21) [18].

I. the oxidized metal ions simply dissolve in the electrolyte and the result is the electropolishing;

II. in presence of O^{2-} ions, the metal cations can form a compact oxide layer;

III. a competition between metal ions dissolution and the creation of an oxide layer can induce a self-organization in nanopores or nanotubes;

IV. a rapid process can lead to disorganized nanotube bundles;

V. other conditions form a mesoporous nanotube layer.

Zwilling *et. al.* [144] first reported the formation of self-organized oxides from the electrochemical anodization of titanium and realized that self-organization was due to low concentrations of fluoride ions in the electrolyte. The pH is also important, since a neutral pH leads to longer nanotubes and consequently to a thicker layer [145]. A further improvement was the elimination of sidewall inhomogeneity and the improved order by using non-aqueous electrolytes[146]; an organic electrolyte like ethylene glycol, in fact, allows the growth of high-ordered hexagonal arrays of long nanotubes (hundreds of µm) [147], though the presence of water in low concentration helps in the oxidation of titanium [148]. Moreover, if the nanotubes are removed, an array of ordered dimples is left on the titanium surface and such dimples can act as guide in a second anodization step, resulting in an even higher ordered hexagonal array [149]. Finally, after the electrochemical anodization process the nanotubes formed are amorphous; nevertheless, a thermal treatment in air can form the desired crystalline phase (350-500 °C for anatase and above 550 °C for rutile) [14]. Annealing also increases the conductivity of TiO_2 nanotubes [150], at the same time the concentration of F and C impurities, left by the synthesis method, decrease [151].

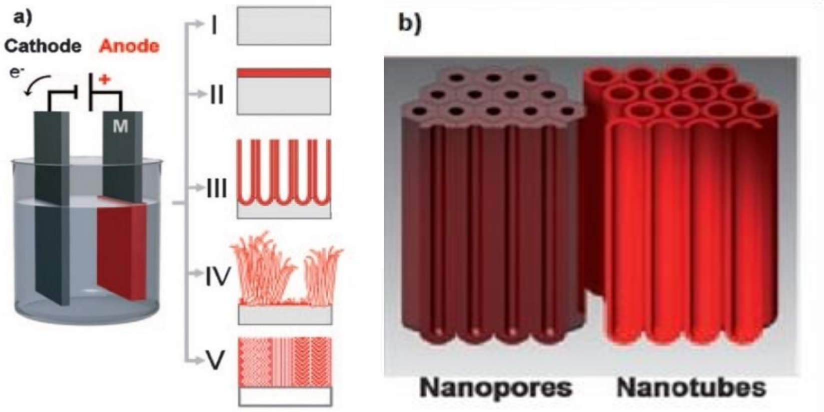

Figure 21. Electrochemical anodization and possible anodic morphologies: (a) I) metal electropolishing, II) compact anodic oxide, III) self-ordered oxides (nanotubes or nanopores), IV) rapid (disorganized) oxide nanotube formation, V) ordered nanoporous layers. (b) Subtle difference between nanopores and nanotubes. Reproduced from [7]

The anodization process can be performed by applying a constant potential (1-60 V for aqueous and 5-150V for non-aqueous electrolytes) and, without fluoride ions, a compact TiO_2 layer forms (Figure 22-a); the growth of the oxide layer is allowed by the migration of ions (Ti^{4+}, O^{2-}) through the oxide itself, due to the high applied potential, and normally occurs at the metal-oxide interface (Figure 22 – b); instead, in presence of F^- ions (0.1-1 wt%) the Ti^{4+} ions can be complexed, when they emerge from the oxide layer, and the already formed TiO_2 is partially dissolved [14]:

$$Ti^{4+} + 6\,F^- \rightarrow [TiF_6]^{2-} \tag{8}$$

$$TiO_2 + 6\,F^- + 4\,H^+ \rightarrow [TiF_6]^{2-} + H_2O \tag{9}$$

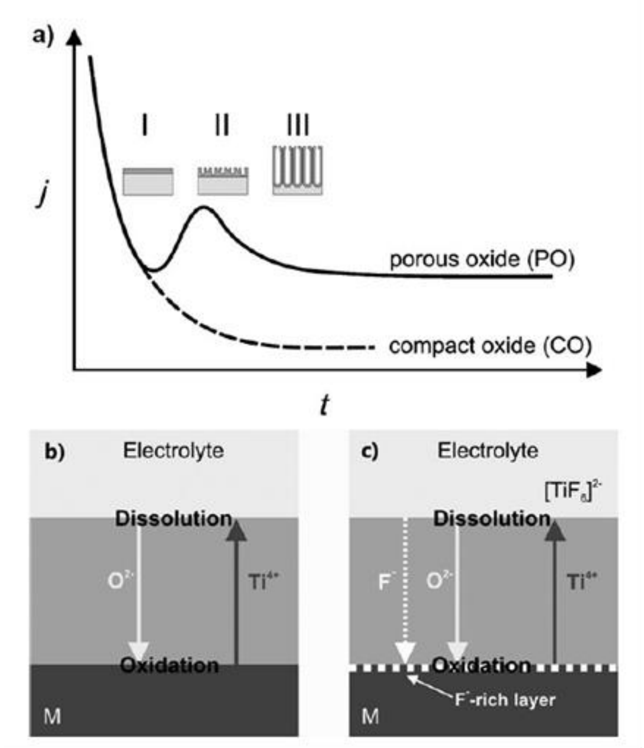

Figure 22. a) Current-time (j-t) characteristics at constant potential in the absence (- - -) and presence (——) of F^-. Three morphological stages (I-III) correspond to different parts of the curve. High-field migration of ions through the oxide in absence (b) and presence (c) of F^-. The high mobility of fluoride ions creates a F^--rich layer at the interface with the metal. Reproduced from [14]

The competition between growth and dissolution leads to a self-ordered structure and, in specific conditions, to the formation of nanotubes; the growth proceeds until the rates of formation at the bottom and dissolution at the top are equal and a steady state is reached [152]. Nanotubes obtained in presence of fluoride ions, present a V-shaped profile [151] and a fluoride-rich layer at the metal-oxide interface, since F^- ions mobility in the oxide layer is higher than that of O^{2-} ions [153]. Due to the growth, this fluoride-rich layer is also present at the boundaries between nanotubes (Figure 23 – a) and, since water can dissolve the species composing this layer, its presence is fundamental for the formation of ribs at the boundaries between nanotubes (Figure 23 – b) [154].

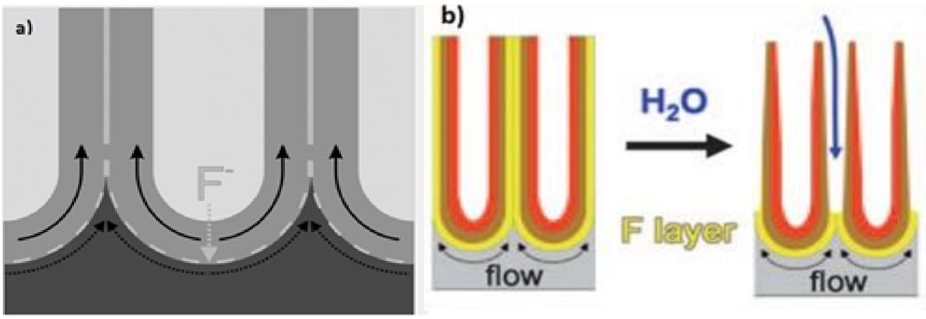

Figure 23. a) Scheme of the flow mechanism that push oxide and fluoride layer up the cell walls [8] c) Scheme of the transition from a porous structure to nanotubes, thanks to the water dissolving the fluoride-rich layer. Reproduced with permission and adapted from Ref. [14]

2.3 Experimental Synthesis results of Titania nanotube

The chosen recipe for the synthesis of nanotubes is a modified version of the method proposed by Lamberti *et. al*. [155]. Initially a titanium foil (Alfa Aesar, Titanium foil 0.25 mm thick, annealed, 99.5 % pure) is pre-treated: first it is sandblasted and then etched in a 40% HCl solution at 60°C for 15 minutes. After that, the real anodization step comes: in the electrochemical configuration used, the cathode is also a Ti foil and the electrolyte is 0.5 wt.% NH_4F and 2.5 vol.% H_2O in ethylene glycol; the anodization is carried out by applying 60 V for 10 min and by using a Teflon electrochemical cell. Due to application of harsh etching, as can be seen in the Field Emission Scanning Electron Microscopy (FESEM) images, the substrate is not smooth enough for the growth of nanotubes which resulted in compact and non-regular nanotubes (see Figure 24). To overcome this issue and also to increase the stability of well-oriented vertical Titania nanotubes, the synthesize method has been modified. This new method includes a titanium foil (Alfa Aesar, Titanium foil 0.25 mm thick, annealed, 99.5 % pure) sandblasted and then etched in a 40% HF solution for 1 minute then anodization process was done as mentioned above. Then the grown nanotubes were removed by sonication of 10 minute in a solution of H_2O_2 to make the substrate ready for the second anodization to take place in the foot print of the removed nanotubes (This process called Aging). Second anodization was done similar to the first anodization. Finally, since the nanotubes are amorphous, they are converted to anatase form by an annealing step, at 450 °C for 1 h, in the oven. The results showed that the effort to use the less harsh etching solution and also resynthesizing the nanotubes in their footprint has been paid off. Indeed, the synthesized nanotubes are well oriented compact Titania nanotubes with the diameter of around 80 nm and the length of less than µm (Figure 25). All the used reactants where purchased from Sigma-Aldrich.

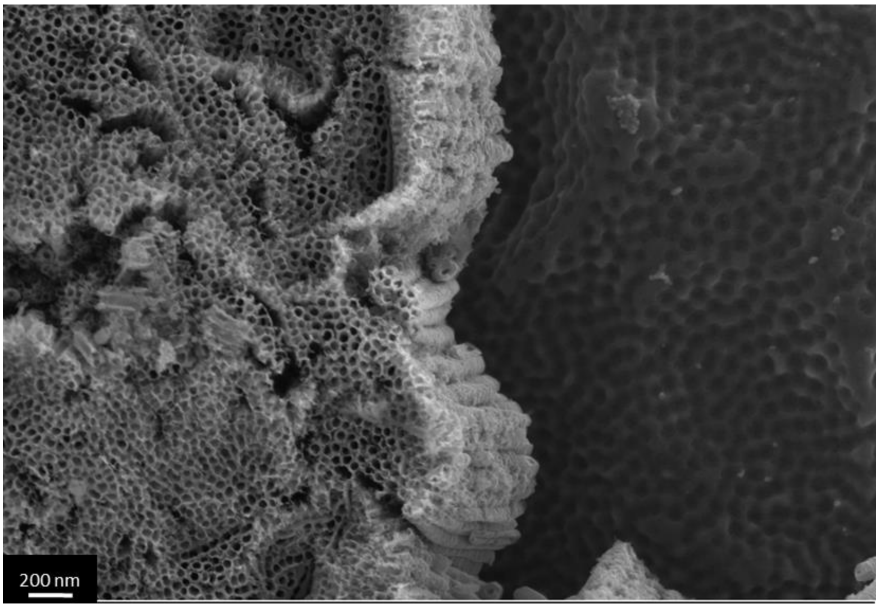

Figure 24. A top view FESEM image of synthesized nanotubes being etched with HCl solution.

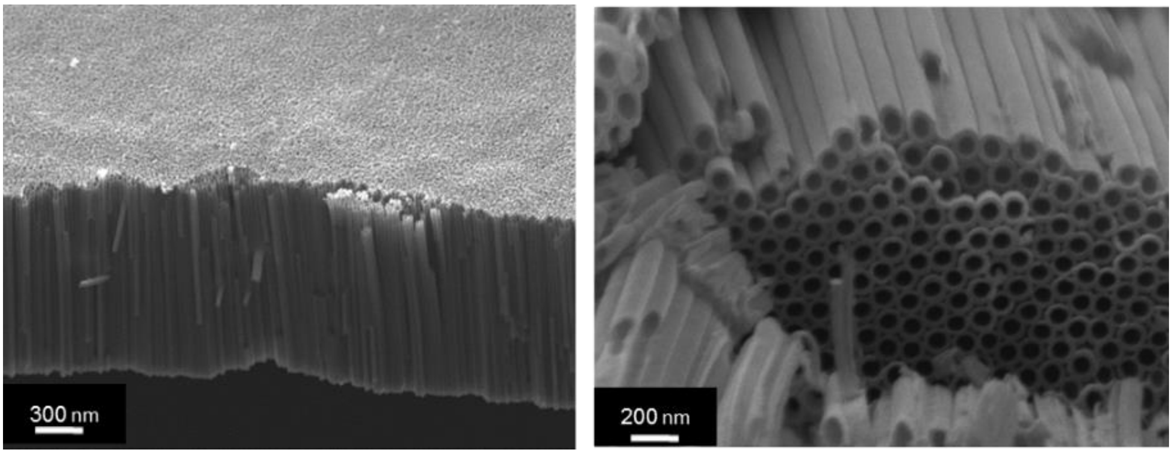

Figure 25. FESEM images of well oriented vertical Titania nanotubes synthesized by Aging process

2.4 Ag deposition

Ag nanoparticles are acting as the major electrocatalyst for CO_2 reduction to CO. Thus, the morphology and the dispersion of these nanoparticles on the substrate can be crucial to the performance of electrocatalyst. Among all the deposition methods, in this work, UV deposition and sputtering has been chosen due to their feasibility and reproducibility.

2.4.1 UV deposition

In this procedure Silver Nitrate ($AgNO_3$) in different concentrations used as Ag precursor. Under the UV illumination the photogenerated electrons reduce the surface-adsorbed metal ions forming metal clusters and being deposited on the substrate as follows;

$$Ag^{+}(aq) + e^{-} \rightarrow Ag(s) \qquad (10\ )$$

Also depending on the time frame of irradiation, bigger clusters can be formed. In the first step to find out the optimal irradiation time for well dispersed Ag nanoparticles, UV deposition has been done in a 0.1M solution of $AgNO_3$ in 1, 5 and 10 minutes. As can be seen in Figure 26, higher irradiation timing will result in higher absorption of electrons by metal ions which then creates bigger clusters with lower active areas for catalytic activity and higher irregularity in the dispersion.

Another parameter which can affect the dispersion of particles is the concentration of precursor. Thus, different concentrations of 0.01M, 0.001M, 0.0001M and 0.00001M of $AgNO_3$ have been used in a constant deposition time of 5 minutes (see Figure 27). Using low concentration of precursor resulted in small Ag particle deposition in a scattered way (Figure 27.c, d). Moreover, higher concentration also can cause bigger agglomeration of Ag particles with less regular dispersion over nanotubes (Figure 27a). The best quasi uniformly dispersed small Ag particles happened in fairly low concentration of 0.001M $AgNO_3$ in 5 minutes of irradiation (Figure 27 b).

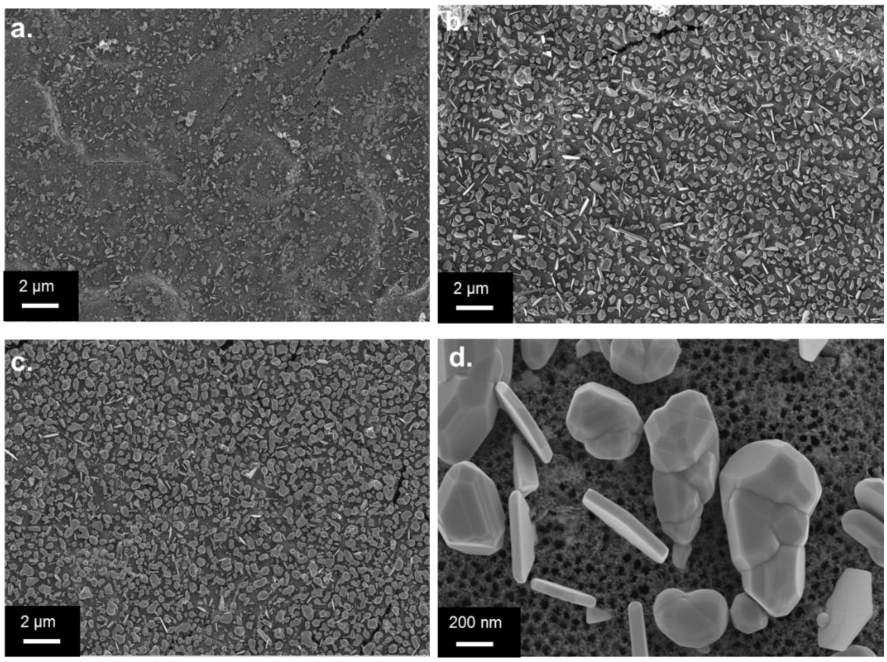

Figure 26. FESEM images of prepared catalyst by UV deposition in 0.1M solution of $AgNO_3$ for a)1 minute b) 5 minutes c)10 minutes of irradiation. d) Magnified image of Ag clusters after irradiation of 10 minutes

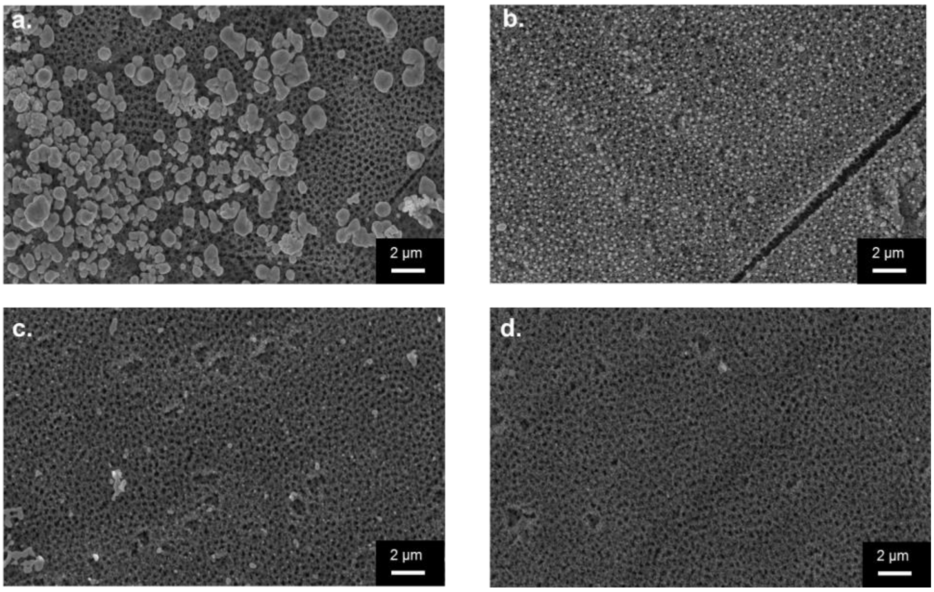

Figure 27. FESEM images of prepared catalyst by UV deposition in 5 minutes of irradiation in a) 0.01M b) 0.001M c) 0.0001M d) 0.00001M solution of $AgNO_3$

2.4.2 Sputtering

The physical sputtering technique is based on the fact that particles colliding on a surface with an energy higher than a threshold value can sputter atoms from the surface in to another substrate. Usually, 200-1000 V are applied between a cathode (target) and an anode (substrate) in a vacuum chamber, containing a heavy inert gas (usually argon); the high potential creates a plasma by ionizing the gas atoms which impact on the cathode and, as a consequence, atoms are ejected from the target surface and deposited onto the substrate (Figure 28) [156].

The use of a metal target allows the deposition of a thin metallic film on a substrate and, in this case, the sputtering technique has been chosen to easily deposit small silver nanoparticles on the TiO_2 substrate.

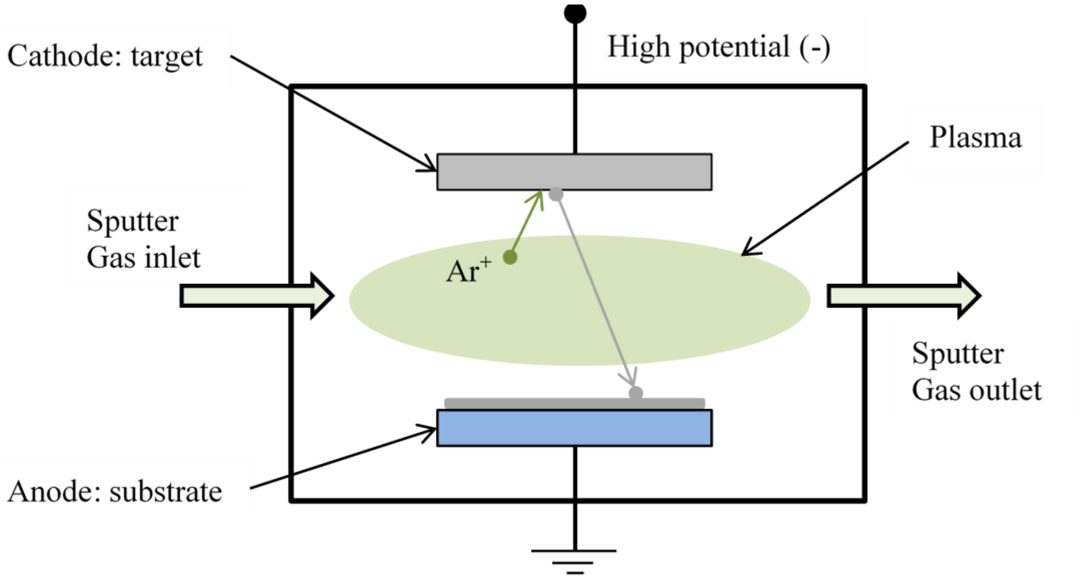

Figure 28.The Scheme of sputtering deposition

However, a sputter coater (Quorum Q150T ES, Figure 29) holding a silver target (Testbourne Ltd, S5-9000-D35 Silver Target 99,99 % pure) have been used to prepare a set of catalysts with different silver loadings, which depends on the sputtering conditions: current and time. It is noteworthy that higher current results in bigger quantities of Silver being ejected from the target and as a result higher amount of Silver will be deposited on the substrate. Also, a higher deposition time can result in higher coating of the substrate and again higher Silver loading. In this work Titania nanotubes were used as the substrate, so different sputtering conditions were used to find a suitable current and time for this deposition method of Ag nanoparticles. The optimum parameters of sputtering are defined as the ones in which Ag nanoparticles are being dispersed uniformly, with a high surface area being exposed to the electrolyte, to increase its electrocatalytic activity. For instance, Figure 30 shows FESEM cross-view images of a sputtered sample by applying the current of 40mA for 90s of deposition (left) and its enlargement (right); from the image on the left one can observe the nanotubes' structure and some aggregates of Ag nanoparticles on the tops of the nanotubes. Furthermore, in the image on the right, small nanoparticles on the internal surface of the nanotubes are notable, which present various sizes: from very few nanometres to 20-30 nm. The images also confirm that the diameter of the nanotubes is about 100 nm.

Figure 29.Sputter coater used for the silver deposition

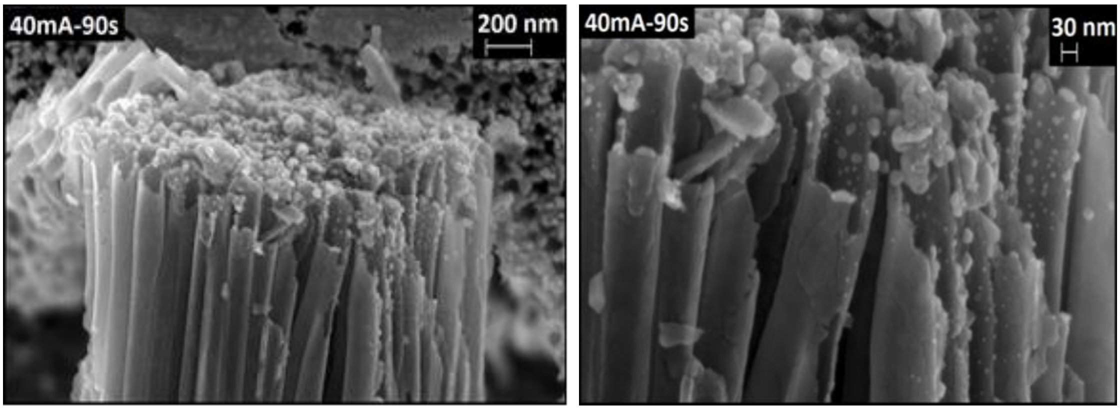

Figure 30.FESEM images of the same piece of Ag sputtered Titania nanotube at 40mA for 90s, at two different scales.

In the present work the sputtering conditions have been used to identify and name the various catalyst samples and, starting from here and for the rest of the discussion, they will be addressed with the structure;

$$(current)mA - (time)s$$

in which the values are being substituted, respectively (e.g. 20mA-90s). Based on this scheme, the list of the prepared catalysts is as indicated in table 6.

Table 6. List of prepared catalysts

Catalyst name	**Catalyst nature**	**Sputtering current and time**	**Ag loading (%)**[1]
20mA-90s	Ag / TiO_2 nanotubes	20 mA, 90 s	4
40mA-90s	Ag / TiO_2 nanotubes	40 mA, 90 s	9
60mA-90s or Ag / TNT	Ag / TiO_2 nanotubes	60 mA, 90 s	16
60mA-120s	Ag / TiO_2 nanotubes	60 mA, 120 s	29
80mA-90s	Ag / TiO_2 nanotubes	80 mA, 90 s	27
Ag / Ti foil	Ag / Ti foil	60 mA, 90 s	N/A
Ag / TNP	Ag / TiO_2 nanoparticles	60 mA, 90 s	N/A
TNT	TiO_2 nanotubes	No silver	0
Ti foil	Ti foil	No silver	0

Figure 31 reports FESEM image comparison between the top views of the catalysts with increasing sputtering current and, consequently, with increasing amounts of silver. As showed before, the nanoparticles form aggregates on the top of the nanotubes and, depending on the amount of silver, the degree of coverage is different. Indeed, this is especially observed when comparing the 40mA-90s sample, where the tops of the nanotubes are not completely covered, with respect to the 80mA-90s sample, which presents a complete coverage of the tops at the point that most of the entrances of the nanotubes internal cavities are totally or partially occluded. Instead, the 60mA-90s sample presents a favourable intermediate situation between the last two cases: the coverage of the nanotubes tops is complete and, at the same time, most of the nanotubes entrances are free. In that case, small nanoparticles which are sputtered inside the nanotubes could be exposed to electrolyte for participation in the reaction and the amount of silver on the tops is maximized. Not only the degree of coverage of the nanotubes changes with the sputtering current, but also the organization and dimension of the nanoparticles/agglomerates on the top. As an example, the 20mA-90s sample shows some big silver clusters (of about 200 nm) that leave the tops of the nanotubes

---

[1] EDS method has been used to measure Ag loading as explained in detail in the next chapter

mostly uncovered. This tendency is reduced by increasing the sputtering current to 40 mA and is no more visible at 60 mA.

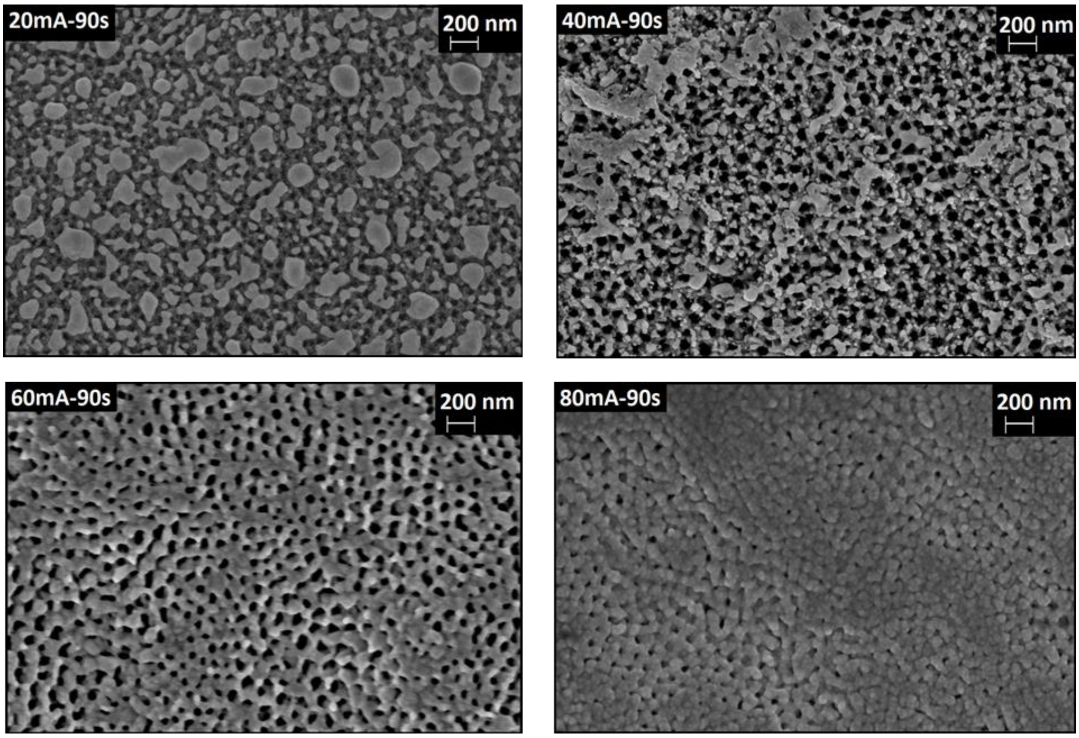

Figure 31.FESEM images of Ag/TNT with different sputtering currents and equal sputtering times.

In addition, Figure 32 shows different views of the electrocatalysts prepared with the same sputtering current (60mA) and different deposition time. The cross-view of the 60mA-90s sample confirms the previous considerations. Instead, the 60mA-120s sample was prepared with a longer sputtering time, which leads to higher amount of silver with respect to 60mA-90s and, similarly to the 80mA-90s sample, the nanotubes entrances are mostly covered.

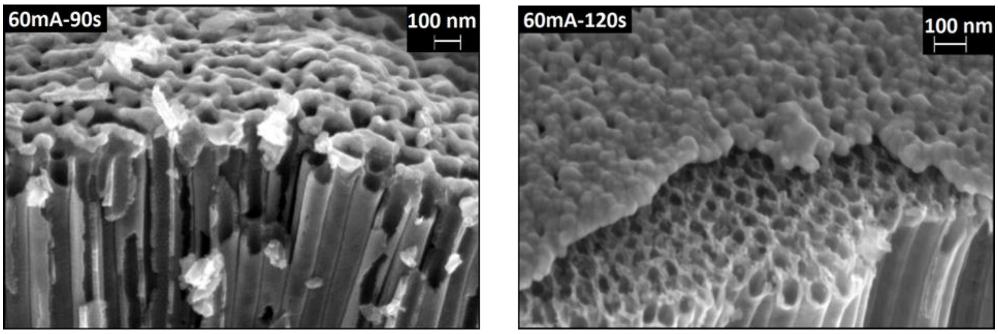

Figure 32. FESEM images of Ag sputtering at 60 mA with 90s and 120s

Moreover to investigate the effect of the substrate on CO_2 reduction to CO, Titania nanoparticles were being synthesized to be used as the substrate for Ag nanoparticles to have comparison versus Titania nanotubes as follows; A titanium foil (Alfa Aesar, Titanium foil 0,25 mm thick, annealed, 99,5 % pure) is sandblasted and rinsed by ethanol and a layer of 30 µm of TiO_2 paste(Dyesole, 18NR-T Titania paste) prepared by doctor blading on the foil. Then dried at 100°C for 30 minutes and calcined at 525°C for one hour.

2.4.2.1 X-ray diffraction (XRD)

To investigate the crystalline form of prepared electrocatalysts X-ray diffraction analysis has been carried out. Figure 33 shows a comparison between the XRD spectra of the Ti foil used to prepare the nanotubes, the TiO_2 nanotubes and the Ag/TNT catalysts sputtered at 60mA with different times or methods. Primarily by the comparison of Ti foil spectra and Titania nanotubes spectra, one can easily distinguish the existence of TiO_2 in its anatase form. Moreover, the small size of the silver peaks is in agreement with the low silver loading, since the minimum quantity for the XRD detection is 1 wt.%. It is also evident that the silver peaks have a low intensity and are rather broad, the latter feature could indicate that the crystallites are small, according to the Scherrer equation 11:

$$D = \frac{K \cdot \lambda}{\beta \cdot \cos\theta} \qquad (11)$$

Where:

D: crystallites size;

K: shape factor;

λ: X-ray wavelength;

β: peak width (line broadening at half the maximum intensity);

θ: Bragg angle.

Furthermore as can be seen in the XRD result (Figure 33), from crystallographic point of view, the dominant facets of Ag are Ag(111), Ag(100) and Ag(200) . Then by increasing the amount of sputtered Ag (from 20mA to 80mA of applied current for sputtering), the majority of Ag(111) facet is more visible. This analysis can confirm the existence of Ag in its metallic form.

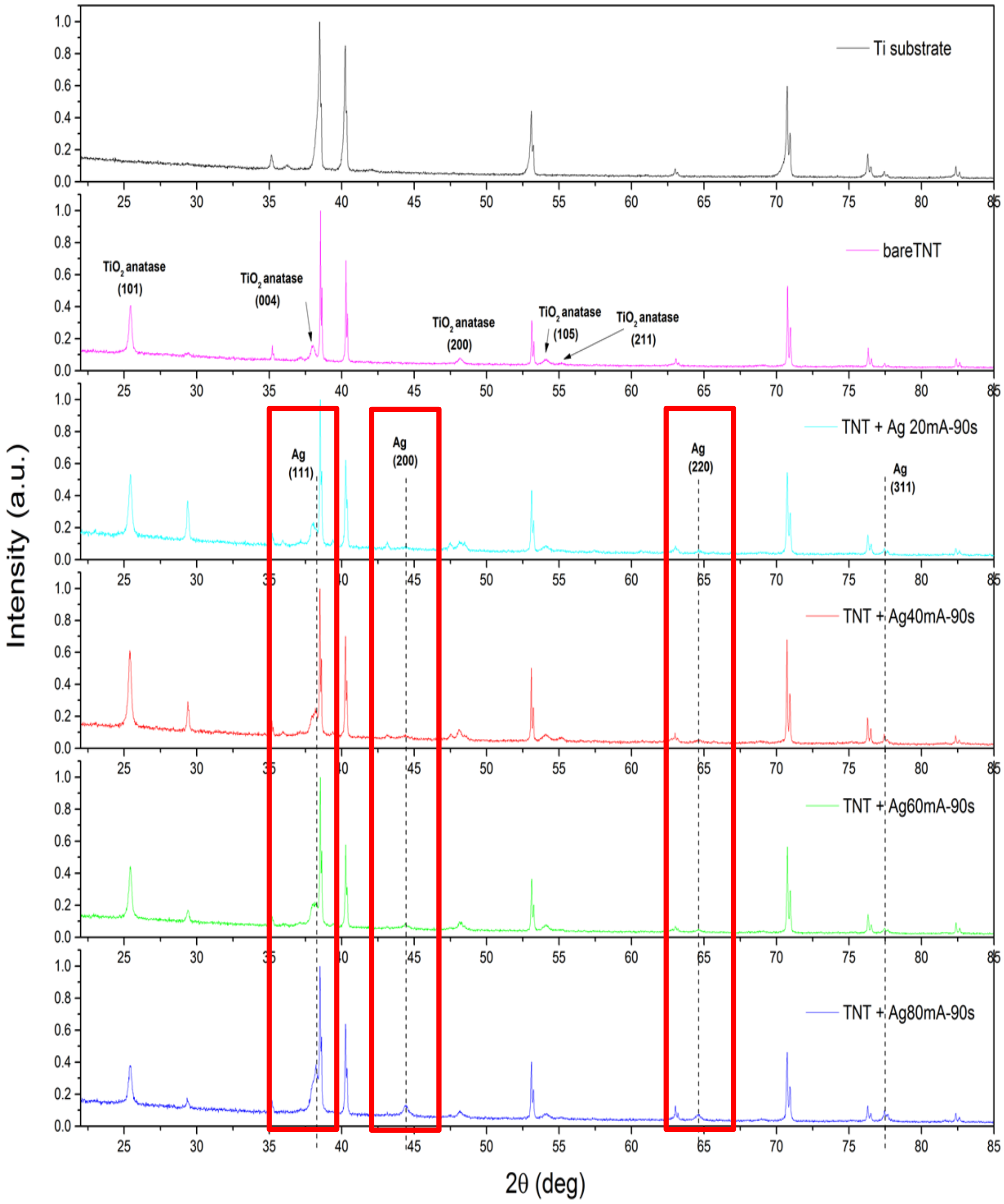

Figure 33. XRD spectra of (from top to bottom): Ti foil, TiO_2 nanotubes, different Ag/TNT samples. The Ag facets are being highlighted in red.

Chapter 3

Electrocatalytic activity test

3.1 Setup and methodology

Performance analysis of the electrocatalysts has been done by thorough quantitative and qualitive analysis as follows:

- Cyclic voltammetry (CV): For reaction kinetic measurement and assess its behavior in different applied potentials
- Chrono amperometry (CA): For quantitative measurement of the products during the reaction at a constant applied potential
- Linear sweep voltammetry (LSV): For reaction kinetic measurement and assess its behavior at different applied potentials
- Electrochemical Impedance Spectroscopy (EIS): For having the responses of the system as a function of the perturbation frequency which can reveal internal dynamics and metal/electrolyte capacitance.
- Electrochemical Surface Area (ECSA): To measure the active surface area of the electrocatalyst to be able to compare and justify the results based on their electrochemical active surface area.

Two different setups have been used for above mentioned tests. One is an electrochemical cell made of poly(methylmethacrylate) (PMMA). This cell consists of two compartments (anodic and cathodic), which are pressed against one another by a four-screw system and sealed by two O-rings; the total internal volume of the reactor is 284 cm^3. The two compartments are separated by a sulfonic membrane (Nafion N117, 178 µm thick), which prevents the mixing of their contents (solutions and gases in the head spaces) and, at the same time, allows the transfer of H^+ ions. Each compartment presents: a) a gas inlet for CO_2 bubbling; b) a gas outlet; c) a magnetic stirrer; d) an inlet, provided with a valve, to fill-in the compartment with the solution and to take liquid samples; e) a pressure indicator; f) a sealed connection for the electric contacts. Moreover, the reactor is equipped with a temperature sensor connected to a cooling system, which maintains the temperature at the desired value, and with a dissolved CO_2 indicator (Mettler Toledo, InPro 5000); this reactor is also designed to perform tests at high pressure, adding two backpressure valves on the reactor outlets, and endures a maximum of 10 atm. It is worth mentioning experiments with this setup carried out in chemical engineering laboratory of TU Delft.

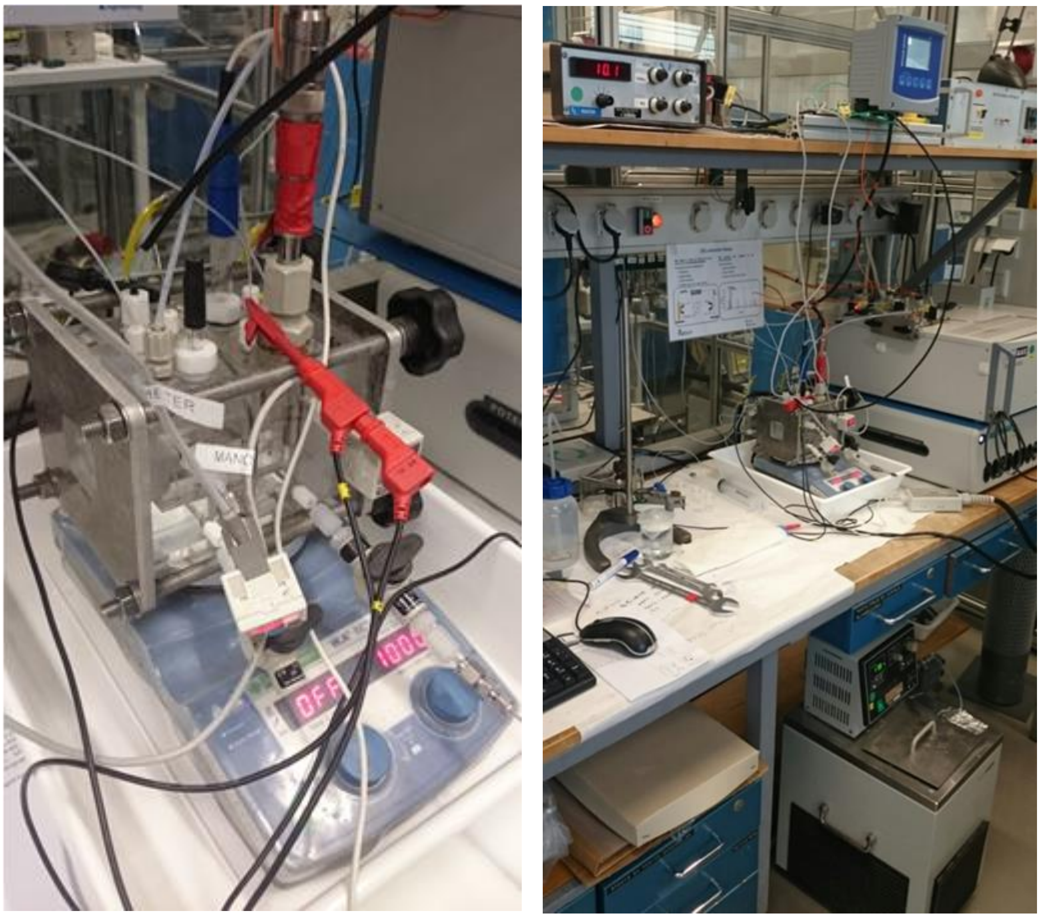

Figure 34. The two-compartment electrochemical cell (left) and the rest of the equipment and fittings being connected to the reactor (right)

As for the rest of the setup, a CO_2 cylinder is connected to the mass flow controllers (Bronkhorst EL-FLOW model F-201CV), which regulate the flow rate of CO_2 fed to the two reactor compartments. Consequently, CO_2 is bubbled directly into the solution ($KHCO_3$, Sigma-Aldrich, purity above 99,95 %) and both compartments are magnetically stirred. A potentiostat (Autolab, PGSTAT302N) applies the desired potential between the working electrode (catalyst) and the reference electrode (Radiometer Analytical, XR300 Ag/AgCl), the counter electrode is a platinum gauze (Mateck, 0,06 mm wire diameter, 5x5 cm^2). The gas flows, that leave the reactor, go to a gas chromatograph (Global Analyser Solutions, Compact GC) which measures the product concentrations. A refrigerating circulator chiller (Lauda, RC 6) is connected to the temperature sensor and keeps the temperature of the solution in the reactor at a constant value. Figure 35 shows a simplified scheme of the setup.

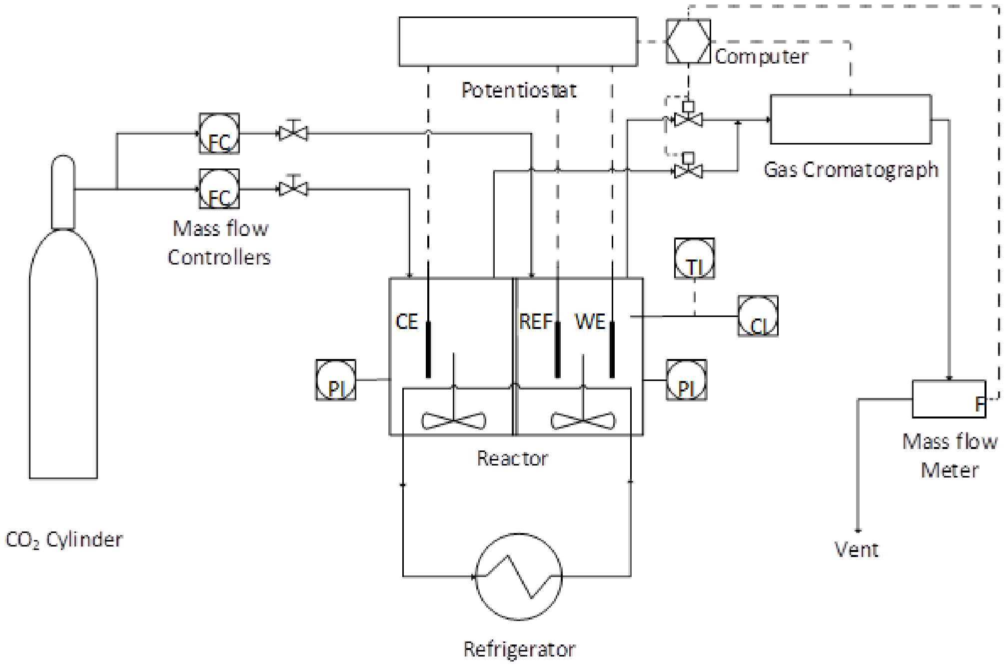

Figure 35. The scheme of the electrochemical cell and its equipment for CO_2 reduction measurements in TU Delft.

The other setup is a one compartment cell made of Teflon, by Hysytech (Figure 36). The CO_2 inlet is immersed in the liquid, to bubble the gas directly into the solution ($KHCO_3$, Sigma-Aldrich, purity above 99,95 %). The electrolyte is magnetically stirred and connected to a potentiostat (Biologic, VS.P-300), which applies the desired potential between the working electrode (catalyst) and the reference electrode (Radiometer Analytical, REF421 saturated calomel electrode). It is noteworthy that the counter electrode is a platinum plate. Because of the inlet flow, a flow rate approximately equal to the feed leaves the reactor from an outlet in the reactor cap and reaches the GC (Inficon, Micro GC Fusion Gas Analyzer), which measures the product concentrations. Moreover, a pressure indicator is connected on the line from the reactor to the GC (Figure 37). It is worth mentioning that all the experiments with this setup carried out in Solarfuel laboratory of PoliTo.

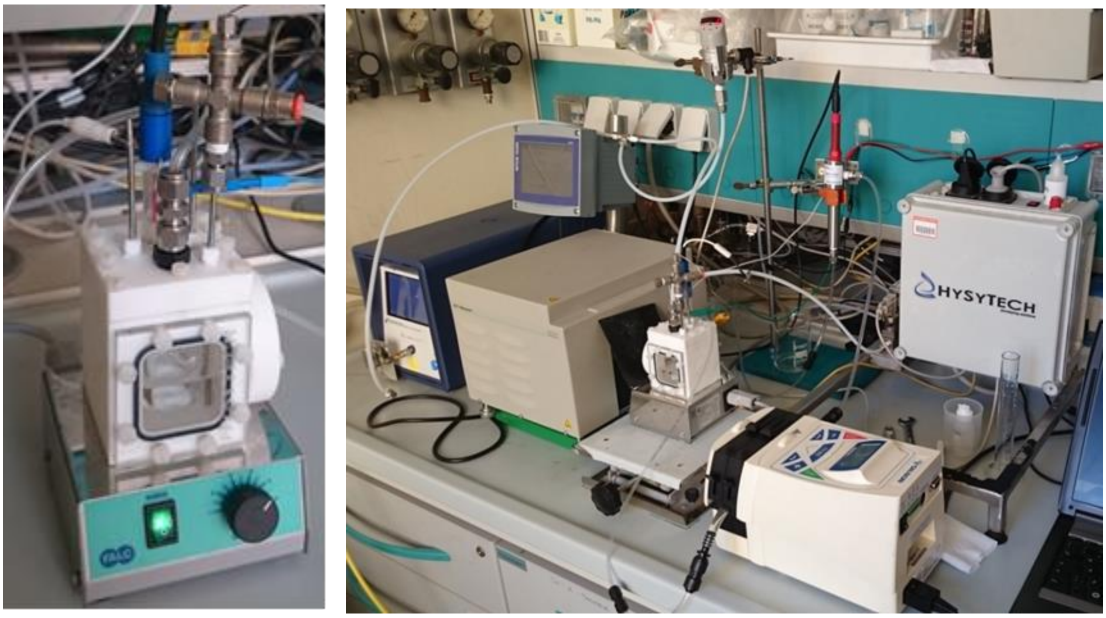

Figure 36. The one compartment electrochemical reactor (left) and all the fittings and equipment and sensors (right) for CO_2 reduction

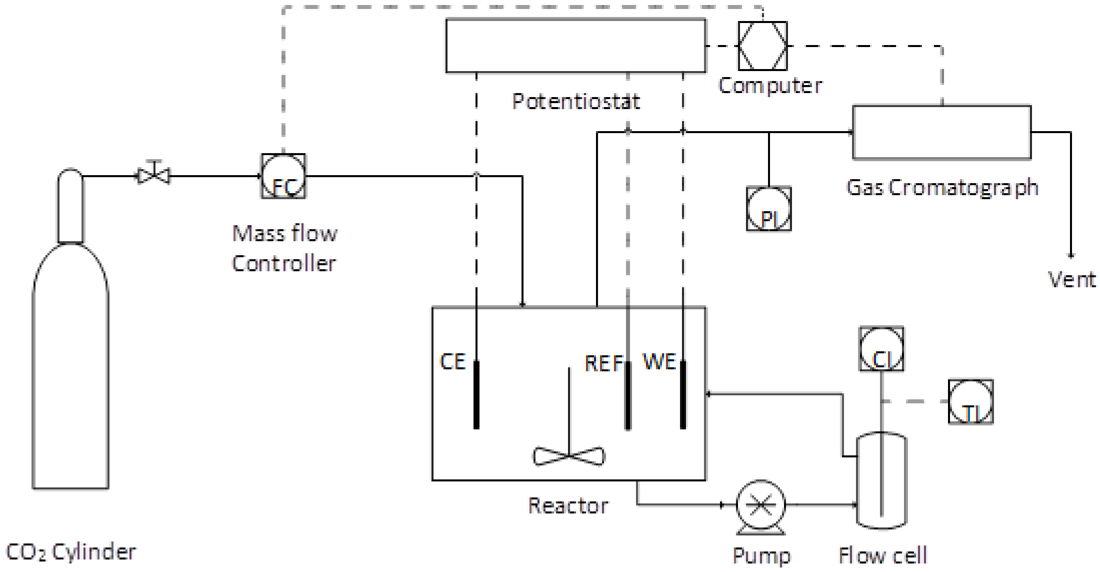

Figure 37. Simplified scheme of one compartment electrochemical reactor and its equipment in PoliTo.

In addition, the data elaboration during the present work and the equations used for calculations have been described as follows; The current can be converted into current density values by dividing it by the electrode geometric area (equation 12):

$$j = \frac{I}{A} \tag{12}$$

Also, from the gas flow rate and the concentrations, it is possible to calculate the production rates and the CO/H_2 ratio as follows (Equations 13-15).

$$\dot{n}_{CO} = \frac{y_{CO} \cdot \dot{V} \cdot P}{R \cdot T \cdot A} \tag{13}$$

$$\dot{n}_{H2} = \frac{y_{H2} \cdot \dot{V} \cdot P}{R \cdot T \cdot A} \tag{14}$$

$$\frac{CO}{H_2} = \frac{\dot{n}_{CO}}{\dot{n}_{H2}} \tag{15}$$

Where:

$\dot{n}_{CO}$, $\dot{n}_{H2}$ $\left(\frac{mol}{s \cdot m^2}\right)$: production rates (molar flow rates per unit area) respectively of CO and H_2;

$\dot{V}\ \left(\frac{m^3}{s}\right)$: gas total volumetric flow rate;

$P\ (Pa)$: pressure;

$R\ \left(\frac{m^3 \cdot Pa}{mol \cdot K}\right)$: gas constant;

$T\ (K)$: temperature;

$A\ (m^2)$: electrode geometric area.

Finally, by using the production rates and the current density, the faradaic efficiency can be calculated (Equations 16, 17).

$$FE_{CO} = \frac{\dot{n}_{CO} \cdot z_{CO} \cdot F}{j} \cdot 100 \tag{16}$$

$$FE_{H2} = \frac{\dot{n}_{H2} \cdot z_{H2} \cdot F}{j} \cdot 100 \tag{17}$$

Where:

$\dot{n}_{CO}\ , \dot{n}_{H2}\ \left(\frac{mol}{s \cdot m^2}\right)$: production rates respectively of CO and H_2;

$z_{CO}\ , z_{H2}\ \left(\frac{mol_{e^-}}{mol}\right)$: moles of electrons needed to form a mole respectively of CO and H_2;

$F\ \left(\frac{C}{mol_{e^-}}\right)$: Faraday constant;

$j\ \left(\frac{A}{m^2}\right)$: current density.

To know the z values, it is sufficient to consider the two half-cell reactions. The value is indeed 2 for both cases (Equations 18, 19).

$$CO_2 + 2\ e^- \rightarrow CO + \frac{1}{2} O_2 \tag{18}$$

$$2H^+ + 2\ e^- \rightarrow H_2 \tag{19}$$

3.2 Performance analysis

In the following sub sessions different performance analysis as mentioned above have been done and the results are being compared and discussed among different catalysis with different Ag loading and deposition methods.

3.2.1 Ag-UV deposited Titania nanotubes

As discussed in previous chapter one of the method which has been chosen for deposition of Ag nanoparticles on Titania nanotube is by irradiation of $AgNO_3$ solution. Based on the FESEM images and morphological analysis of them, 5 minutes was chosen to be the optimum deposition time in order to avoid the agglomeration of Ag particles and for a uniform dispersion. Among different concentrations of $AgNO_3$ as precursor, 0.001 M showed to have the best dispersion with the most uniform nano-sized particles over the nanotubes (Figure 27-b). For the performance analysis of this electrocatlyst a chrono amperometry test has been done in the conditions mentioned in table 7 in the two-compartment cell reactor (Figure 34).

The results of an 80 minutes test on each potential showed a very unstable behavior of the selected electrocatalyst of Ag-UV deposited TNT. As can be seen in Figure 38 within the first 45 minutes the production of CO increased in all three applied cathodic potentials but after that a drastically decrease of CO production happened which indicated a deactivation of this electrocatalyst. This behavior seems to be as a result of loss of Ag nanoparticles during the reaction. XPS and EDS analysis before and after the reaction also confirm the loss of a significant portion of Ag nanoparticles (Figure A-1 & A-2 in the appendix). This could be due to low nuclei adhesive forces during the deposition and agglomeration of Ag particles.

Table 7. Experiment conditions for CA test in the two-compartment cell

Parameter	**Value**
Temperature	20 °C
Pressure	1 atm (except for one test)
Electrolyte (aqueous solution)	$KHCO_3$ 0,1M (85 ml)
Potentials	-1,4 / -1,5 / -1,6 V vs. SHE
CO_2 flow rate	600 Nml/h
Stirring	600 rpm
Electrode geometric area	2,4 cm^2

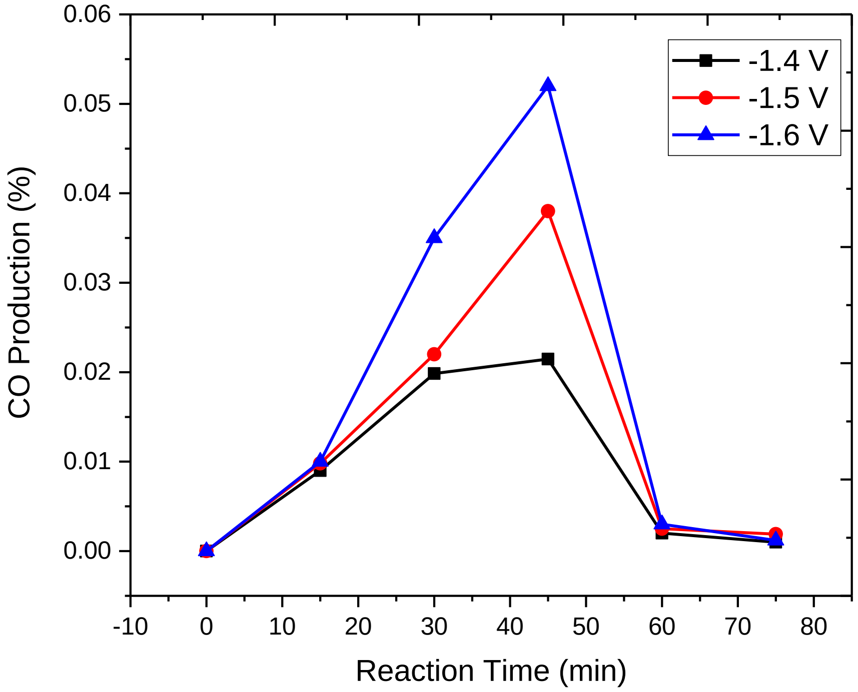

Figure 38. CO production in 3 different potentials during reduction of CO_2 in the two-compartment cell

3.2.2 Ag sputtered Titania nanotube

To investigate the performance of the prepared Ag-based electrocatalyst, chrono amperometry test has been done in the conditions mentioned in table 7. Figures 39-42 are presenting the results of complete analysis of Titania nanotubes being sputtered with Ag for different applied currents with different deposition time. Furthermore, the effect of pressure and a thorough electrochemical analysis have been discussed in the following sub sessions.

3.2.2.1 Different sputtering conditions

As can be seen in Figure 39 the results of chrono amperometry test of Titania nanotubes being sputtered in different applied currents with the same deposition time of 90s are illustrated. It is noteworthy to mention that these tests have been carried out in three different applied potentials as stated in table 7. The more detailed analysis of these tests has been presented in the appendix (Figure A-3).

Evidently, as mentioned before Ag is the main responsible electrocatalyst for CO_2 reduction to CO. Thus, the most general trend in the results can be defined as follows; by increasing the amount of Ag, which in fact is due to increase in sputtering applied current, more CO will be produced. In another word, higher Ag results in higher CO production. Also increasing the applied potential pushes the reactions' tendency toward HER instead of CO_2 reduction. Furthermore, regardless of the amount of Ag nanoparticles, current density is almost the same for all the electrocatalyst at each potential. The only deviation from the above-mentioned trend happened at -1.6 V in which the best performance does not belong to the electrocatalyst with higher Ag loading. In fact, the 60mA90s sample, presents a maximum of both CO production and selectivity and, at the same time, a minimum of the H_2 production and current density. In particular, at -1,6 V it is also evident that the trend of H_2 production rate, H_2 faradaic efficiency and current density are similar. This suggests that a higher current can be correlated to an increase in hydrogen evolution and to a decrease in CO selectivity, which is confirmed by the CO/H_2 ratio graph. This result suggests that although higher amount of Ag should result in higher CO but there are other morphological parameters other than just the amount of Ag which effect the performance of Ag-TNT electrocatalyst. Based on these results 60mA 90s seems to be the optimum conditions for Ag sputtering on TNT for this purpose.

It is notable that the sum of the faradaic efficiencies of the gas products was in average 97-99 %, depending on the silver loading. In fact, such value slightly increased with the amount of silver, nonetheless it presents fluctuations (± 1 %) due to the combination of experimental errors and various variables involved in the calculation. The average difference between the gas products FE and the overall FE, which is about 1-3 %, can be attributed to the production of small amounts of liquid products. This justification is confirmed by the HPLC analysis of the solution of the following longer tests, which revealed the presence of formic acid (Figure 40).

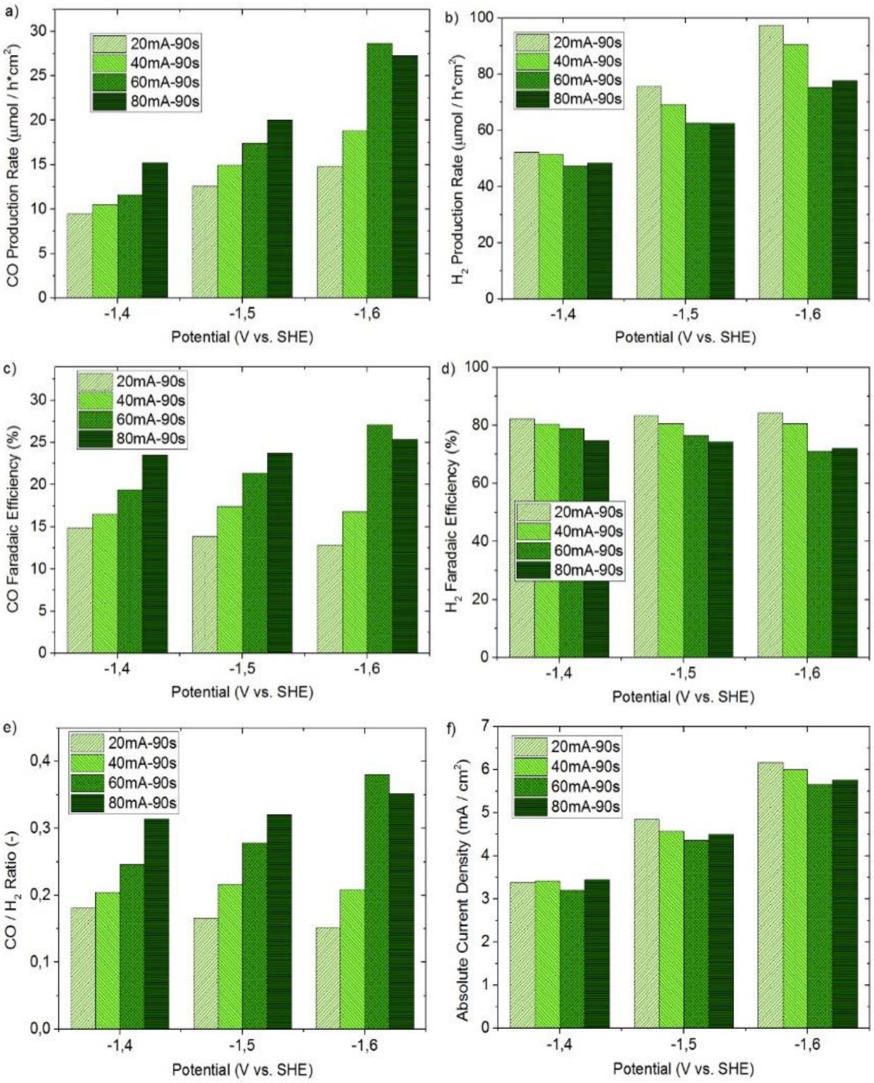

Figure 39. Comparison between the results (vs. potential) of catalysts with the same sputtering time and different sputtering current (90 minutes of test at each potential): a,b) CO and H_2 production rates, c,d) CO and H_2 faradaic efficiencies, e) CO/H_2 ratio, f) absolute current density.

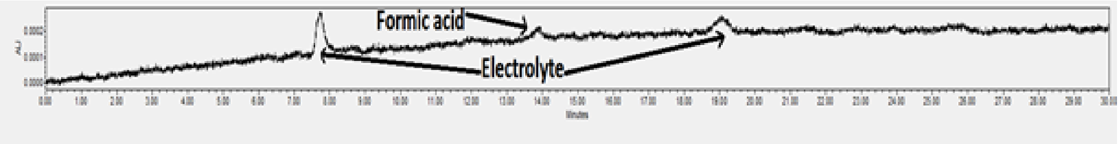

Figure 40. HPLC chromatogram of the solution after a test (sample: 60mA-90s) The peaks for electrolyte correlate with water and bicarbonate.

To investigate whether a longer sputtering treatment leads to a better performance, the results obtained with a 60mA120s sputtered sample has been compared to those of the 60mA90s electrode. The comparison of the final results at each potential is shown in the Figure 41, while the complete curves vs. time are reported in the appendix (Figure A-4).

The sample sputtered for longer time (120 s) behaved better at the lowest potential and worse at the higher potentials, than the 60mA-90s catalyst. That is more explicit from CO faradaic efficiency graph, where the selectivity increased for the 60mA-90s and decreases for 60mA-120s electrode by increasing the potential. The H_2 faradaic efficiency slightly presented a reversal trend, so that in CO/H_2 ratio the trend of the CO faradaic efficiency is accentuated. The H_2 production and current density graphs are rather regular, with 60mA-120s, always presenting a higher value and with values that increased at higher applied potentials. As a matter of fact, the best result obtained in these first tests was still that of the 60mA-90s electrode at -1,6 V vs. SHE. Therefore, this catalyst and the related sputtering conditions has been chosen as the best/reference electrocatalyst in the following experimental activities.

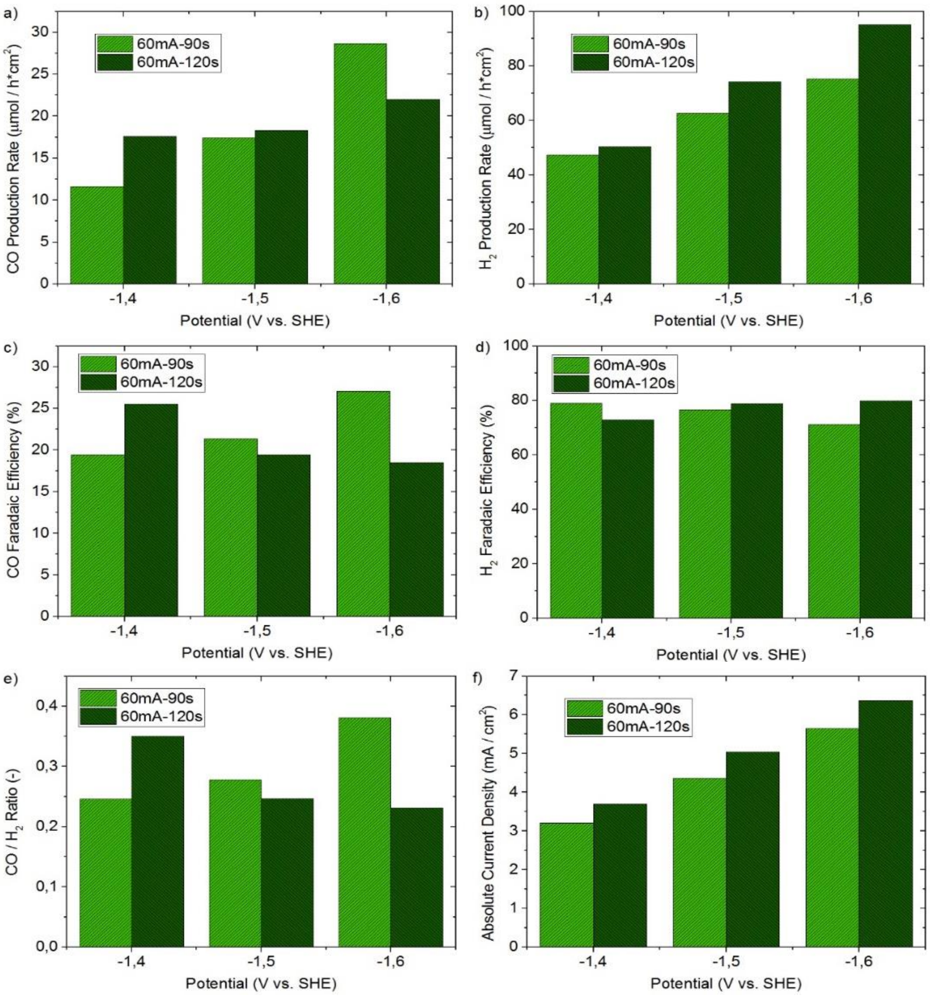

Figure 41. Comparison between the results (vs. potential) of catalysts with the same sputtering current and different sputtering time (90 minutes of test at each potential): a,b) CO and H_2 production rates, c,d) CO and H_2 faradaic

Furthermore, to measure the maximum current density which can be achieved by the electrocatalyst, one should remove all the barriers which prevents the electrons to pass through from the surface of the catalyst to electrolyte and finally reduce the dissolved CO_2. The major barrier to this phenomenon is mass transfer diffusion resistance in electrolyte. One way to minimize this effect is to use rotating disk as working electrode. As the disk turns, some of the solution described as the hydrodynamic boundary layer is dragged by the spinning disk and the resulting centrifugal force flings the solution away from the center of the electrode. Hence, solution flows up, perpendicular to the electrode, from the bulk to replace the boundary layer. The sum result is a laminar flow of solution towards and across the electrode. The rate of the solution flow can be controlled by the electrode's angular velocity and modeled mathematically. This flow can quickly achieve conditions in which the steady-state current is controlled by the solution flow rather than diffusion [160]. This is a contrast to still and unstirred experiments where the steady-state current is limited by the diffusion of species in solution. For this reason, an LSV (linear sweep voltammetry) has been done in a RDE with 1600 rpm using TNT/Ag 60mA90s in the same electrolyte of $KHCO_3$ 0.1M. Initially, LSV test has been done with N_2 bubbling and then the electrolyte has been saturated by CO_2 and the same test has been repeated. As can be seen in Figure 42, a higher onset potential can be noticed when CO_2 reduction is happening which can be as a result of formation of $CO_2^{-\cdot}$ radical, which has its own kinetical barrier compared to the process with the tests under the N_2 flow for which only HER (blue line) should happen. But when the applied potential increases the current density increases drastically with respect to the test with N_2 bubbling. This difference in current can be attributed to CO_2 reduction reaction (CO_2-RR). It is noteworthy that the highest current density for CO_2 reduction achieved at -1.6V vs SHE was of -65 mA/cm^2. Thus, due to the abovementioned advantages of RDE's, the obtained current density with RDE were higher than those obtained with static electrodes.

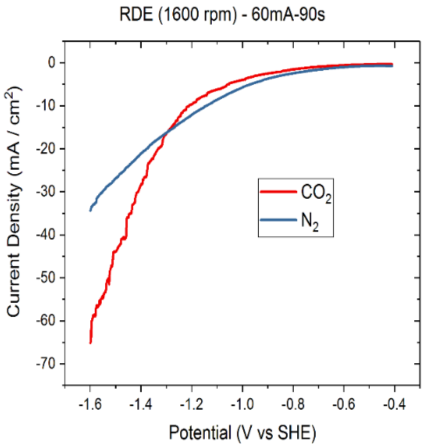

Figure 42. LSV test in RDE for Ag/TNT 60mA-90s with N_2 bubbling (blue) and CO_2 bubbling (red)

3.2.2.2 Pressure effect

Another parameter which can affect the performance of electrocatalyst in CO_2 reduction is pressure. Due to low solubility of CO_2 in aqueous media, lowering the temperature and increasing the pressure can increase its solubility and as a result higher feedstock for production rate of products. For this purpose, decreasing the temperature is not an option because it effects the kinetics of the reaction by reducing the reaction rate for CO_2 reduction. In another hand, although increasing the pressure can increase the solubility and production rate of the products but maintaining the reaction to take place in a high pressure has its own challenges naming; proper fitting and proper reactor which can handle high pressures. Hence, the high capital cost is the major drawback for this process.

To investigate this effect a test at higher pressure has been performed with the 60mA90s electrocatalyst and the results are compared with the test performed at atmospheric pressure under similar conditions (Figure 43). Also, complete curves vs. time are reported in the appendix (Figure A-5).

It is evident from the results that CO production drastically increased at 7 atm. Indeed, at -1,4 V vs SHE this value was more than doubled if compared to the one obtained at atmospheric pressure. Nevertheless, this effect is far more evident at the lowest potential and the difference between two CO productions decreased by increasing the potential. An explanation can be find in the dissolved CO_2 values, since the saturation value (2280 mg/l) was increased by more than 40 % at 7 atm with respect to the corresponding value at atmospheric pressure. In other words, the maximum difference of dissolved CO_2 (which is an indication of CO_2 participating in the electrochemical reduction) registered during the test, with respect to the initial value, is higher at 7 atm (13 % at 1,6 V vs. SHE and 7 atm; with respect to 8 % at 1 atm). Moreover, the decrease in selectivity, by increasing the potential, can be attributed to the fact that at higher applied potentials HER reaction becomes the dominant one instead of CO_2 reduction and as a result, it makes the effect of higher reactant concentration, less important. Also, the H_2 production was higher at 7 atm and, instead, in this case the difference becomes larger by increasing the potential. As a matter of fact, considering CO faradaic efficiency, it can be noticed that at 1 atm the CO selectivity increased with the potential, while at 7 atm it decreased to a lower value than the one at 1 atm. Probably the reason behind the latter is that, as mentioned before, the percentage decrease of CO_2 dissolved is higher at 7 atm; thus, at the highest applied voltage, the reactant concentration is proportionally lower (with respect to the saturation value) at high pressure. The H_2 follows exactly the reversal trend and, as a result, in the CO/H_2 ratio the trend is accentuated. The current density was always higher at 7 atm and, obviously, it increased with the applied potential.

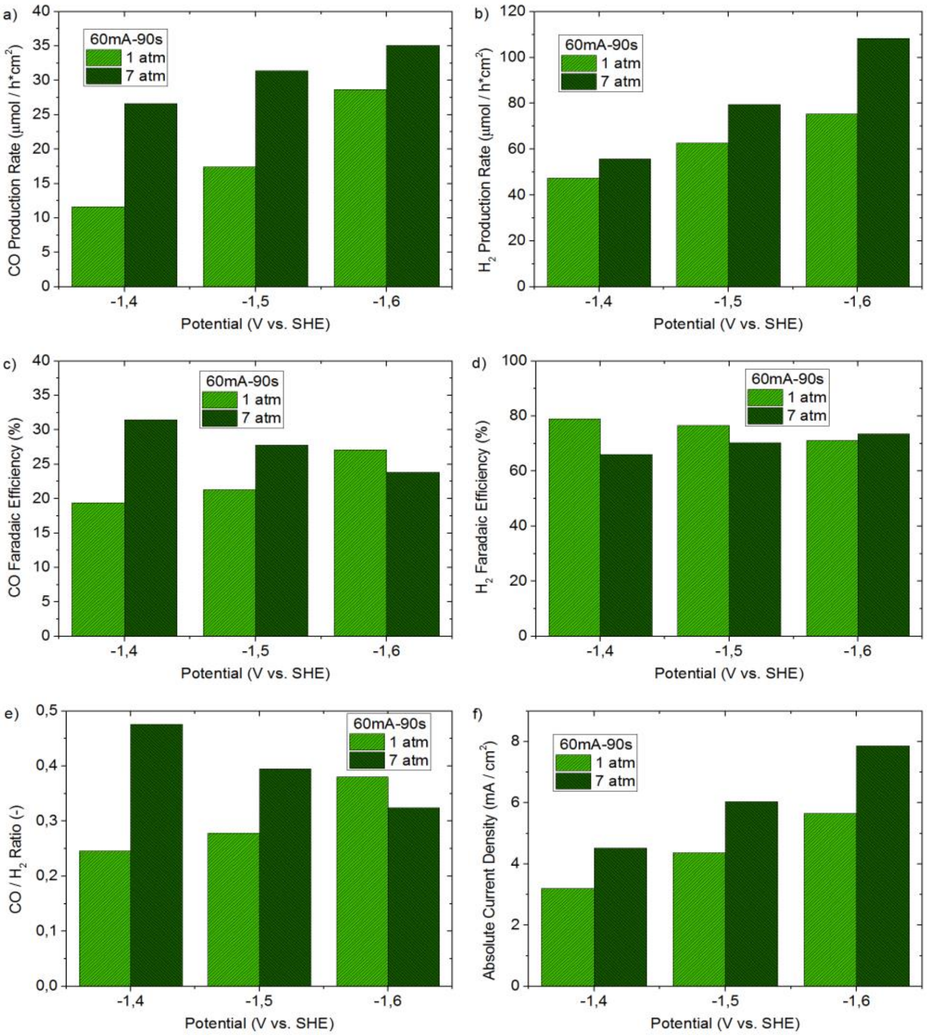

Figure 43. Comparison between the results (vs. potential) of 60mA90s tested at two different pressure values (90 minutes of test at each potential): a,b) CO and H_2 production rates, c,d) CO and H_2 faradaic efficiencies, e) CO/H_2 ratio, f) absolute current density.

3.2.2.3 Stability analysis

One of the most important parameter in performance analysis of a catalyst is stability test to find out the durability of its performance and in many cases to find out the reasons for a decay in the activity performance of such catalyst to be able to eventually improve it. To do so, a CA test for 21 hours has been carried out for the best electrocatalyst among the above-mentioned ones (60mA90s). The results showed a decay for CO production and increase in H_2 production after a peak of production within the first 3 hours which clearly signals a deactivation of electrocatalyst over the time which pushes the reaction toward HER instead of CO_2-RR. The details of these experiment can be found in the appendix (Figure A-6). The analysis for this deactivation has been discussed in the following by surface qualitative and quantitative analysis.

The Primary analysis to investigate this issue would be the surface analysis. Thus, to study the effect of coverage of Ag nanoparticles on electrochemical active surface area of the catalyst, a measurement based on double-layer capacity has been carried out. The goal for this analysis is to compare electrochemical active surface area of each electrocatalyst before and after reaction. The context of this method is based on the storage of electrical energy by means of electrical double layer effect. This effect can be distinguished on a conductive electrode and adjacent liquid electrolyte. In fact this is the zone in which the two layers of ions are separated by a single layer of solvent molecules that adheres to the surface of the electrode and acts like a dielectric in a conventional capacitor [157].

Usually to measure electrochemically active surface area (ECSA), voltammetric curves are needed to be recorded in the mere double layer region at various scan rates and then a plot of the current in the middle of the potential window vs. scan rate should be constructed and the slope of this linear line is an indicative ratio of ECSA of the catalyst as follows [158]:

$$i = dQ/dt = (dQ/dE) \cdot (dE/dt) = C \cdot V \qquad (20)$$

ECSA can be calculated by referring the obtained capacity to the reference value of capacity per the unit area (Cref);

$$ECSA = C / Cref \qquad (21)$$

Hence, with this method by comparing the slope of the current vs. scan rate in the double layer capacity zone, the ratio of ECSA for different catalysts can be distinguished. As can be seen in Figure 44, ECSA trend among the fresh catalysts considered to be that, higher Ag resulted in higher active surface for electrocatalytic activity of Ag nanoparticles and indeed these differences among higher Ag loading (60mA-90s and 80mA-90s) are less significant. On the other hand, after 4 hours of reaction, the trend is not the same anymore. The 60mA90s sample has shown to have higher ECSA than all the other samples even the 80mA90s sample. These results also can justify the higher productivity of 60mA90s at higher potentials (-1.6V) and its durability during the reaction which started at -1.4 V vs. SHE and continuously the potential increased up to -1.6V (Figure 41).

A possible reason for the reduction on the ECSA of most samples could be the loss of Ag nanoparticles from the surface of catalyst. To investigate this hypothesis Ag loading of the surface of TNT has been measured before and after the reaction (Figure 46). It is worth mentioning that this measurement has been done by EDS. Using EDS for this analysis is a bit tricky cause Titania nanotubes are synthesized on Ti foils and Ti foil do not act as a co-catalyst in the reaction. So, to be able to achieve measuring the right Ag loading on only Titania nanotubes, initially we should find out the right intensity of beam in which the depth of measurement would be equal to Ag layer plus Titania nanotubes and avoiding the dispersion of cone in to Ti substrate. To achieve this goal different measurement have been taken in different beam intensity in such a way that molar composition of Ti to O remained 1 to 2. Increasing the beam means formation of bigger cone and by increasing continuously the intensity, at a certain point the molar ratio of Ti to O is not 1 to 2 anymore because the cone passed Titania nanotubes and measuring Ti in both nanotubes and substrate. That point can indicate us up to which beam intensity we can cover the measurement for electrocatalyst composition and not the substrate (Figure 45).

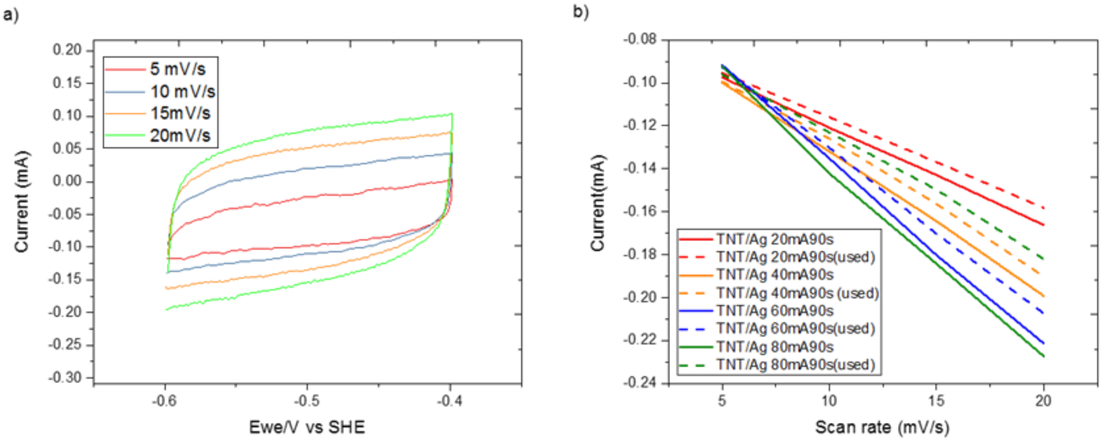

Figure 44. Cyclic voltammetry in different scan rates at double capacity layer b) ECSA ratio for different catalyst before and after the reaction

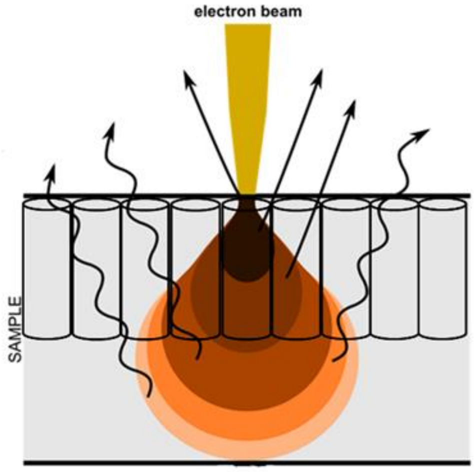

Figure 45. Schematic of cone formation of EDS beam based on applied beam intensity

Evidently, it is clear form Figure 46 that some Ag particles were being spread through the electrolyte during the reaction. The existence of Ag particles has been confirmed by ICP analysis. It is evident that the percentage loss of Ag nanoparticles from the surface of catalyst is higher in lower Ag loading (20mA90s and 40mA90s) which also can describe the decrease in the activity and ECSA of electrocatalyst.

But this trend is not clear for higher Ag loading (60mA90s and 80mA90s). Another reason to the loss of activity and ECSA of the catalyst seems to be the agglomeration of Ag nanoparticles which then causes lower active surface area of nanoparticles. The possible proposed reasons for this agglomeration seems to happen due to the difference in charge of Ag particles with different sizes. In another word, the larger particle has a partial negative charge and the smaller particle a partial positive charge at electrical equilibrium, due to the greater work function of the larger particle. At the surface of electrocatalyst the larger nanoparticle accepts an electron from a neighboring smaller particle through the conducting substrate. In this moment smaller nanoparticle becomes more positively charged and reestablishes equilibrium by dissolving an Ag^+ ion into solution [15] (Figure 47). This phenomenon results in agglomeration of bigger Ag particles and dissolution of smaller Ag nanoparticles.

These agglomerations seem to be more significant for higher Ag loading as a result of higher amount of Ag nanoparticles in the vicinity of each other and resulted in lowering the activity and durability of the 80mA90s sample.

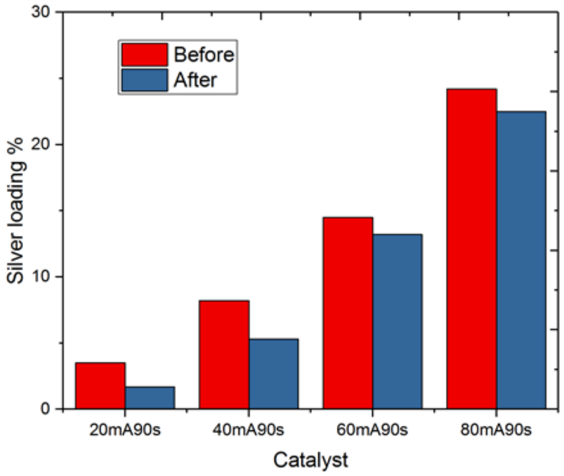

Figure 46.Ag loading for different catalyst before and after the reaction

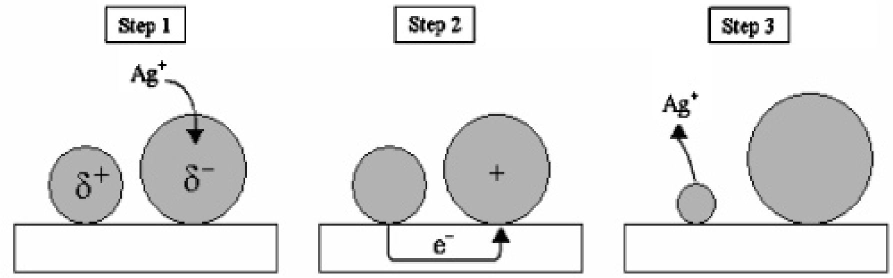

Figure 47. The schematic of agglomeration and dissolution mechanism of smaller Ag nanoparticles to bigger ones. With permission from [15]

In FESEM images which were taken after the reaction of the above mentioned electrocatalyst, the reshaping and agglomeration of Ag particles are evident. As can be seen in Figure 48, some of Ag nanoparticles are attached to each other and agglomerated in a huge cubic form. Others simply just detached and scattered in different part of the surface. For further analysis of this phenomenon TEM analysis has been done before and after the reaction for 60mA90s. These analyses also confirmed the destruction and reshaping of Ag nanoparticles. Scattering and reshaping of these particles, apart from disorientation of surface, also caused some Ag particles to fall from the surface of nanotubes in to the inner part of the tubes (Figure 49 & 50). This seems to happen to Ag particles which didn’t agglomerated during the repositioning and reshaping due to a non-completely uniform charge transfer.

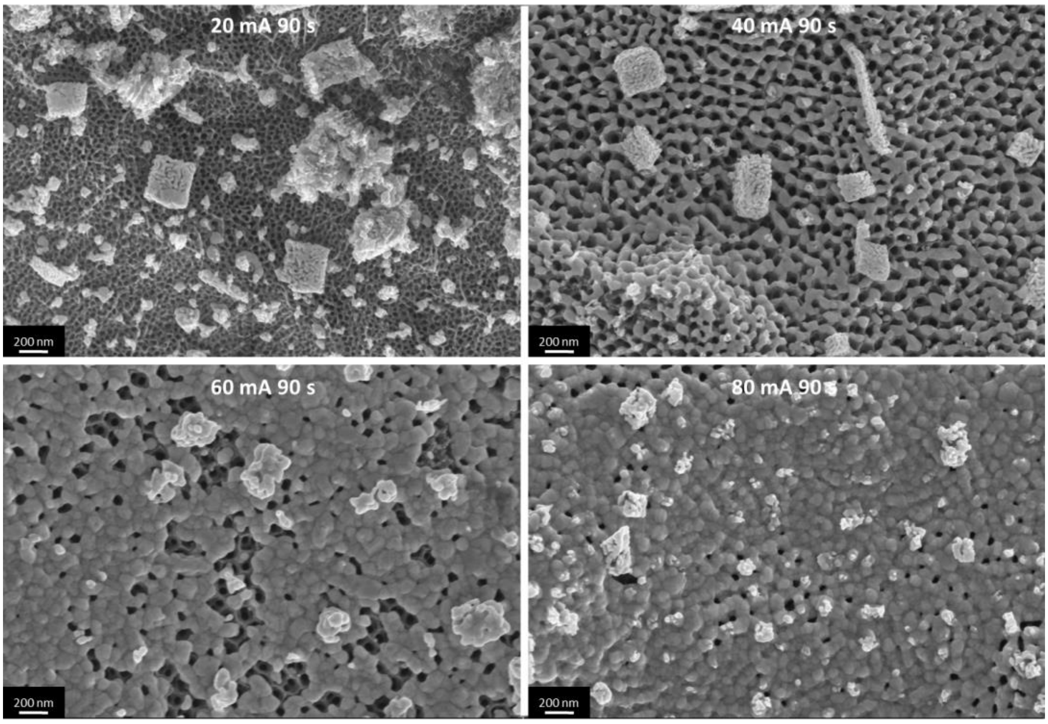

Figure 48. FESEM top view images of different catalysts after 4 hours of reaction

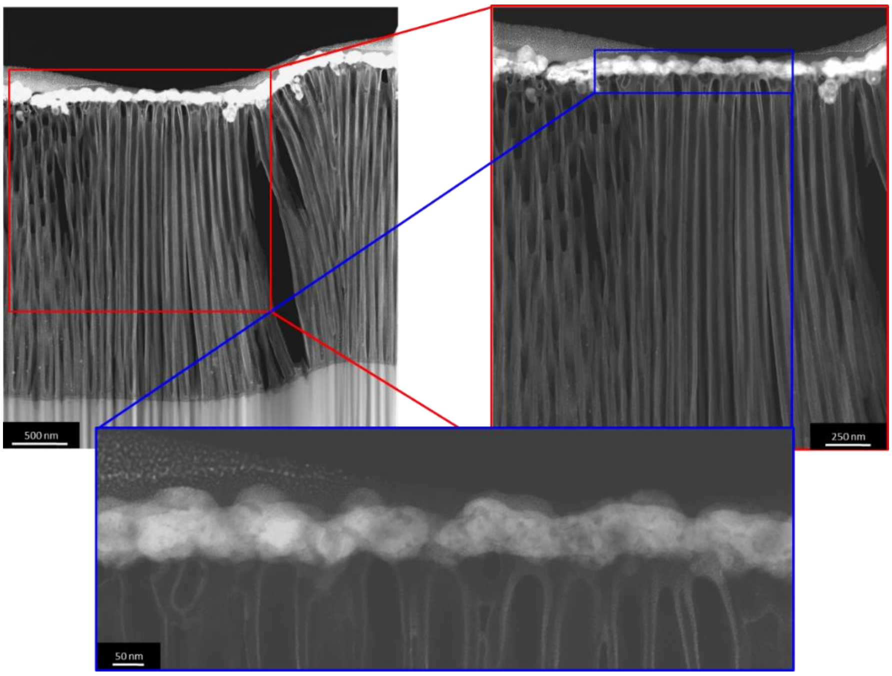

Figure 49. TEM side view image of 60mA90s before the reaction

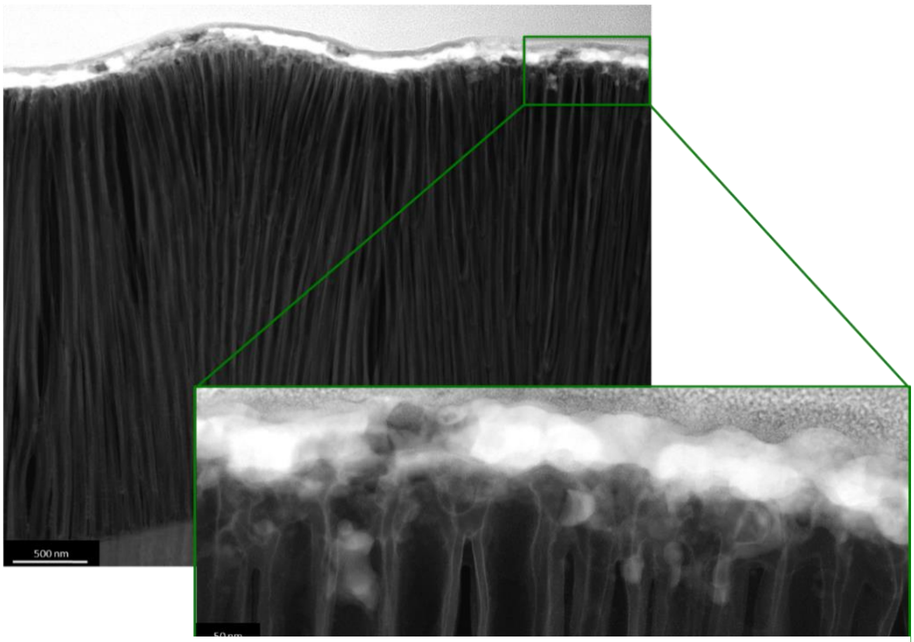

Figure 50. TEM side view image of 60mA90s after the reaction

3.2.3 The role of Titania nanotubes

To investigate the effect of Titania nanotube which has been used as the substrate for Ag nanoparticles in CO_2 reduction, different quantitative and qualitive tests have been done. To have a comparable result, in these experiments the best sputtering conditions which previously showed to be 60mA 90s, has been used for all the catalyst to maintain the Ag nanoparticle loading in different electrocatalyst and only changing the substrate. Electrocatalysts which has been used in this session for comparison are as follows;

1) Ag / TiO_2 nanotubes;
2) Ag / Ti foil;
3) Ag / TiO_2 nanoparticles;
4) TiO_2 nanotubes;
5) Ti foil.

To do a thorough analysis on the role of Titania nanotubes, initially CA test has been done for the above mentioned electrocatalysts. Then, for further analysis and to justify the results of CA tests, ECSA and CV tests have been carried out. In table 8 the experiment conditions of CA for these electrocatalysts has been presented.

As for the CA tests, these experiments were performed at three different increasing potentials, for 90 minutes at each potential (conditions mentioned below in table 8). The final results vs. potential are reported in Figure 51; while the complete curves vs. time are in the appendix (Figures from A-7 to A-10).

Before analysing the performance of these electrocatalyst it is evident from Figure 51 that Titania and Titanium foil solely cannot act as an electrocatalyst for CO_2 reduction and that’s why the graph of solely Titania nanotube and Titanium foil are overlapping at zero for the production of CO. Moreover, it is clear from CO production graph (Figure.51-a) that Ag/TNT behaves better than the other samples; indeed, its CO production rate was the highest at every potential value and increased by rising the potential. On the other hand, the other Ag-containing samples, using Ti foil or TNP as a support, showed a decreasing CO production rate when the potential was increased. This difference suggests that the change in morphology, supposedly induced on Ag nanoparticles due to the applied potential, could be more critical in the case of electrodes having Ti foil or TiO_2 nanoparticles as the support. It is possible that the change in the Ag morphology, reduces the catalyst specific surface due to the formations of bigger silver clusters as described in the previous sub-session. However, the performance of the Ag/TNP sample was initially higher than that of Ag/Ti foil, though it decayed faster with the potential. A possible reason is that the adherence force of Ag nanoparticles to Titania nanoparticle layer is less resistant to high potentials than in the case of the TiO_2 nanotubes or Titanium foil, thus, it undergoes through some kind of deterioration.

In addition, evidently from H_2 production rate and current density graphs, the sample Ag/TNT produced less Hydrogen than the others, although the hydrogen production also increased with the potential, as expected. A similar behaviour was presented by Ag/Ti foil sample, but the H_2 produced was higher and the difference with respect to the Ag/TNT sample increased with the applied potential. The current density obtained with the Ag/Ti foil, instead, was lower than that of Ag/TNT, probably because of the small superficial area due to the lack of nanostructured arrangements. On the other hand, for Ag/TNP the situation is completely different: both H_2 production and current density rapidly increased with the potential. This could be due to the fact that the nanoparticles' layer was about 30 times thicker than the nanotubes layer (only 4 µm), and, therefore, with respect to the layer thickness, the percentage of Ag coverage in Ag/TNP is less than the one in Ag/TNT. Moreover, lower current density of Ag/TNP compared to Ag/TNT sample at -1,4 V vs. SHE could be explained by the inter-crystalline contacts of nanoparticles that increase the electrical resistance [159]. Instead, at higher potentials, the effect of higher available surface area could be dominant in accordance with the faradaic efficiency values for the H_2 production which are close to 100 %.

The selectivity for CO decreased with the applied potential for all samples, but with different rates. Among the tested electrodes, Ag/TNT is assuredly the best, nevertheless the trend for hydrogen production is not exactly in accordance with respect to that observed in previous experiments. This is possible because of the difference on the range of applied potential. In another words, because of resistance compensation in these tests the real applied potential is higher and can push the reaction toward HER. Moreover, the H_2 faradaic efficiency graph confirmed the fact that the TiO_2 nanotubes are able to form traces of liquid products, since there is a difference of 1-2 % between the faradaic efficiencies of TNT and Ti foil (the latter approximately correspond to 100 %). A further observation should be dedicated to the Ag/Ti foil, which shows a good CO production and selectivity and suggests that the sputtering method is a valuable deposition method, since it can activate the flat surface of a metal foil with Ag nanoparticles, by using a small amount of silver.

Table 8. Experimental scenario of the chronoamperometry tests[2]

Parameter	**Value**
Temperature	24 °C (average)
Pressure	1 atm
Electrolyte (aqueous solution)	$KHCO_3$ 0,1M (67 ml)
Potentials (with IR compensation)	-1,4 / -1,5 / -1,6 V vs. SHE
CO_2 flow rate	38 ml/min
Stirring	400 rpm
Electrode geometric area	2,4 cm^2

---

[2] It is noteworthy that although the nominal values of applied potential were the same as used before, but by using the IR compensation (software compensation, 85 %) the real potentials applied in these experiments were higher. The measured electrical resistance between reference electrode and cathode was 27 Ω, while the total cell resistance was of 41 Ω. Besides, the cell used in these tests is smaller and does not contain a membrane for the separation of anodic and cathodic chambers, thus presenting a lower electrical resistance; This, together with the higher applied potentials, implies that higher current densities and production rates were obtained with respect to the tests performed in previous session and suggests that a direct comparison between results, obtained in the two different cells at the same nominal potential, shall not be made.

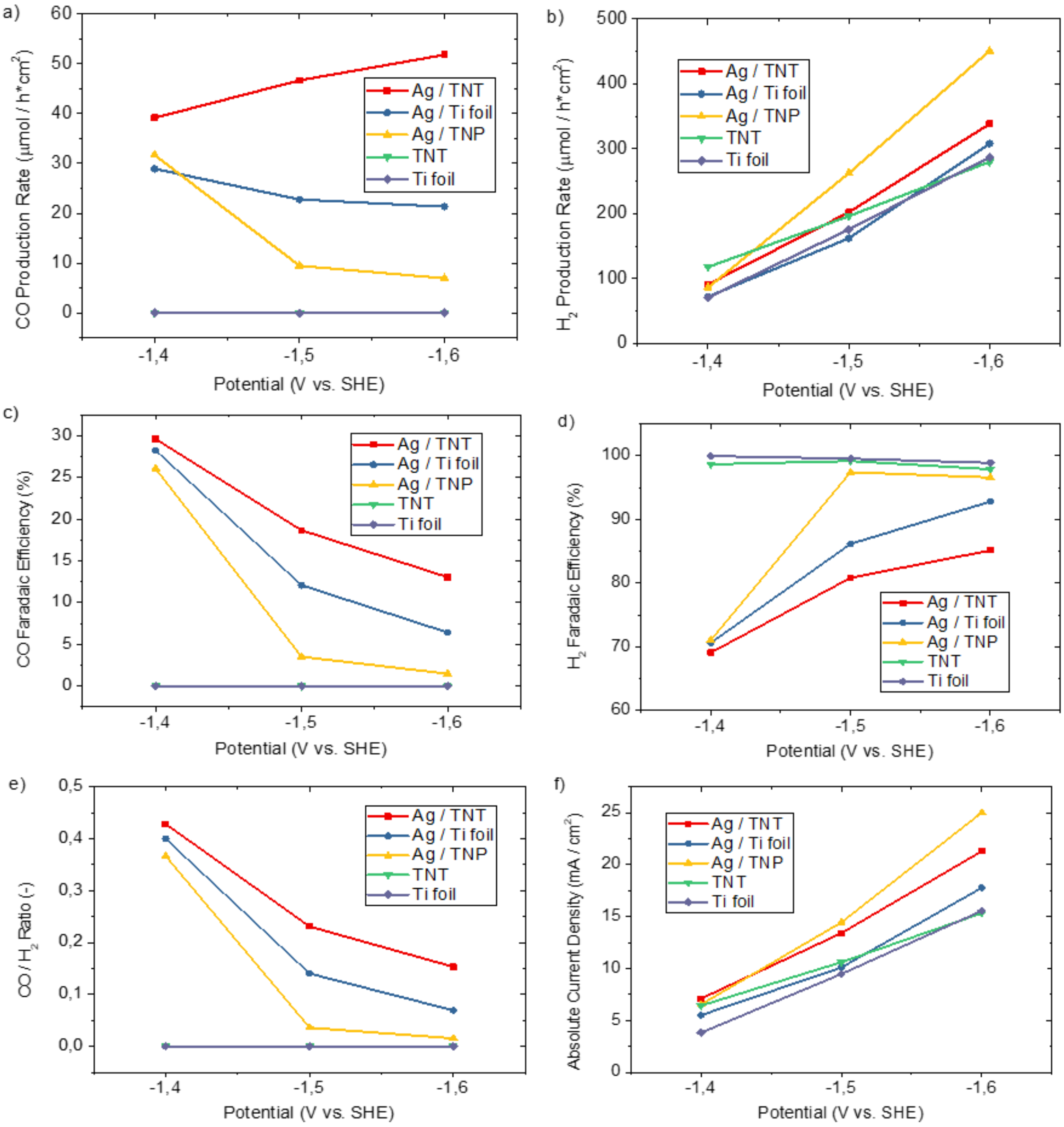

Figure 51. Comparison between the results (vs. potential) of silver on titania nanotubes and blank samples (sputtering conditions: 60 mA and 90 seconds): a,b) CO and H_2 production rates, c,d) CO and H_2 faradaic efficiencies, e) CO/H_2 ratio, f) absolute current density. All the potentials were applied with IR compensation

To investigate more the effect of Titania nanotube as a substrate, an Electrochemical Impedance Spectroscopy (EIS) test has been done. In this method a perturbative characterization of the dynamics of an electrochemical process has been carried out. Evidently this method consists of analyzing the response of an electrochemical system (cell) to an applied potential. The frequency dependence of this impedance can reveal underlying chemical processes [160]. These measured values contain information about electrical resistances, any contact resistance between the electrolyte and electrode, and any mass transport losses, so lower the resistance, lower is the contact resistance and mass transport losses through the electrochemical reaction. At first glance, it appears that the impedance related to Ag/Ti foil sample is quite larger with respect to the other two samples, in agreement with the results discussed above. In addition, also the shape of the spectrum in the low frequency region is quite different. In fact, usually the typical spectrum of an electrode immersed in an electrolytic solution during an electroreduction process is characterized by a high frequency feature (*i.e.* a leftmost arc). So, the process at high frequencies is related to the faster process, *i.e.* charge transport in the electrode bulk. Then, the lower frequency arc is related to the slower process, *i.e.* charge transfer at the electrode-electrolyte interface, which could account for the Warburg diffusion [161]. The high frequency process, which is related to the extent of the electroreduction can be modeled through a parallel between the charge transport resistance R_1 and the double layer capacitance C_1, while the low frequency one, which accounts for the mass transport limitations, can be modeled through a Warburg impedance, characterized by the resistance R_2; the series resistance R_s models the ohmic losses (Figure 52a) [162]. It is noteworthy that for the mass transport limitation a Warburg Short element has been used. This element is the extension of Warburg element to represent the finite length diffusion, *i.e.* where no bulk electrolyte condition is present in the analyzed system [163]. The equivalent circuit composed by these elements was used to fit the experimental impedance data: the fitting procedure was proved to be good for the electrode based on titanium oxide (see the solid curves in Figure 53), while gave origin to not reliable results when used for Ti foil-based electrode.

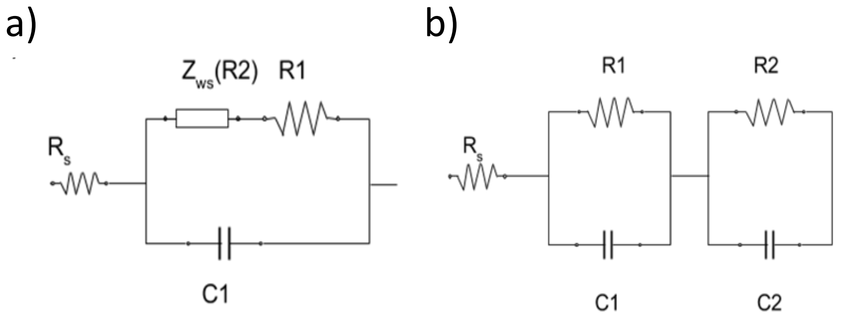

Figure 52. The schematic of applied circuit for EIS fittings: Circuit used for a) Ag/TNT and Ag/TNP b) Ag/Ti foil. Zw_s represents the Warburg Short diffusion

The reason for the observed discrepancy can be attributed to the supposed capability of TiO_2 to stabilize the reaction intermediates which favors the CO_2 electroreduction: this characteristic is not evidenced in Ti foil, thus causing a double layer formation at the Ti/Ag interface, which limits the overall reaction. This hypothesis is supported by the fact that a good fitting can be obtained by substituting the Warburg impedance with a low frequency double layer process, characterized by a resistance R_2 and a capacitance C_2 (see Figure 52b): the curve calculated using this model is reported in Figure 53 (blue curve). The values of the resistances obtained through the fitting procedure are reported in the inset of Figure 53; as it demonstrates, Ag/Ti sample is characterized by larger resistances, and the low frequency process becomes the limiting step of the reaction. On the contrary, Ag/TNT electrode exhibits the lowest impedance, thanks to the fast electron path provided by mono-dimensional structuration.

The obtained results were successfully confirmed by the electrochemical active surface area measurements reported in Figure 54. It is supposed that the higher surface area exposed by the TiO_2 nanotubes, as well as the expected stabilization of the CO_2 reduction intermediates, resulted in a higher active surface area of the deposited Ag nanoparticles, which induced a lower electrons transfer resistance (see Figure 53-inset).

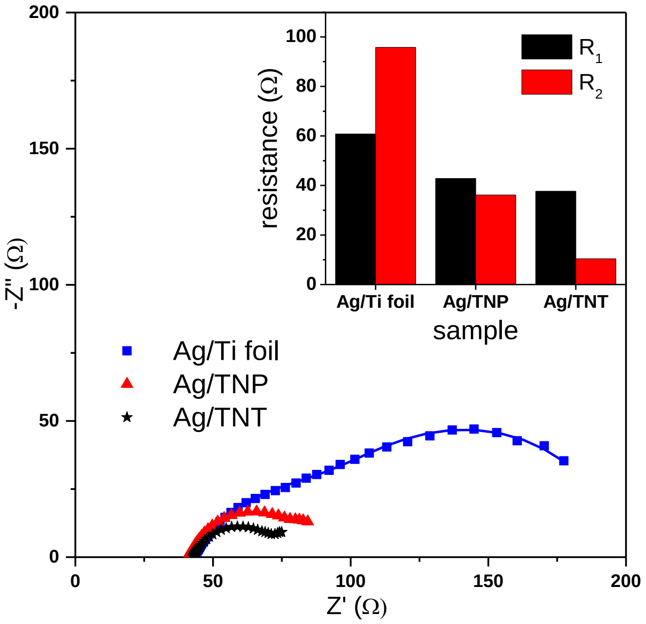

Figure 53. EIS analysis for 3 different substrates with the same Ag loading

Furthermore, as described before, ECSA ratio has been measured for the above-mentioned electrocatalysts by comparing the slope of the current vs. scan rate in the double layer capacity zone. It is evident that the slope for ECSA ratio for Ag nanoparticles being deposited on Titania nanotubes is by far bigger than the others. Thus, it can be concluded that Ag nanoparticles being deposited on Titania nanotubes have higher electrochemical active surface area than Ti foil and Titania nanoparticles. These analyses again confirm the role of Titania nanotubes as the substrate for Ag nanoparticles to improve the performance of electrocatalyst. This is due to the increase in the active surface area and stabilizing the rate determining radicals by facilitating the electron transfer route.

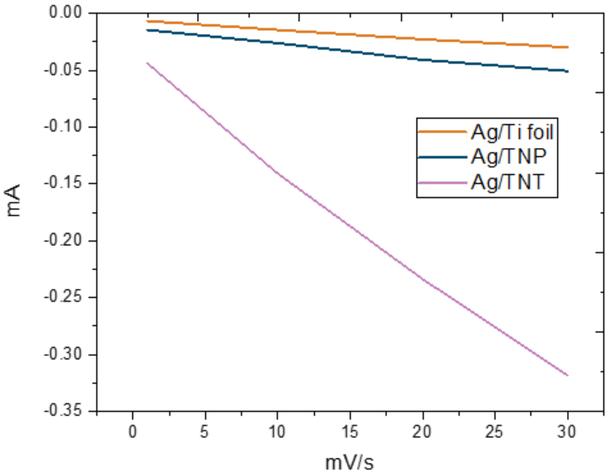

Figure 54.ECSA ratio measurement for different Ti substrate

Moreover, in order to understand the role of Titania nanotubes in the process of CO_2 reduction to CO by Ag nanoparticles, it is noteworthy to present the mechanism of CO_2 on Ag electrode; according to Kortlever *et. al*.[164] the reaction pathway for electroreduction of CO_2 to form CO on Ag electrodes consists of these steps:

$$CO_2(g) + *^{3} + H^+(aq) + e^- \leftrightarrow COOH^* \quad (22)$$

$$CO_2(g) + * + e^- \leftrightarrow COO^{-*} \quad (23)$$

$$COO^{-*} + H^+(aq) \leftrightarrow COOH^* \quad (24)$$

---

[3] The * sign represents the adsorption status on the surface of electrode

$$COOH^* + H^+(aq) + e^- \leftrightarrow CO^* + H_2O\ (l) \tag{25}$$

$$CO^* \leftrightarrow CO\ (g) + * \tag{26}$$

The first initial steps can occur either as a one-step Proton Coupled Electron Transfer (equation 22) or two step mechanism (equations 23, 24). In an interesting recent work Firet *et. al*. [165] confirmed these mechanism by monitoring the thin film Ag electrode by operando infrared spectroscopy. Based on this proposition by applying higher potentials the mechanism moves from one step PCET to two step reaction. In both high and low overpotential the formation of COO^{-*} ($CO_2{}^-{}_{ads}$) for CO production is very significant.

In addition, DFT calculations by Yangt *et. al*. [166] showed that the presence of Ag nanoparticles can substantially modify CO_2 adsorption on anatase TiO_2 (101). This calculation suggested that Ag particles affect the CO_2 adsorption on TiO_2 sites where there is no binding between CO_2 and the particle itself which can be described as a form of modification of properties of TiO_2 as it donates electron density to the surface [166]. In order to compare the above proposed mechanism with electrochemical behavior of Ag-decorated Titania nanotubes, a comparison of cyclic voltammetry of TNT/Ag and Ti/Ag with CO_2 bubbling has been done so one can differentiate the mechanism of CO_2 reduction. As has been shown in Figure 55, the major difference in CV between using Ti and TNT are the existence of the reduction peak of 1 and 3 which can be described as attributed to the reactions for Ti^{IV} in theTiO_2 and Ti^{III} species, thus can act as a redox electron carrier to facilitate some reactions, which include CO_2 reduction [167]. Also, the onset potential of CO_2 based on the comparison of CV's with Ar bubbling and CO_2 bubbling (Figure 42) can describe the point 2 as the onset potential for CO_2 reduction which in case of TNT happened in lower overpotentials compared to Ti co-catalyst. This description confirms the redox behavior of Ti^{IV}/Ti^{III} for $CO_{2\ ads}$. reduction to $CO_2{}^-{}_{ads}$ as a necessary rate determining step for CO_2 reduction to CO. This analysis of redox behavior of Titania and its role in the process of CO_2 reduction with the presences of Ag nanoparticle has been illustrated as described above in Figure 56.

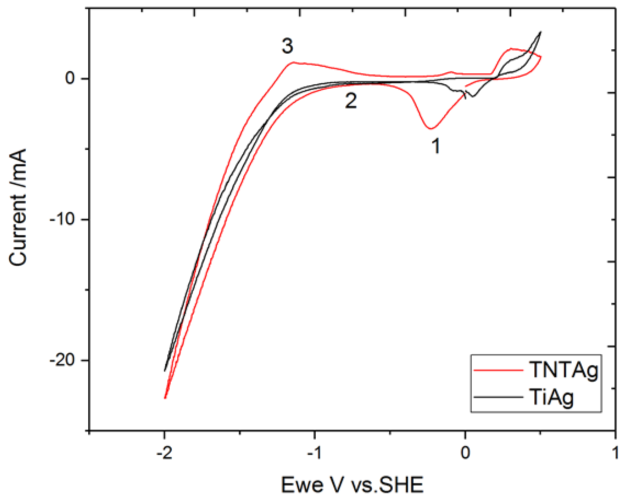

Figure 56. Cyclic voltammetry of Ti foil with deposited Silver (black line) and Titania nanotube deposited with Silver (redline)

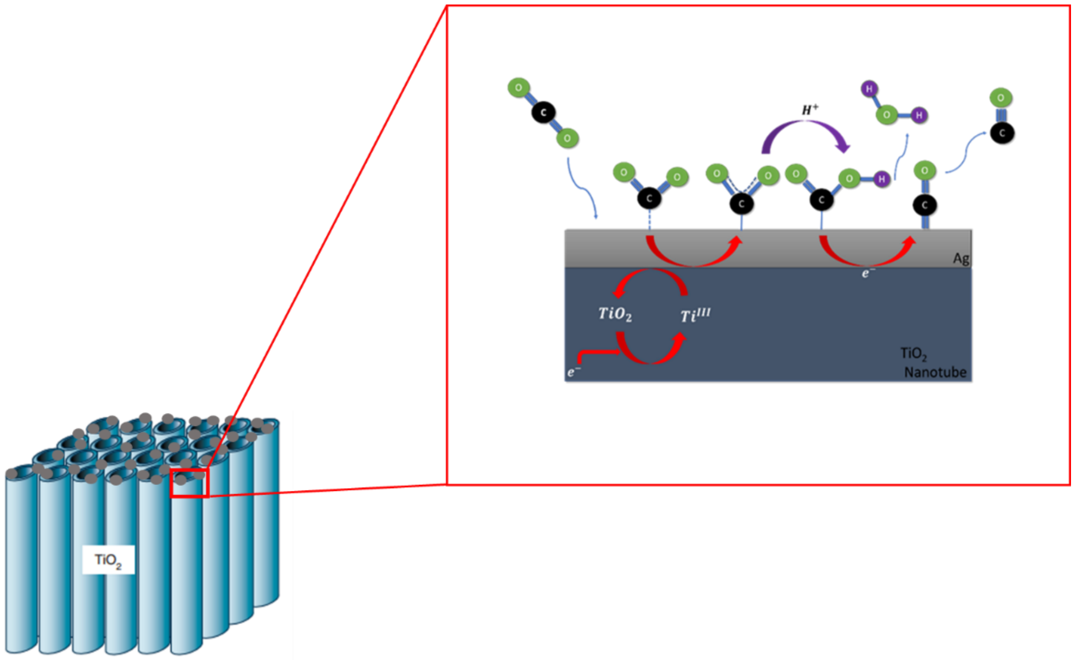

Figure 55. The schematic of the mechanism of CO_2 reduction over Ag-decorated Titania nanotube in aqueous electrolyte.

Conclusion

In this work electrocatalytic reduction of CO_2 to syngas by Ag decorated Titania nanotubes has been discussed. Among different possible noble metals which are being used recently as the electrocatalyst, Ag has been chosen in its nanoparticle structure. Also, Titania nanotubes have been selected as the Co-catalyst for this process. For the substrate synthesis, a modified anodization method has been used to grow well oriented compact Titania nanotubes on Titania foil. In addition, two approaches for the deposition of Ag nanoparticles have been carried out; Ag deposition by UV illumination and Sputtering. As for the UV deposition, different Ag loading achieved by changing time of illumination and concentration of Ag solution. These deposited electrocatalyst showed a very unstable behavior during the reaction due to dissolution of Ag particles into electrolyte and also agglomeration of Ag nanoparticles on the surface of electrolyte. On the other hand, sputtering method showed to be more adjustable for different Ag loading. The adjustments carried out by different applied currents and deposition times. Among different configuration of sputtered Ag on Titania nanotubes, the one sputtered at 60 mA with the deposition time of 90 seconds showed to have the best performance among the tested electrodes in which the maximum current density of 60 mA /cm^2 at cathodic potential of -1.6 vs SHE with the CO/H_2 ratio of 1 to 3 has been achieved. Furthermore, long duration tests showed a decay in the activity of the aforementioned electrocatalysts. Evidently, from morphological analysis of these electrodes before and after the reaction (TEM &FESEM) due to charge transfer during the process, a change on the structural shape of Ag in the form of agglomeration has been noticed. ECSA analysis of the tested electrocatalysts, also showed a decay on electrochemical active surface area ratio after the reaction due to the abovementioned phenomenon. Surprisingly, these analyses confirmed that high amount of Ag as the electrocatalyst not necessarily can result in better performance. In fact, morphological and structural parameters can also play an important role for the performance of these electrocatalysts.

Moreover, to investigate the role of Titania nanotubes, different samples with the same Ag loading and different substrates have been prepared and tested. The results showed the electrode with Titania nanotube as the substrate performed significantly better than the ones with Titania nanoparticles and Titanium.

Interestingly, further electrochemical analysis showed that Titania can act as a redox couple and help facilitate the transfer of electrons to Ag electrocatalyst and stabilize the rate determining radicals on the surface. Also, Titania in its nanotube form, showed to have the advantage of higher active sites and less resistance against mass transfer and electrical transportation in the double layer zone which again increased the overall performance of the electrode toward electrocatalytic reduction of CO_2. Although the novel application of Titania nanotube in this work showed to increase the performance of electrocatalyst and Ag as a noble metal used in low quantities respect to other reported experiments, but it cannot be considered as a persistent electrocatalyst for long lasting industrial processes. Also, the production rate of syngas is still far from the commercializing and industrial scales but being able to modify and increase the performance of the electrocatalysts, can open up new paths toward industrializing syngas production by electrocatalytic reduction of CO_2.

References

1. Hernandez, S., et al., *Syngas production from electrochemical reduction of CO2: current status and prospective implementation.* Green Chemistry, 2017. **19**(10): p. 2326-2346.
2. Jones, J.P., et al., *Electrochemical CO_2 Reduction: Recent Advances and Current Trends.* Israel Journal of Chemistry, 2014. **54**(10): p. 1451-1466.
3. Ma, S.C., et al., *Silver Supported on Titania as an Active Catalyst for Electrochemical Carbon Dioxide Reduction.* Chemsuschem, 2014. **7**(3): p. 866-874.
4. Delacourt, C., et al., *Mathematical Modeling of CO_2 Reduction to CO in Aqueous Electrolytes I. Kinetic Study on Planar Silver and Gold Electrodes.* Journal of the Electrochemical Society, 2010. **157**(12): p. B1902-B1910.
5. Delacourt, C., et al., *Design of an electrochemical cell making syngas ($CO+H_2$) from CO_2 and H_2O reduction at room temperature.* Journal of the Electrochemical Society, 2008. **155**(1): p. B42-B49.
6. Verma, S., et al., *The effect of electrolyte composition on the electroreduction of CO_2 to CO on Ag based gas diffusion electrodes.* Physical Chemistry Chemical Physics, 2016. **18**(10): p. 7075-7084.
7. Roy, P., et al., *TiO_2 Nanotubes: Synthesis and Applications.* Angewandte Chemie-International Edition, 2011. **50**(13): p. 2904-2939.
8. Houser, J.E., et al., *The role of viscous flow of oxide in the growth of self-ordered porous anodic alumina films.* Nat Mater, 2009. **8**(5): p. 415-420.
9. Dufek, E.J., et al., *Bench-scale electrochemical system for generation of CO and syn-gas.* Journal of Applied Electrochemistry, 2011. **41**(6): p. 623-631.
10. Hori, Y., et al., *Formation of hydrocarbons in the electrochemical reduction of carbon dioxide at a copper electrode in aqueous solution.* Journal of the Chemical Society, Faraday Transactions 1: Physical Chemistry in Condensed Phases, 1989. **85**(8): p. 2309-2326.
11. McCrory, C.C.L., et al., *Benchmarking Hydrogen Evolving Reaction and Oxygen Evolving Reaction Electrocatalysts for Solar Water Splitting Devices.* Journal of the American Chemical Society, 2015. **137**(13): p. 4347-4357.

12. Li, Y.C., et al., *Electrolysis of CO_2 to Syngas in Bipolar Membrane-Based Electrochemical Cells.* ACS Energy Letters, 2016. **1**(6): p. 1149-1153.
13. Kuhl, K.P., et al., *New insights into the electrochemical reduction of carbon dioxide on metallic copper surfaces.* Energy & Environmental Science, 2012. **5**(5): p. 7050-7059.
14. Roy, P., et al., *TiO_2 Nanotubes: Synthesis and Applications.* Angewandte Chemie International Edition, 2011. **50**(13): p. 2904-2939.
15. Redmond, P.L., et al., *Electrochemical Ostwald ripening of colloidal Ag particles on conductive substrates.* Nano Letters, 2005. **5**(1): p. 131-135.
16. Wu, K.N., et al., *Modeling and Experimental Validation of Electrochemical Reduction of CO_2 to CO in a Microfluidic Cell (vol 162, pg F23, 2015).* Journal of the Electrochemical Society, 2015. **162**(3): p. X6-X6.
17. Dufek, E.J., et al., *Operation of a Pressurized System for Continuous Reduction of CO_2.* Journal of the Electrochemical Society, 2012. **159**(9): p. F514-F517.
18. Pang, Y.L., et al., *A critical review on the recent progress of synthesizing techniques and fabrication of TiO_2-based nanotubes photocatalysts.* Applied Catalysis a-General, 2014. **481**: p. 127-142.
19. Gupta, N., et al., *Calculation for the cathode surface concentrations in the electrochemical reduction of CO_2 in $KHCO_3$ solutions.* Journal of Applied Electrochemistry, 2006. **36**(2): p. 161-172.
20. Kubacka, A., et al., *Advanced Nanoarchitectures for Solar Photocatalytic Applications.* Chemical Reviews, 2012. **112**(3): p. 1555-1614.
21. Roy, S.C., et al., *Toward Solar Fuels: Photocatalytic Conversion of Carbon Dioxide to Hydrocarbons.* Acs Nano, 2010. **4**(3): p. 1259-1278.
22. Demirbas, A., *Potential applications of renewable energy sources, biomass combustion problems in boiler power systems and combustion related environmental issues[*Progress in Energy and Combustion Science, 2005. **31**(2): p. 171-192.
23. Kelemen, P.B. and J. Matter, *In situ carbonation of peridotite for CO2 storage.* Proceedings of the National Academy of Sciences, 2008. **105**(45): p. 17295-17300.
24. Aresta, M., A. Dibenedetto, and A. Angelini, *Catalysis for the Valorization of Exhaust Carbon: from CO_2 to Chemicals, Materials, and Fuels. Technological Use of CO_2.* Chemical Reviews, 2014. **114**(3): p. 1709-1742.

25. *Syngas and Derivatives Market Trends: A Global Strategic Business Report*. [cited 2016 Sept. 22nd]; Available from: http://www.strategyr.com/MCP-7590.asp.

26. Zhang, K., et al., *Catalytic conversion of cellulose for efficient ethylene glycol production and insights into the reaction pathways.* Rsc Advances, 2016. **6**(81): p. 77499-77506.

27. Akhter, P., et al., *Environmental issues regarding CO2 and recent strategies for alternative fuels through photocatalytic reduction with titania-based materials.* Journal of Environmental Chemical Engineering, 2016. **4**(4, Part A): p. 3934-3953.

28. Zhu, W.L., et al., *Monodisperse Au Nanoparticles for Selective Electrocatalytic Reduction of* CO_2 *to CO.* Journal of the American Chemical Society, 2013. **135**(45): p. 16833-16836.

29. Bard, A.J.F., et al., *Electrochemical Methods: Fundamentals and Applications*. 2001: wiley.

30. B.P. Sullivan , et al., *Electrochemical and Electrocatalytic Reactions of Carbon Dioxide*. 1993: Elsevier B.V.

31. R.G. Lerner, G.L.T., *Encyclopaedia of Physics (2nd Edition)*. 1991: VHC publishers.

32. Kumar, B., et al., *Photochemical and Photoelectrochemical Reduction of* CO_2. Annual Review of Physical Chemistry, Vol 63, 2012. **63**: p. 541-569.

33. Lamy, E., et al., *Standard Potential and Kinetic-Parameters of Electrochemical Reduction of Carbon-Dioxide in Dimethylformamide.* Journal of Electroanalytical Chemistry, 1977. **78**(2): p. 403-407.

34. Hori, Y., et al., *Electrochemical Reduction of Carbon-Dioxide to Carbon-Monoxide at a Gold Electrode in Aqueous Potassium Hydrogen Carbonate.* Journal of the Chemical Society-Chemical Communications, 1987(10): p. 728-729.

35. Hu, B.X., et al., *Thermal, electrochemical, and photochemical conversion of* CO_2 *to fuels and value-added products (vol 1, pg 18, 2013).* Journal of Co2 Utilization, 2013. **2**: p. 64-64.

36. Rosen, B.A., et al., *Ionic Liquid-Mediated Selective Conversion of* CO_2 *to CO at Low Overpotentials.* Science, 2011. **334**(6056): p. 643-644.

37. Bang, J.H., et al., *Porous carbon supports prepared by ultrasonic spray pyrolysis for direct methanol fuel cell electrodes.* Journal of Physical Chemistry C, 2007. **111**(29): p. 10959-10964.

38. Sharma, S., et al., *Support materials for PEMFC and DMFC electrocatalysts-A review.* Journal of Power Sources, 2012. **208**: p. 96-119.
39. Zhou, F., et al., *Highly selective electrocatalytic reduction of carbon dioxide to carbon monoxide on silver electrode with aqueous ionic liquids.* Electrochemistry Communications, 2014. **46**: p. 103-106.
40. Hori, Y., et al., *Silver-coated ion exchange membrane electrode applied to electrochemical reduction of carbon dioxide.* Electrochimica Acta, 2003. **48**(18): p. 2651-2657.
41. Sastre, F., et al., *Efficient Electrochemical Production of Syngas from* CO_2 *and* H_2O *by using a Nanostructured* $Ag/g\text{-}C_3N_4$ *Catalyst.* Chemelectrochem, 2016. **3**(9): p. 1497-1502.
42. Lu, Q., et al., *A selective and efficient electrocatalyst for carbon dioxide reduction.* Nature Communications, 2014. **5**.
43. Subiao Liu, H.T., et al., *Shape-Dependent Electrocatalytic Reduction of* CO_2 *to CO on Triangular Silver Nanoplates.* J. Am. Chem. Soc, 2017. **139**: p. 4.
44. Tornow, C.E., et al., *Nitrogen-Based Catalysts for the Electrochemical Reduction of* CO_2 *to CO.* Journal of the American Chemical Society, 2012. **134**(48): p. 19520-19523.
45. F. Sastre , et al., *Efficient electrochemical production of syngas from* CO_2 *and* H_2O *using a nano-structured* Ag/C_3N_4 *catalyst.* Submitted, 2016.
46. Hatsukade, T., et al., *Insights into the electrocatalytic reduction of* CO_2 *on metallic silver surfaces.* Physical Chemistry Chemical Physics, 2014. **16**(27): p. 13814-13819.
47. Hara, K., et al., *Large current density* CO_2 *reduction under high pressure using gas diffusion electrodes.* Bulletin of the Chemical Society of Japan, 1997. **70**(3): p. 571-576.
48. Lu, Q., et al., *Nanostructured Metallic Electrocatalysts for Carbon Dioxide Reduction.* Chemcatchem, 2015. **7**(1): p. 38-47.
49. Ma, S.C., et al., *Carbon nanotube containing Ag catalyst layers for efficient and selective reduction of carbon dioxide.* Journal of Materials Chemistry A, 2016. **4**(22): p. 8573-8578.
50. Ronge, J., et al., *Monolithic cells for solar fuels.* Chemical Society Reviews, 2014. **43**(23): p. 7963-7981.
51. Osterloh, F.E., *Inorganic nanostructures for photoelectrochemical and photocatalytic water splitting.* Chemical Society Reviews, 2013. **42**(6): p. 2294-2320.

52. Tang, J.W., et al., *Mechanism of photocatalytic water splitting in TiO(2). Reaction of water with photoholes, importance of charge carrier dynamics, and evidence for four-hole chemistry.* Journal of the American Chemical Society, 2008. **130**(42): p. 13885-13891.

53. Chen, Y.H., et al., *Aqueous CO_2 Reduction at Very Low Overpotential on Oxide-Derived Au Nanoparticles.* Journal of the American Chemical Society, 2012. **134**(49): p. 19969-19972.

54. Huan, T.N., et al., *CO_2 Reduction to CO in Water: Carbon Nanotube-Gold Nanohybrid as a Selective and Efficient Electrocatalyst.* Chemsuschem, 2016. **9**(17): p. 2317-2320.

55. Ohmori, T., et al., *Influence of sputtering parameters on electrochemical CO2 reduction in sputtered Au electrode.* Journal of Electroanalytical Chemistry, 2001. **514**(1-2): p. 51-55.

56. Ohmori, T., et al., *Photovoltaic water electrolysis using the sputter-deposited a-Si/c-Si solar cells.* International Journal of Hydrogen Energy, 2001. **26**(7): p. 661-664.

57. Hara, K., et al., *High-Efficiency Electrochemical Reduction of Carbon-Dioxide under High-Pressure on a Gas-Diffusion Electrode Containing Pt Catalysts.* Journal of the Electrochemical Society, 1995. **142**(4): p. L57-L59.

58. Li, C.W., et al., *Electroreduction of carbon monoxide to liquid fuel on oxide-derived nanocrystalline copper.* Nature, 2014. **508**(7497): p. 504-507.

59. Li, C.W., et al., *CO_2 Reduction at Low Overpotential on Cu Electrodes Resulting from the Reduction of Thick Cu2O Films.* Journal of the American Chemical Society, 2012. **134**(17): p. 7231-7234.

60. Kas, R., et al., *Three-dimensional porous hollow fibre copper electrodes for efficient and high-rate electrochemical carbon dioxide reduction.* Nature Communications, 2016. **7**.

61. Qing Li, J.F., et al., *Tuning Sn-Catalysis for Electrochemical Reduction of CO2 to CO via the Core/Shell Cu/SnO2 Structure.* J. Am. Chem. Soc, 2017. **139**(12): p. 4290–4293.

62. Medina-Ramos, et al., *Efficient Reduction of CO_2 to CO with High Current Density Using in Situ or ex Situ Prepared Bi-Based Materials.* Journal of the American Chemical Society, 2014. **136**(23): p. 8361-8367.

63. Froehlich, J.D., et al., *Homogeneous CO_2 Reduction by Ni(cyclam) at a Glassy Carbon Electrode.* Inorganic Chemistry, 2012. **51**(7): p. 3932-3934.

64. Parkin, A., et al., *Rapid and efficient electrocatalytic CO_2/CO interconversions by Carboxydothermus hydrogenoformans CO dehydrogenase I on an electrode.* Journal of the American Chemical Society, 2007. **129**(34): p. 10328-10329.

65. Ragsdale, S.W., *Life with carbon monoxide.* Critical Reviews in Biochemistry and Molecular Biology, 2004. **39**(3): p. 165-195.

66. Asadi, M., et al., *Nanostructured transition metal dichalcogenide electrocatalysts for CO_2 reduction in ionic liquid.* Science, 2016. **353**(6298): p. 467-470.

67. Zhao, G.Y., et al., *Electrochemical reduction of supercritical carbon dioxide in ionic liquid 1-n-butyl-3-methylimidazolium hexafluorophosphate.* Journal of Supercritical Fluids, 2004. **32**(1-3): p. 287-291.

68. Rosen, J., et al., *Electrodeposited Zn Dendrites with Enhanced CO Selectivity for Electrocatalytic CO_2 Reduction.* Acs Catalysis, 2015. **5**(8): p. 4586-4591.

69. Beley, M., et al., *Electrocatalytic Reduction of Co2 by Ni Cyclam^{2+} in Water - Study of the Factors Affecting the Efficiency and the Selectivity of the Process.* Journal of the American Chemical Society, 1986. **108**(24): p. 7461-7467.

70. Yamamoto, T., et al., *Electrochemical reduction of CO_2 in the micropores of activated carbon fibers.* Journal of the Electrochemical Society, 2000. **147**(9): p. 3393-3400.

71. Wu, J.J., et al., *Achieving Highly Efficient, Selective, and Stable CO^2 Reduction on Nitrogen-Doped Carbon Nanotubes.* Acs Nano, 2015. **9**(5): p. 5364-5371.

72. Medina-Ramos, J., et al., *Efficient Conversion of CO^2 to CO Using Tin and Other Inexpensive and Easily Prepared Post-Transition Metal Catalysts.* Journal of the American Chemical Society, 2015. **137**(15): p. 5021-5027.

73. Kaneco, S., et al., *Electrochemical reduction of high pressure carbon dioxide at a Cu electrode in cold methanol with CsOH supporting salt.* Chemical Engineering Journal, 2007. **128**(1): p. 47-50.

74. Ikeda, S., et al., *Selective Formation of Formic-Acid, Oxalic-Acid, and Carbon-Monoxide by Electrochemical Reduction of Carbon-Dioxide.* Bulletin of the Chemical Society of Japan, 1987. **60**(7): p. 2517-2522.

75. Gao, D.F., et al., *Size-Dependent Electrocatalytic Reduction of CO^2 over Pd Nanoparticles.* Journal of the American Chemical Society, 2015. **137**(13): p. 4288-4291.

76. Costentin, C., et al., *A Local Proton Source Enhances CO_2 Electroreduction to CO by a Molecular Fe Catalyst.* Science, 2012. **338**(6103): p. 90-94.

77. Hall, A.S., et al., *Mesostructure-Induced Selectivity in CO^2 Reduction Catalysis.* Journal of the American Chemical Society, 2015. **137**(47): p. 14834-14837.

78. DiMeglio, J.L., et al., *Selective Conversion of CO_2 to CO with High Efficiency Using an Inexpensive Bismuth-Based Electrocatalyst.* Journal of the American Chemical Society, 2013. **135**(24): p. 8798-8801.

79. Rasul, S., et al., *A Highly Selective Copper-Indium Bimetallic Electrocatalyst for the Electrochemical Reduction of Aqueous CO_2 to CO.* Angewandte Chemie-International Edition, 2015. **54**(7): p. 2146-2150.

80. Zhou, F., et al., *Highly selective and stable electro-catalytic system with ionic liquids for the reduction of carbon dioxide to carbon monoxide.* Electrochemistry Communications, 2015. **55**: p. 43-46.

81. Huei-Ru Molly Jhong, C.E.T., et al., *A Nitrogen-Doped Carbon Catalyst for Electrochemical CO2 Conversion to CO with High Selectivity and Current Density.* ChemSusChem, 2016. **9**.

82. Asadi, M., et al., *Robust carbon dioxide reduction on molybdenum disulphide edges.* Nat Commun, 2014. **5**.

83. Smieja, J.M., et al., *Manganese as a Substitute for Rhenium in CO_2 Reduction Catalysts: The Importance of Acids.* Inorganic Chemistry, 2013. **52**(5): p. 2484-2491.

84. Shin, W., et al., *Highly selective electrocatalytic conversion of CO_2 to CO at -0.57V (NHE) by carbon monoxide dehydrogenase from Moorella thermoacetica.* Journal of the American Chemical Society, 2003. **125**(48): p. 14688-14689.

85. Badawy, W.A., et al., *Cathodic hydrogen evolution on molybdenum in NaOH solutions.* International Journal of Hydrogen Energy, 2013. **38**(23): p. 9625-9632.

86. Jaksic, J.M., et al., *Kinetic analysis of hydrogen evolution at Ni-Mo alloy electrodes.* Electrochimica Acta, 2000. **45**(25-26): p. 4151-4158.

87. N. Pentland, J.O.M.B.a.E.S., *Hydrogen evolution reaction on copper, gold, molybdenum, palladium, rhodium, and iron mechanism and measurement technique under high purity conditions.* J Electrochem Soc, 1957. **104**(3): p. 182-194.

88. Conway, B.E., et al. *Determination of the Adsorption Behavior of Overpotential-Deposited Hydrogen-Atom Species in the Cathodic

Hydrogen-Evolution Reaction by Analysis of Potential-Relaxation Transients. Journal of the Chemical Society-Faraday Transactions I, 1985. **81**: p. 1841-1862.

89. Lasia, A., et al., *Kinetics of Hydrogen Evolution on Nickel Electrodes.* Journal of Electroanalytical Chemistry, 1990. **294**(1-2): p. 123-141.

90. Jaccaud, M., et al., *New Chlor-Alkali Activated Cathodes.* Materials Chemistry and Physics, 1989. **22**(1-2): p. 105-119.

91. Kotz, E.R., et al., *Ruthenium Dioxide as a Hydrogen-Evolving Cathode.* Journal of Applied Electrochemistry, 1987. **17**(6): p. 1190-1197.

92. Safizadeh, F., et al., *Electrocatalysis developments for hydrogen evolution reaction in alkaline solutions - A Review.* International Journal of Hydrogen Energy, 2015. **40**(1): p. 256-274.

93. Shervedani, R.K., et al., *Electrocatalytic Activities of Nickel-phosphorous Composite Coating Reinforced with Codeposited Graphite Carbon for Hydrogen Evolution Reaction in Alkaline Solution.* Journal of New Materials for Electrochemical Systems, 2008. **11**(4): p. 259-265.

94. Elezovic, N.R., et al., *Kinetics of the hydrogen evolution reaction on Fe-Mo film deposited on mild steel support in alkaline solution.* Electrochimica Acta, 2005. **50**(28): p. 5594-5601.

95. Grgur, B.N., et al., *Electrodeposition and characterization of Fe-Mo alloys as cathodes for hydrogen evolution in the process of chlorate production (vol 70, pg 879, 2005).* Journal of the Serbian Chemical Society, 2005. **70**(8-9): p. 1131-1131.

96. Rosalbino, F., et al., *Electrocatalytic properties of Fe-R (R = rare earth metal) crystalline alloys as hydrogen electrodes in alkaline water electrolysis.* Journal of Alloys and Compounds, 2005. **403**(1-2): p. 275-282.

97. Rosalbino, F., et al., *Characterization of Fe-Zn-R (R = rare earth metal) crystalline alloys as electrocatalysts for hydrogen evolution.* International Journal of Hydrogen Energy, 2008. **33**(11): p. 2660-2667.

98. Cesiulis, H., et al., *Electrodeposition of CoMo and CoMoP alloys from the weakly acidic solutions.* Surface Engineering and Applied Electrochemistry, 2010. **46**(5): p. 406-415.

99. Gomez, E., et al., *Electrodeposited cobalt-molybdenum magnetic materials.* Journal of Electroanalytical Chemistry, 2001. **517**(1-2): p. 109-116.

100. Gomez, E., et al., *Detection and characterization of molybdenum oxides formed during the initial stages of cobalt-molybdenum electrodeposition.* Journal of Applied Electrochemistry, 2003. **33**(3-4): p. 245-252.

101. Kublanovsky, V., et al., *Cobalt-molybdenum-phosphorus alloys: Electroplating and corrosion properties.* Protection of Metals and Physical Chemistry of Surfaces, 2009. **45**(5): p. 588-594.

102. Podlaha, E.J., et al., *Induced codeposition .1. An experimental investigation of Ni-Mo alloys.* Journal of the Electrochemical Society, 1996. **143**(3): p. 885-892.

103. Spasojevic, M., et al., *The Evolution of Hydrogen on Cobalt-Molybdenum Coating - Polarization Characteristics.* Journal of Applied Electrochemistry, 1984. **14**(2): p. 265-266.

104. Subramania, A., et al., *Electrocatalytic cobalt-molybdenum alloy deposits.* International Journal of Hydrogen Energy, 2007. **32**(14): p. 2843-2847.

105. O'Brien TF, B.T., et al., *Overview of the chloralkali industry. Handbook of chlor-alkali technology. Fundamentals*. Vol. I. 2005: Springer science.

106. Goldman, L.M., et al., *Short Wavelength Compositionally Modulated Ni/Ni-P Films Prepared by Electrodeposition.* Journal of Applied Physics, 1986. **60**(4): p. 1374-1376.

107. Krstajic, N.V., et al., *Non-noble metal composite cathodes for hydrogen evolution. Part I: The Ni-MoOx coatings electrodeposited from Watt's type bath containing MoO3 powder particles.* International Journal of Hydrogen Energy, 2011. **36**(11): p. 6441-6449.

108. Krstajic, N.V., et al., *Non-noble metal composite cathodes for hydrogen evolution. Part II: The Ni-MoO*^{2} *coatings electrodeposited from nickel chloride-ammonium chloride bath containing MoO*^{2} *powder particles.* International Journal of Hydrogen Energy, 2011. **36**(11): p. 6450-6461.

109. Rashkov, R., et al., *NiW/TiOx composite layers as cathode material for hydrogen evolution reaction.* International Journal of Hydrogen Energy, 2009. **34**(5): p. 2095-2100.

110. Wang, M.Y., et al., *The enhanced electrocatalytic activity and stability of NiW films electrodeposited under super gravity field for hydrogen evolution reaction.* International Journal of Hydrogen Energy, 2011. **36**(5): p. 3305-3312.

111. Solmaz, R., et al., *Electrochemical deposition and characterization of NiFe coatings as electrocatalytic materials for alkaline water electrolysis.* Electrochimica Acta, 2009. **54**(14): p. 3726-3734.

112. Ullal, Y., et al., *Electrodeposition and electro-catalytic study of nanocrystalline Ni-Fe alloy.* International Journal of Hydrogen Energy, 2014. **39**(20): p. 10485-10492.

113. Marini, S., et al., *Stable and inexpensive electrodes for the hydrogen evolution reaction.* International Journal of Hydrogen Energy, 2013. **38**(26): p. 11484-11495.

114. I. Arul Raj, K.I.V., *Transition metal-based hydrogen electrodes in alkaline solution — electrocatalysis on nickel based binary alloy coatings.* Journal of Applied Electrochemistry, 1990. **20**(1): p. 32-38.

115. Fenwick, A.Q., et al., *Electrocatalytic Reduction of Nitrogen and Carbon Dioxide to Chemical Fuels: Challenges and Opportunities for a Solar Fuel Device.* J. Photochem. Photobiol. B: Biol, 2015. **152**(Pt A): p. 47-57.

116. Cachet, C., et al., *Influence of Perfluorinated and Hydrogenated Surfactants Upon Hydrogen Evolution on Gold Electrodes.* Electrochimica Acta, 1994. **39**(18): p. 2743-2750.

117. Hamelin, A., *Cyclic voltammetry at gold single-crystal surfaces .1. Behaviour at low-index faces.* Journal of Electroanalytical Chemistry, 1996. **407**(1-2): p. 1-11.

118. Hamelin, A., et al., *Cyclic voltammetry at gold single-crystal surfaces .2. Behaviour of high-index faces.* Journal of Electroanalytical Chemistry, 1996. **407**(1-2): p. 13-21.

119. Hamelin, A., et al., *Some Electrochemical Consequences of Potential-Induced Surface Reconstruction on Au(100) - Double-Layer Nonuniformity and Electrode-Kinetics.* Journal of Electroanalytical Chemistry, 1994. **365**(1-2): p. 47-57.

120. Perez, J., et al., *Hydrogen evolution reaction on gold single-crystal electrodes in acid solutions.* Journal of Physical Chemistry B, 1998. **102**(52): p. 10931-10935.

121. Xu, Y.H., *The hydrogen evolution reaction on single crystal gold electrode.* International Journal of Hydrogen Energy, 2009. **34**(1): p. 77-83.

122. Khanova, L.A., et al., *Kinetics of the hydrogen evolution reaction on gold electrode. A new case of the barrierless discharge.* Journal of Electroanalytical Chemistry, 2011. **660**(2): p. 224-229.

123. Smiljanic, M., et al., *Catalysis of Hydrogen Evolution on Au(111) Modified by Spontaneously Deposited Pd Nanoislands.* Electrocatalysis, 2012. **3**(3-4): p. 369-375.

124. Danilovic, N., et al., *Electrocatalysis of the HER in acid and alkaline media.* Journal of the Serbian Chemical Society, 2013. **78**(12): p. 2007-2015.

125. Afkhami, A., et al., *Highly sensitive and selective determination of thiocyanate using gold nanoparticles surface decorated multi-walled*

carbon nanotubes modified carbon paste electrode. Sensors and Actuators B-Chemical, 2014. **196**: p. 467-474.

126. R. S. Sai Siddhardha , V.L.b.S.S.R., *Spot-free catalysis using gold carbon nanotube & gold graphene composites for hydrogen evolution reaction.* Journal of Power Sources, 2015. **288**: p. 441-450.

127. Prakash, G.K.S., et al., *Electrochemical reduction of* CO^2 *over Sn-Nafion (R) coated electrode for a fuel-cell-like device.* Journal of Power Sources, 2013. **223**: p. 68-73.

128. Li, H. , et al., *Development of a continuous reactor for the electro-reduction of carbon dioxide to formate - Part 2: Scale-up.* Journal of Applied Electrochemistry, 2007. **37**(10): p. 1107-1117.

129. Mistry, H., et al., *Exceptional Size-Dependent Activity Enhancement in the Electroreduction of CO2 over Au Nanoparticles.* Journal of the American Chemical Society, 2014. **136**(47): p. 16473-16476.

130. Jhong, H.R., et al., *Electrochemical conversion of* CO^2 *to useful chemicals: current status, remaining challenges, and future opportunities.* Current Opinion in Chemical Engineering, 2013. **2**(2): p. 191-199.

131. Hori, Y., et al., *Electrochemical reduction of CO at a copper electrode.* Journal of Physical Chemistry B, 1997. **101**(36): p. 7075-7081.

132. Gattrell, M., et al., *A review of the aqueous electrochemical reduction of* CO^2 *to hydrocarbons at copper.* Journal of Electroanalytical Chemistry, 2006. **594**(1): p. 1-19.

133. Thorson, M.R., et al., *Effect of Cations on the Electrochemical Conversion of* CO_2 *to CO.* Journal of the Electrochemical Society, 2013. **160**(1): p. F69-F74.

134. Wu, J.J., et al., *Electrochemical Reduction of Carbon Dioxide I. Effects of the Electrolyte on the Selectivity and Activity with Sn Electrode.* Journal of the Electrochemical Society, 2012. **159**(7): p. F353-F359.

135. Salehi-Khojin, A., et al., *Nanoparticle Silver Catalysts That Show Enhanced Activity for Carbon Dioxide Electrolysis.* Journal of Physical Chemistry C, 2013. **117**(4): p. 1627-1632.

136. Zhou, F., et al., *Highly selective electrocatalytic reduction of carbon dioxide to carbon monoxide on silver electrode with aqueous ionic liquids.* Electrochemistry Communications, 2014. **46**: p. 103-106.

137. Iijima, S., *Helical Microtubules of Graphitic Carbon.* Nature, 1991. **354**(6348): p. 56-58.

138. Fujishima, A., et al., *Electrochemical Photolysis of Water at a Semiconductor Electrode.* Nature, 1972. **238**(5358): p. 37-+.

139. Nakade, S., et al., *Influence of TiO_2 nanoparticle size on electron diffusion and recombination in dye-sensitized TiO_2 solar cells.* Journal of Physical Chemistry B, 2003. **107**(33): p. 8607-8611.

140. Lamberti, A., et al., *As-grown vertically aligned amorphous TiO_2 nanotube arrays as high-rate Li-based micro-battery anodes with improved long-term performance.* Electrochimica Acta, 2015. **151**: p. 222-229.

141. Ou, H.-H., et al., *Review of titania nanotubes synthesized via the hydrothermal treatment: Fabrication, modification, and application.* Separation and Purification Technology, 2007. **58**(1): p. 179-191.

142. Hoyer, P., *Formation of a Titanium Dioxide Nanotube Array.* Langmuir, 1996. **12**(6): p. 1411-1413.

143. Kasuga, T., et al., *Formation of Titanium Oxide Nanotube.* Langmuir, 1998. **14**(12): p. 3160-3163.

144. Zwilling, V., et al., *Structure and physicochemistry of anodic oxide films on titanium and TA6V alloy.* Surface and Interface Analysis, 1999. **27**(7): p. 629-637.

145. Macak, J.M., et al., *Self-organized porous titanium oxide prepared in Na2SO4/NaF electrolytes.* Electrochimica Acta, 2005. **50**(18): p. 3679-3684.

146. Macak, J.M., et al., *Smooth anodic TiO_2 nanotubes.* Angewandte Chemie International Edition, 2005. **44**(45): p. 7463-7465.

147. Albu, S.P., et al., *250 µm long anodic TiO_2 nanotubes with hexagonal self-ordering.* physica status solidi (RRL) – Rapid Research Letters, 2007. **1**(2): p. R65-R67.

148. Nischk, M., et al., *Ordered TiO_2 nanotubes: The effect of preparation parameters on the photocatalytic activity in air purification process.* Applied Catalysis B: Environmental, 2014. **144**: p. 674-685.

149. Macak, J.M., et al., *Towards ideal hexagonal self- ordering of TiO_2 nanotubes.* physica status solidi (RRL)-Rapid Research Letters, 2007. **1**(5): p. 181-183.

150. Tighineanu, A., et al., *Conductivity of TiO_2 nanotubes: Influence of annealing time and temperature.* Chemical Physics Letters, 2010. **494**(4–6): p. 260-263.

151. Albu, S.P., et al., *Formation of Double-Walled TiO_2 Nanotubes and Robust Anatase Membranes.* Advanced Materials, 2008. **20**(21): p. 4135-4139.

152. Yasuda, K. , et al., *Control of morphology and composition of self-organized zirconium titanate nanotubes formed in* $(NH_4)_2SO_4/NH_4F$ *electrolytes.* Electrochimica Acta, 2007. **52**(12): p. 4053-4061.

153. Habazaki, H., et al., *Fast migration of fluoride ions in growing anodic titanium oxide.* Electrochemistry Communications, 2007. **9**(5): p. 1222-1227.

154. Valota, A., et al., *Influence of water content on nanotubular anodic titania formed in fluoride/glycerol electrolytes.* Electrochimica Acta, 2009. **54**(18): p. 4321-4327.

155. Lamberti, A., et al., *Vertically aligned* TiO_2 *nanotube array for high rate Li-based micro-battery anodes with improved durability.* Electrochimica Acta, 2013. **102**: p. 233-239.

156. Lieberman, M.A., et al., *Principles of plasma discharges and materials processing*. 2005: John Wiley & Sons.

157. *Double-layer capacitance*. Available from: https://en.wikipedia.org/wiki/Double-layer_capacitance.

158. Lukaszewski, M., et al., *Electrochemical Methods of Real Surface Area Determination of Noble Metal Electrodes - an Overview.* International Journal of Electrochemical Science, 2016. **11**(6): p. 4442-4469.

159. Pang, Y.L., et al., *A critical review on the recent progress of synthesizing techniques and fabrication of TiO 2-based nanotubes photocatalysts.* Applied Catalysis A: General, 2014. **481**: p. 127-142.

160. Naughton, M.S., et al., *Quantitative Analysis of Single-Electrode Plots to Understand In-Situ Behavior of Individual Electrodes.* Journal of the Electrochemical Society, 2012. **159**(6): p. B761-B769.

161. Delmondo, L., et al., *Nanostructured MnxOy for oxygen reduction reaction (ORR) catalysts.* Applied Surface Science, 2016. **388**: p. 631-639.

162. Chang, K.W., et al., *Layer-separable and gap-tunable topological insulators.* Physical Chemistry Chemical Physics, 2017. **19**(5): p. 3932-3936.

163. Sacco, A., *Electrochemical Impedance spectroscopy: Fundamentals and application in dye-sensitized solar cells.* Renewable and sustainable energy reviews, 2017. **79**: p. 15.

164. Kortlever, R., et al., *Catalysts and Reaction Pathways for the Electrochemical Reduction of Carbon Dioxide.* Journal of Physical Chemistry Letters, 2015. **6**(20): p. 4073-4082.

165. Firet, N.J., et al., *Probing the Reaction Mechanism of* CO_2 *Electroreduction over Ag Films via Operando Infrared Spectroscopy.* Acs Catalysis, 2017. **7**(1): p. 606-612.

166. Yang, C.T., et al., CO_2 *Adsorption on Anatase* TiO_2 *(101) Surfaces in the Presence of Subnanometer Ag/Pt Clusters: Implications for* CO_2 *Photoreduction.* Journal of Physical Chemistry C, 2014. **118**(45): p. 26236-26248.

167. Ma, S.C., et al., *Support materials for catalysts for electrochemical reduction of* CO_2 *to value added products.* Abstracts of Papers of the American Chemical Society, 2013. **246**.

Appendix

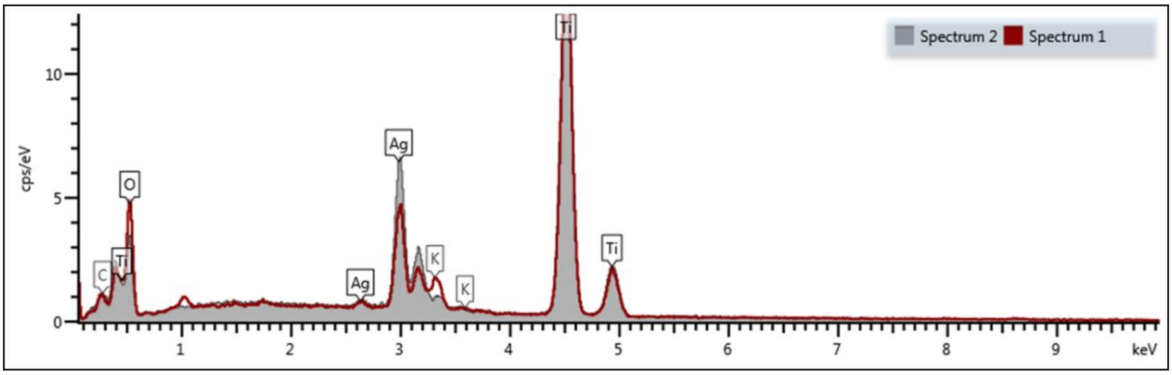

Figure A-1. EDS analysis before (spectrum 2) and after (spectrum 1) the reaction for Ag UV deposited electrocatalyst

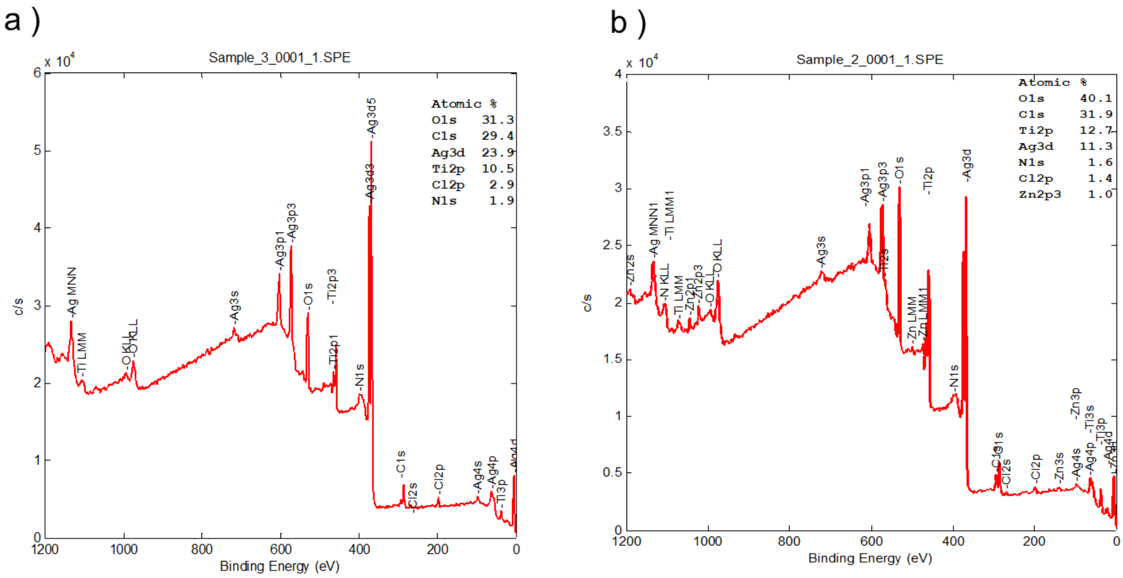

Figure A-2. XPS analysis a) before b) after the reaction for Ag/TNT 20mA90s

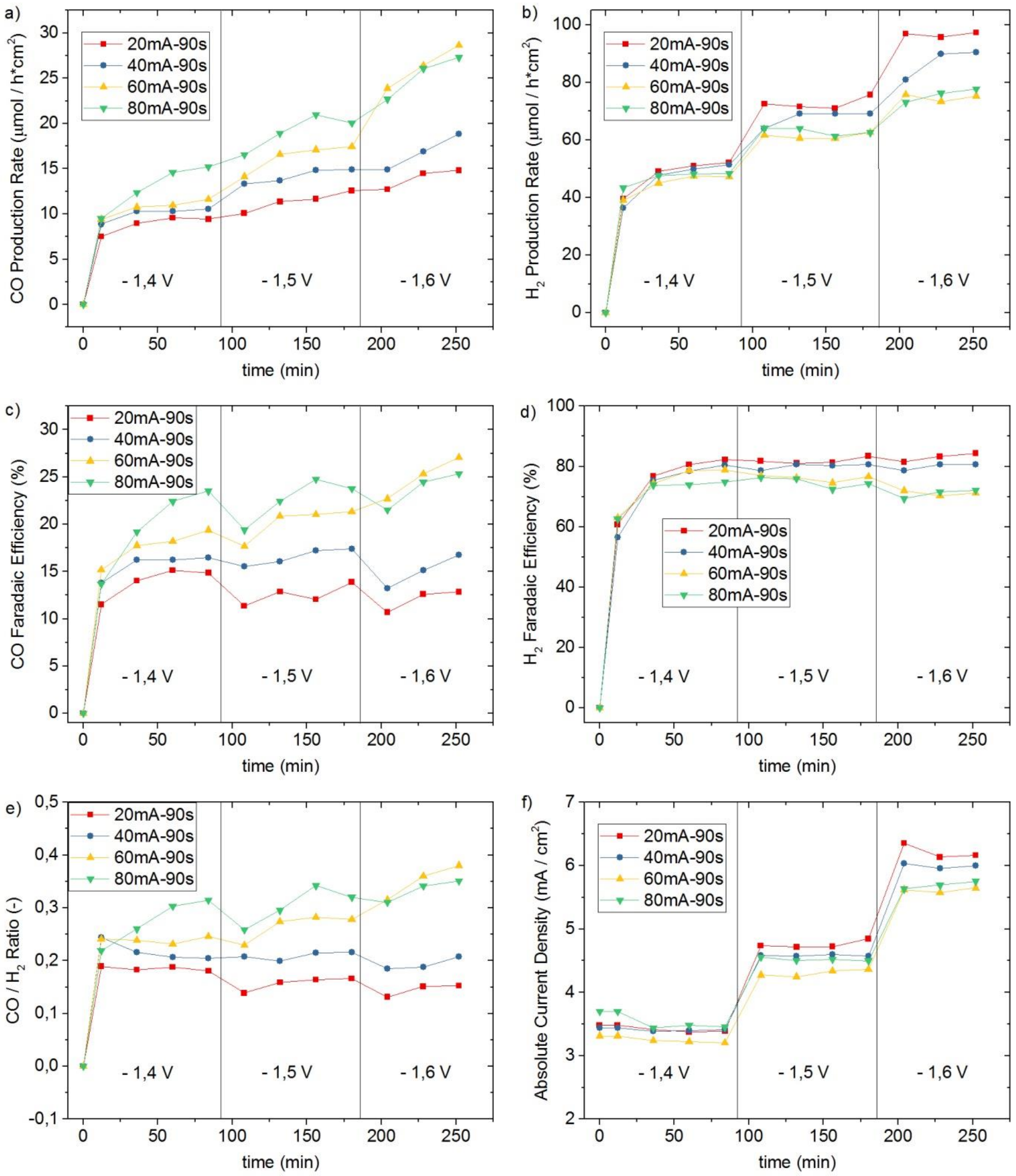

Figure A-3. Comparison between the results (vs. time) of catalysts with the same sputtering time and different sputtering current (90 minutes of test at each potential): a,b) CO and H_2 production rates, c,d) CO and H_2 faradaic efficiencies, e) CO/H_2 ratio, f) absolute current density. All the potential values are in V vs. SHE.

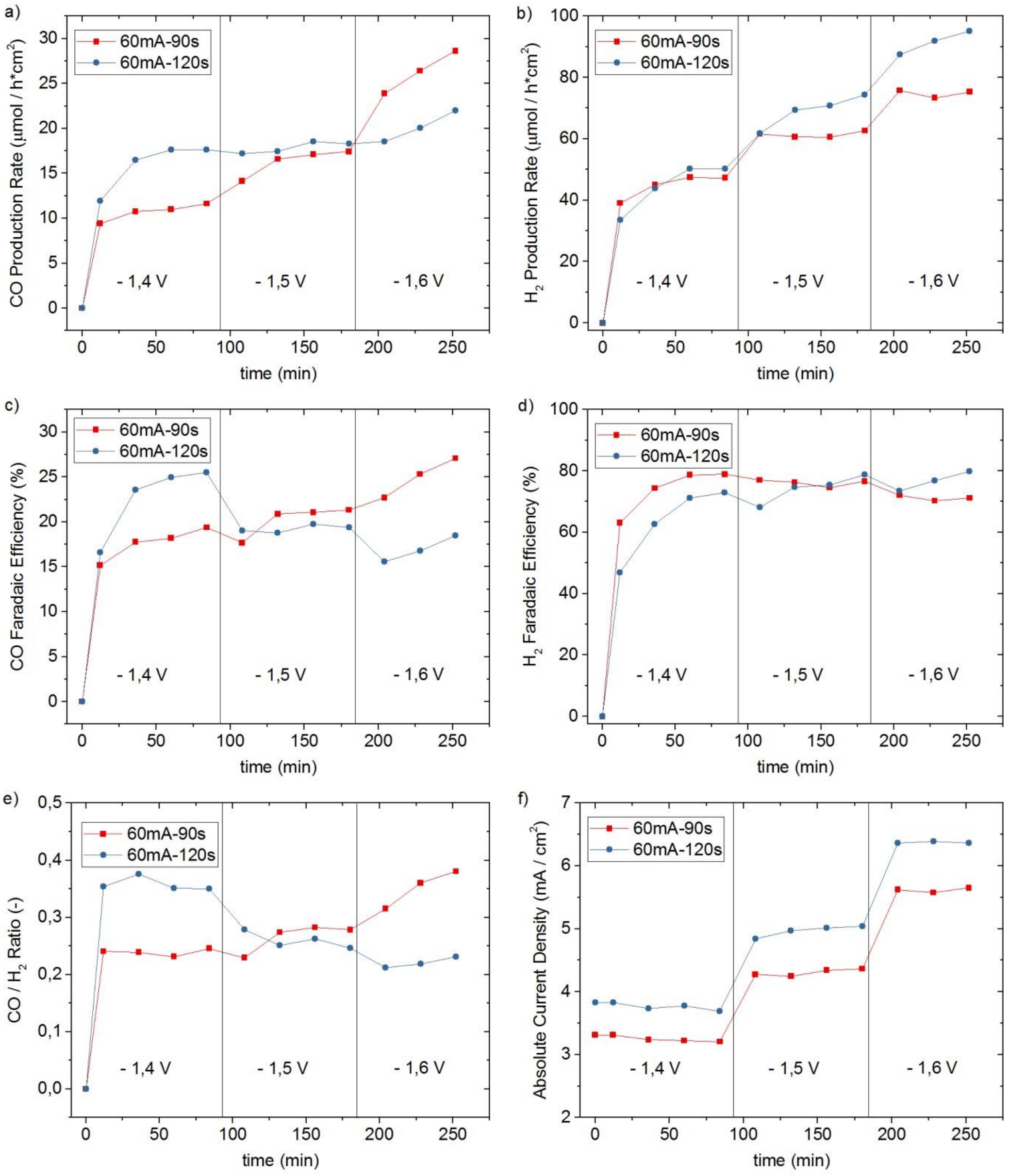

Figure A-4. Comparison between the results (vs. time) of catalysts with the same sputtering current and different sputtering time (90 minutes of test at each potential) : a,b) CO and H_2 production rates, c,d) CO and H_2 faradaic efficiencies, e) CO/H_2 ratio, f) absolute current density. All the potential values are in V vs. SHE

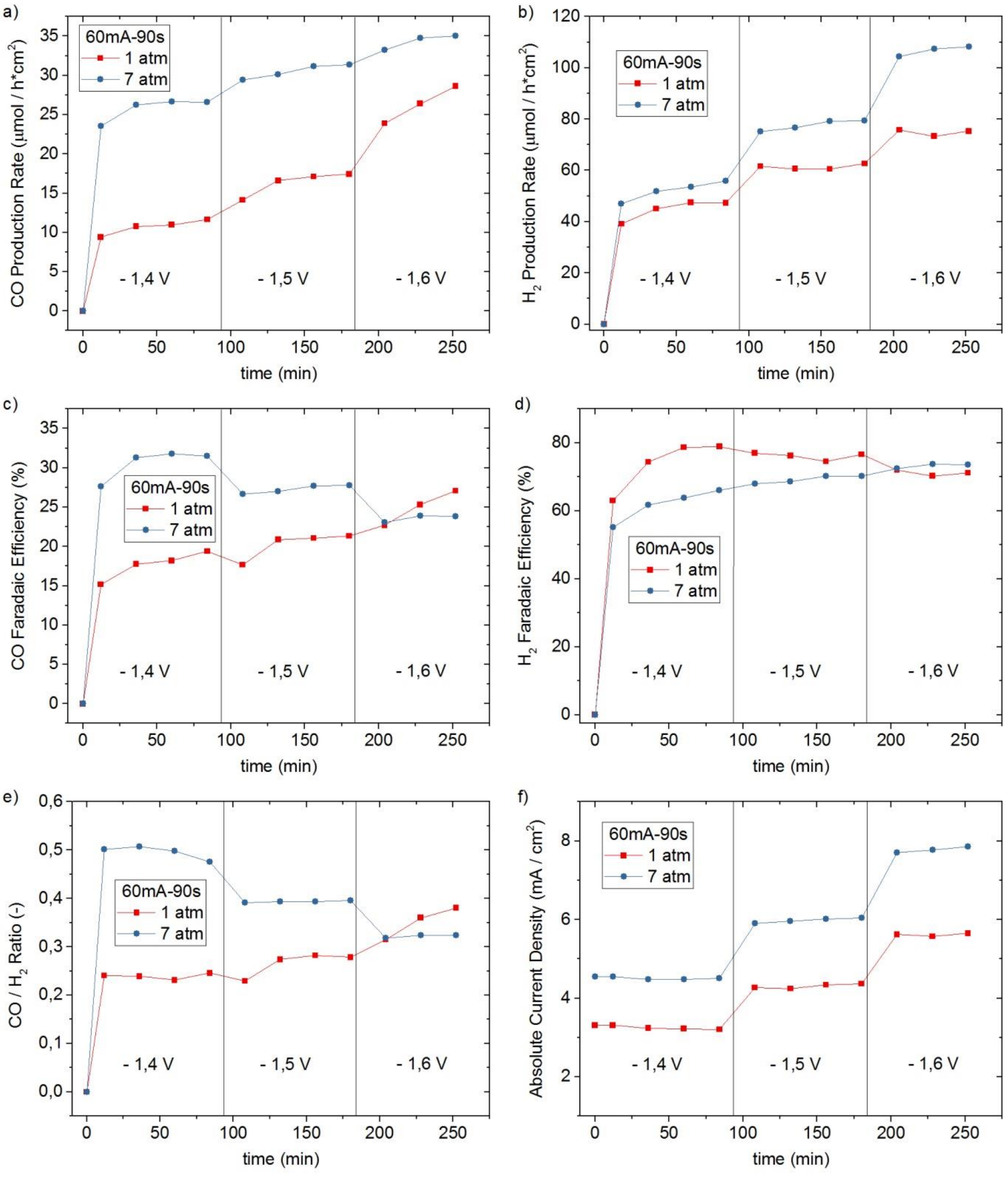

Figure A-5. Comparison between the results (vs. time) of 60mA90s tested at two different pressure values (90 minutes of test at each potential): a,b) CO and H_2 production rates, c,d) CO and H_2 faradaic efficiencies, e) CO/H_2 ratio, f) absolute current density. All the potential values are in V vs. SHE.

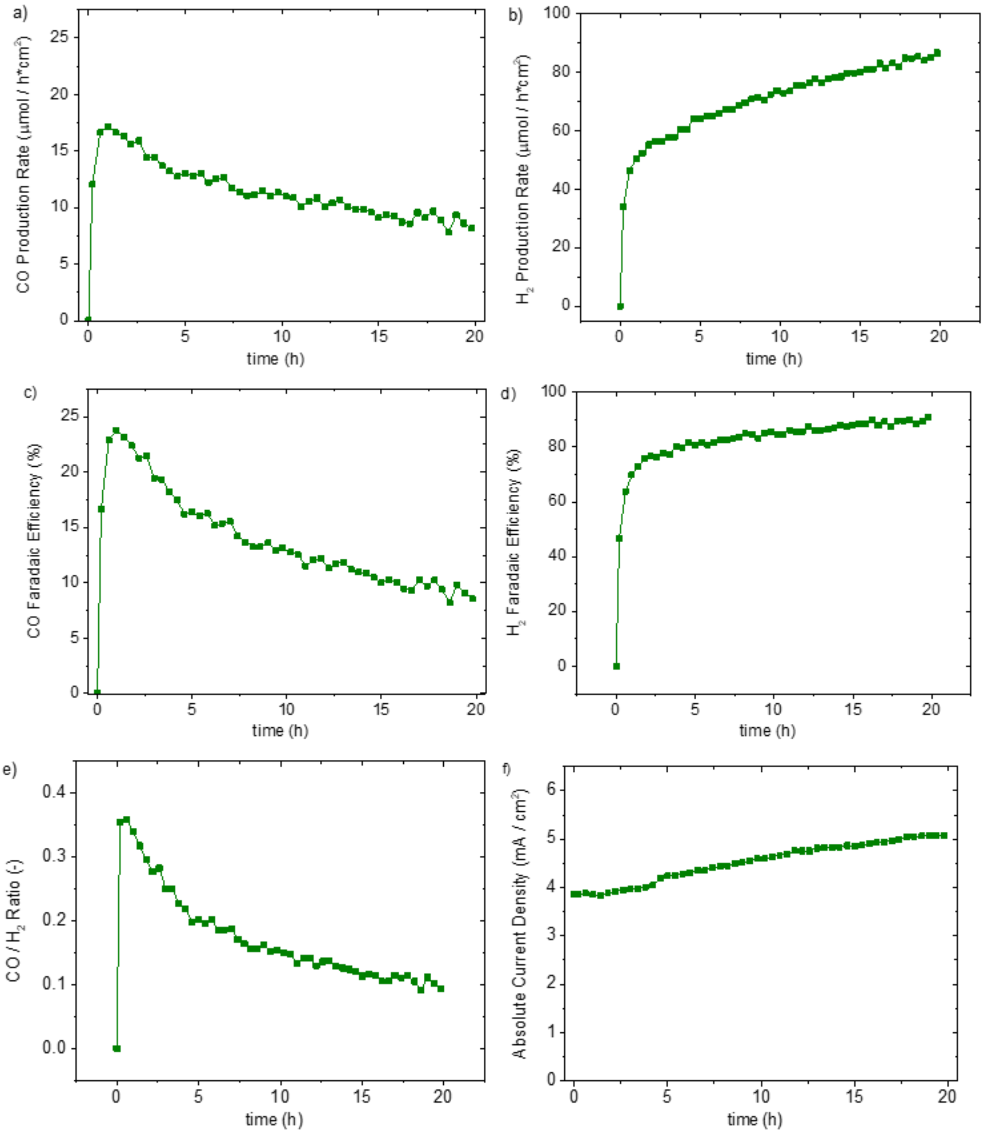

FigureA-6. Long duration test for 60mA90s at -1.4V vs. SHE. a) CO production b) H_2 production c) CO faradaic efficiency d) H2 faradaic efficiency e) CO/H_2 ratio f) absolute current density vs hours of reaction

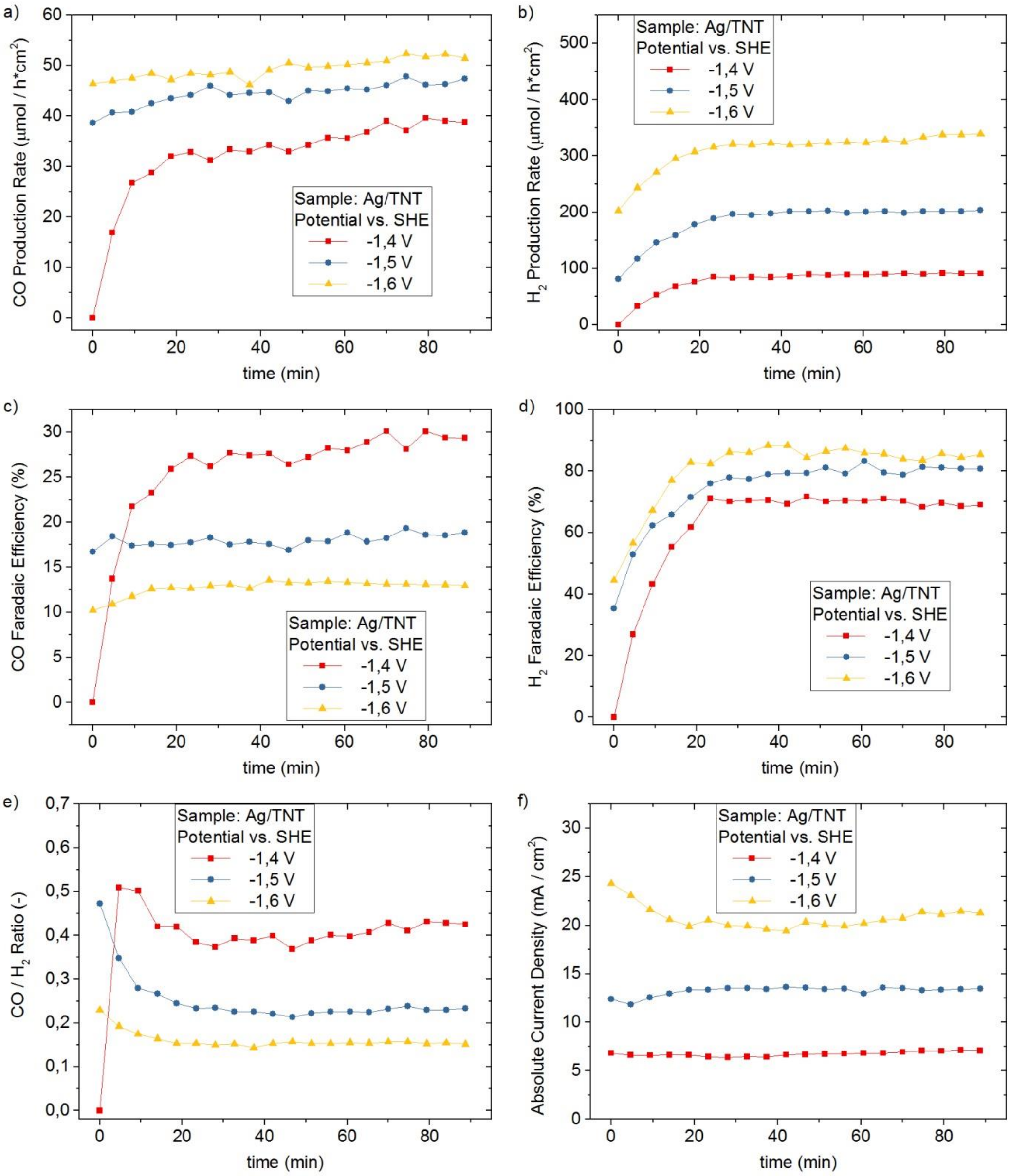

Figure A-7. Results (vs. potential) of Ag/TNT 60mA-90s: a,b) CO and H_2 production rates, c,d) CO and H_2 faradaic efficiencies, e) CO/H_2 ratio, f) absolute current density. All the potentials were applied with IR compensation.

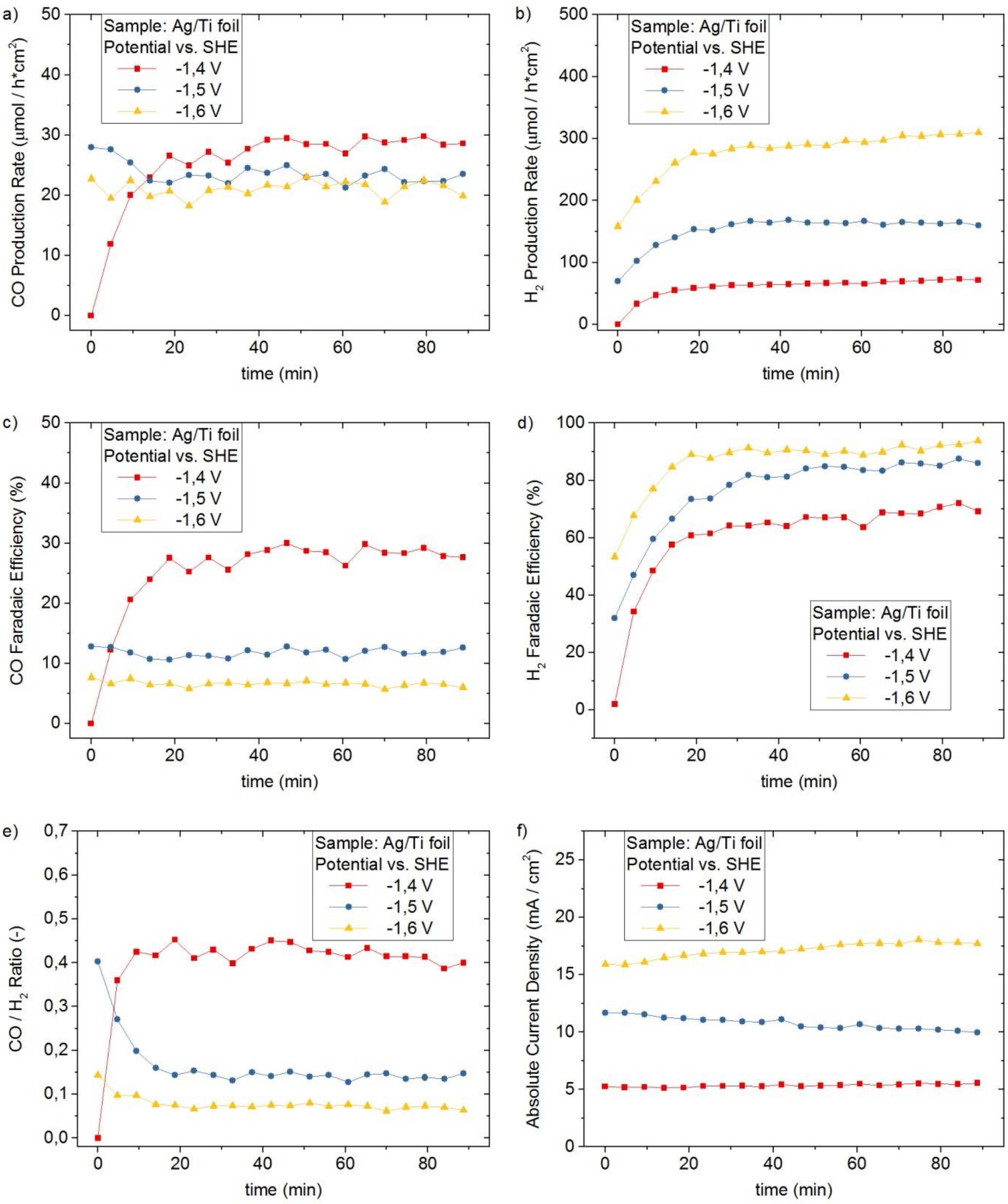

Figure A-8. Results (vs. potential) of Ag/Ti foil 60mA-90s sputtered: a,b) CO and H_2 production rates, c,d) CO and H_2 faradaic efficiencies, e) CO/H_2 ratio, f) absolute current density. All the potentials were applied with IR compensation.

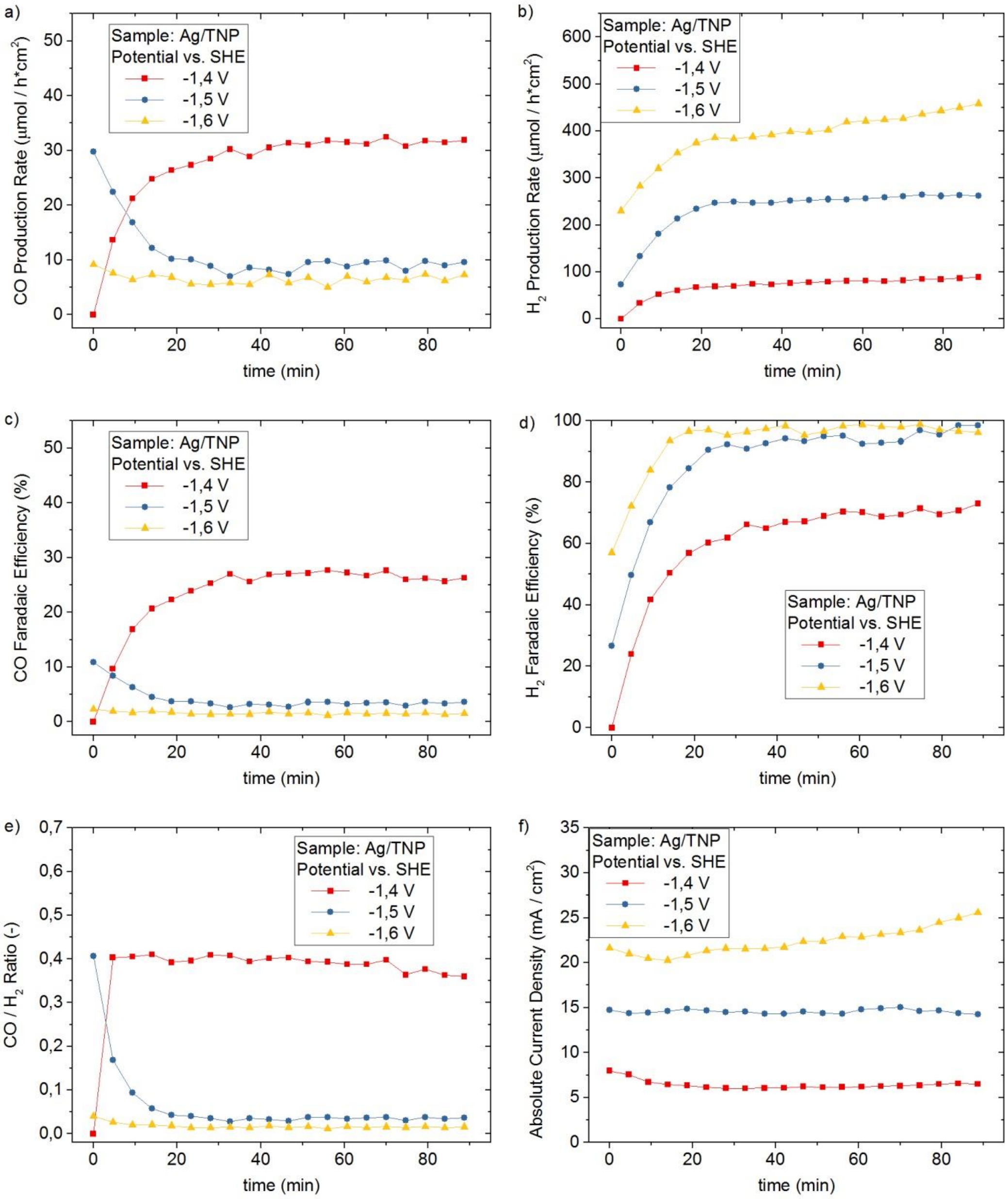

Figure A-9. Results (vs. potential) of Ag/TNP 60mA-90s sputtered: a,b) CO and H_2 production rates, c,d) CO and H_2 faradaic efficiencies, e) CO/H_2 ratio, f) absolute current density. All the potentials were applied with IR compensation.

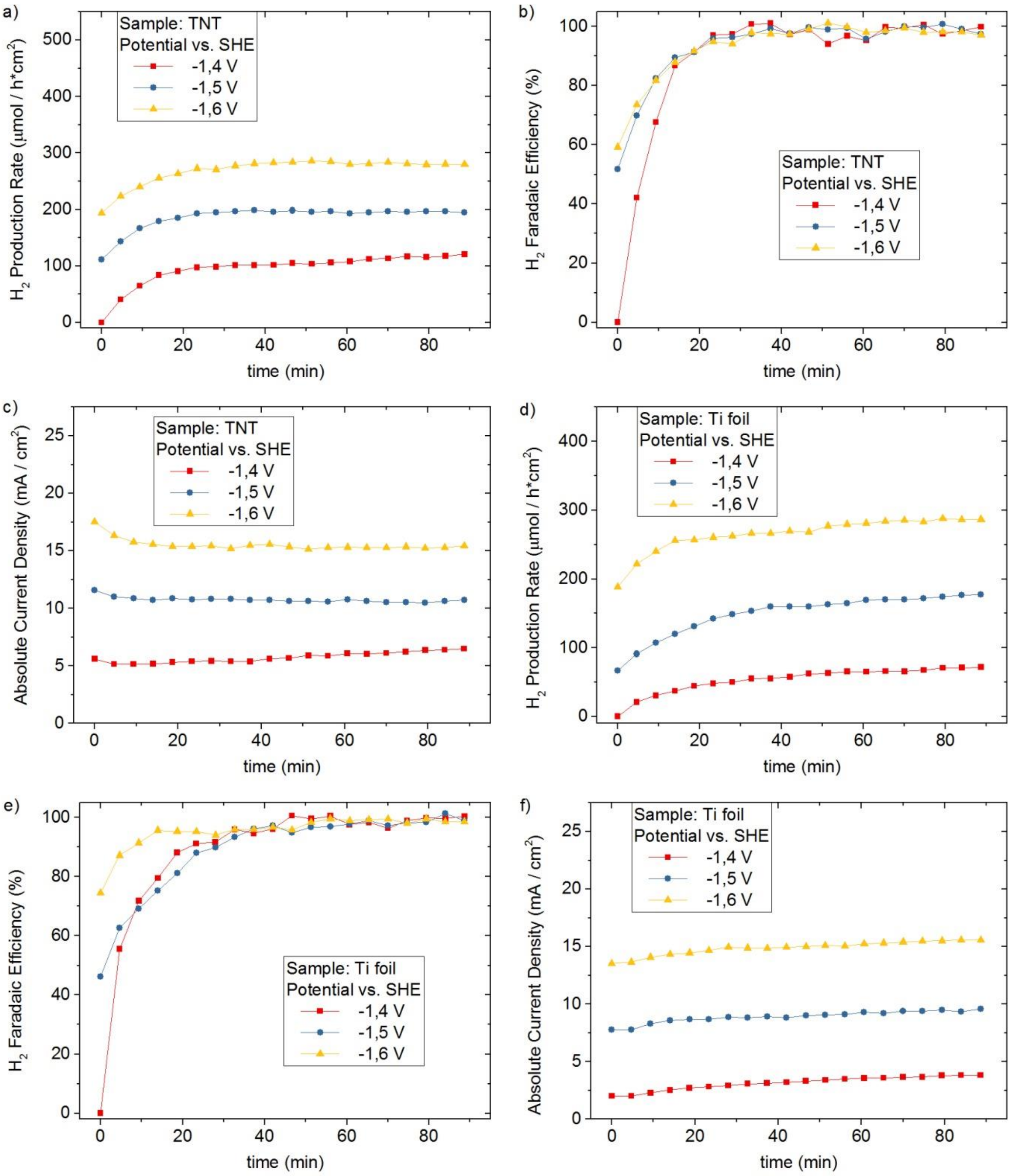

Figure A-10. Results (vs. potential) of TNT and Ti foil: a,b) CO and H_2 production rates, c,d) CO and H_2 faradaic efficiencies, e) CO/H_2 ratio, f) absolute current density. All the potentials were applied with IR compensation.